Dissertation

Untersuchungen an mechanosensitiven Ionenkanälen in benignen und malignen humanen Mammaepithel – Zelllinien

eingereicht von

Msc.

Chouyang LI

zur Erlangung des akademischen Grades

Doktor der Medizinischen Wissenschaft

(Dr. scient. med.)

an der

Medical University of Graz

Institut for Biophysik

unter der Anleitung von

Ao.Univ.-Prof. Dr.phil. Wolfgang SCHREIBMAYER

2015

Dissertation

A STUDY ON MECHANOSENSITIVE ION CHANNELS IN BENIGN AND CANCEROUS HUMAN MAMMARY EPITHELIAL CELL LINES

submitted by

Msc.

Chouyang LI

for the Academic Degree of

Doctor of Medical Science

(Dr. scient. med.)

at the

Medical University of Graz

Institute for Biophysics

under the Supervision of

Ao.Univ.-Prof. Dr.phil. Wolfgang SCHREIBMAYER

2015

“Declaration

I hereby declare that this dissertation is my own original work and that I have fully acknowledged by name all of those individuals and organizations that have contributed to the research for this dissertation. Due acknowledgement has been made in the text to all other material used. Throughout this dissertation and in all related publications I followed the guidelines of “Good Scientific Practice” Date 09.07.2015”.

A STUDY ON MECHANOSENSITIVE ION CHANNELS IN BENIGN AND CANCEROUS HUMAN MAMMARY EPITHELIAL CELL LINES

CONTENT

KEYWORDS

Mechanosensitive Ion Channel / Piezo1 / MCF-7 / MCF-10A / HEK-293 / mammary gland / Breast Cancer /

ABBREVIATIONS

EP_{50}: effective pressure required for half maximal activation of mechanosensitive ion channels

eGFP: green fluorescent protein, enhanced version

eYFP: yellow fluorescent protein, enhanced version.

Fam38A: Family With Sequence Similarity 38, Member A (Gene encoding Piezo1)

Fam38B: Family With Sequence Similarity 38, Member B (Gene encoding Piezo2)

GAPDH: Glycerinaldehyd-3-phosphat-Dehydrogenase

GEO:Gene Expression Omnibus

G_{Λ}: single channel conductance

GsMTx-4: toxin isolated from the Chilean rose tarantula (Grammostola rosea) venom

HEK-293: Human Embryonic Kidney 293 cells

MCF-7: Michigan Cancer Foundation – 7 cell line

MCF-10A: Michigan Cancer Foundation – 10A cell line

XX^{WT}: Wild type XX cell

$XX^{hG1y\#Y}$: XX cell transfected with human GIRK1 y construct, clone #Y

$XX^{G\beta\gamma}$: XX cell transfected with G-protein βγ subunit

XX^{hP1}: XX cell transfected with human Piezo1 protein

$XX^{ZZ\_k.o}$: XX cell transfected with dominant negative ZZ construct

MEC: mammary epithelial cell

mRNA: messenger Ribonucleic acid

MSC: mechanosensitive ion channel

nMSC: non-mechanosensitive ion channel

MTC: mechanical triggered ion channel

BC: big channel

Dr: delayed rectifier

n.p.: negative pressure used inside the patch clamp pipette to activate mechanosensitive ion channels

PFS: pipette filling solution

q-PCR: quantitative real-time PCR

TrpC: canonical transient receptor potential (Genes encoding TrpC channels)

ZBS: zeroing bathing solution

ZUSAMMENFASSUNG

Die Transduktion von mechanischen Reizen wird, bei der gesunden lactierenden Milchdrüse, aber auch während der Kanzerogenese und Metastasierung von Brustgewebe, als wichtiger Prozess erachtet. In der vorliegenden Dissertation wurden benigne und maligne Mammaepithel – Zelllinien auf die Existenz von funktionellen mechanosensitiven Ionenkanälen (MSC's) untersucht, existierende MSC's wurden einem Genprodukt zugeordnet und eine mögliche Bedeutung bei vitalen Prozessen wurde eruiert

Die benigne MCF-10A und die maligne MCF-7 humanen Zelllinien wurden mittels der Patch Clamp Methode auf die Existenz von MSC's untersucht. In 157 von 291 patches von MCF-7 Zellen konnten funktionelle MSC's nachgewiesen werden ("cell attached" mode), die damit, unter den vorgegeben experimentellen Bedingungen, die am häufigsten vorkommende Ionenkanalspezies in dieser Zelllinie war (konstantes Membranpotenzial, die Pipettenlösung enthielt hauptsächlich Na^+, K^+ and Cl^-). In völligem Gegensatz dazu, konnten MSC's in der MCF-10A Zelllinie überhaupt nicht nachgewiesen werden. (N=30). MSCs in MCF-7 wurden in saturierbarer Weise durch Anlegen eines Unterdrucks an der Membranaussenseite aktiviert (EP_{50}: 41.2 ± 0.5 mbar (N=13)). Die Einzelkanalleitfähigkeit (G_Λ) betrug 25.6 ± 0.4 pS (N=8) für 153 mmole/L K^+. Die Permeabilität für monovalente Kationen stieg in der nachfolgend angegebenen Reihenfolge an: $Li^+ < Na^+ < K^+ \tilde{} Rb^+ \tilde{} Cs^+$. Divalente Kationen permeierten ebenso, wobei Ca^{2+} besser permeierte als Ba^{2+}. Wenn das kürzlich beschriebene humane Piezo1 (hP1) Ionenkanal Protein in HEK293 Zellen überexprimiert wurde, konnten Ionenkanäle, die bezüglich G_Λ für Li^+, K^+ und Ca^{2+} ident mit den MSC's in MCF-7 Zellen waren, gefunden werden. Daraus folgern wir, daß MSC's in MCF-7 Zellen durch das hP1 Protein gebildet werden. Wegen des Fehlens eines geeigneten Antikörpers, um hP1 in Western Blots nachweisen zu können, wurde quantitative RT-PCR (qPCR) durchgeführt um die hP1 mRNA expression level zu analysieren. hP1 mRNA konnte in MCF-10A nachgewiesen werden, aber zu signifikant niedrigeren Werten als in MCF-7. Wenn MCF-10A Zellen mit plasmiden welche für hP1 kodieren transformiert wurden, konnten schliesslich MSC's mit G_Λ ident zu MSC's in MCF7 Zellen beobachtet werden. Die Motilität von MCF-7 Zellen, mit und ohne GsMTx4, einem Taranteltoxin und spezifischem Blocker von MSC's, wurde über 72 h mit dem "Cell-Observer" untersucht. Sowohl die Motilität wie mittlere Geschwindigkeit von MCF-7 Zells wurden durch GsMTx4 reduziert.

Wir folgern daraus, daß das hP1 Protein in der Plama Membran von Brustkrebszellen als Mechanosensor fungiert und die zelluäre Motilität reguliert. Eine mögliche Bedeutung von hP1 in Tumorigenese and Metastasierung von humanen Mammaepithelzellen wird durch eine significant erhöhte “Hazard Ratio” (HR) für die Sterberate in Patientinnen, wenn hP1 mRNA im Tumor überexprimiert wird, angezeigt (HR=1.63 (95% Konfidenzintervall: 1.26 – 2.09); $p<0.00013$; N=1115; KM Plotter ("http://www.ncbi.nlm.nih.gov/pubmed/20020197" mit der 2014 Datenbank), wie beschrieben bei: Gyorffy et al., Breast Cancer Res Treatment, 123(3), 725-31, 2010).

ABSTRACT

Perception of and reaction to mechanical stress is regarded to play meaningful roles in the lactating healthy mammary gland but also during cancerogenesis and metastasation of breast cancer. We investigated whether non-cancerous and cancerous breast cells possess functional MSCs within their plasma membranes, identified the molecular nature of the MSCs detected and assessed possible vital roles.

The non-cancerous MCF-10A and the cancerous MCF-7 human cell lines were screened for MSCs with the patch clamp method, using cell-attached membrane patches. MSCs were detected in 157 out of 291 cell-attached membrane patches derived from MCF-7 (various kinds of pipette filling solution were used), being by far the most abundant ion channel species in this cell line under the conditions used (i.e. constant membrane potential; predominant ions within the patch pipette were Na^+, K^+ and Cl^-). In contrast, MSCs were completely absent in MCF-10A cells under the same conditions (N=30). MSCs in MCF-7 were activated by negative pressure at the outer side of the membrane in a saturable manner (EP_{50}: 41.2 ± 0.5 mbar (N=13)). Single channel conductance exerted to be 25.6 ± 0.4 pS (N=8) for 153 mmole/L K^+. Permeability for monovalent cations exerted to be: $Li^+ < Na^+ < K^+ \sim Rb^+ \sim Cs^+$. Divalent cations also permeated substantially with Ca^{2+} permeating better when compared to Ba^{2+}. When a recently discovered MSC protein, human Piezo1 (hP1), was heterologously overexpressed in HEK-293 cells, ion channels with single channel conductances for Li^+, K^+ and Ca^{2+} that were indistinguishable from those observed in MCF-7 cells, were detected. Hence we conclude that MSCs in MCF-7 cells are formed by the hP1 protein. Due to a lack of an available antibody for detection of hP1 by Western Blots, quantitative RT-PCR was performed in order to assess hP1 mRNA expression levels. Messenger RNA encoding hP1 was present in MCF-10A but at significantly lower amounts when compared to MCF-7. When MCF-10A cells are transfected with plasmids encoding hP1, MSCs with single channel conductance indistinguishable to MSC in MCF-7 cells are observed. Motility of MCF-7 cells with and without GsMTx4, a tarantula toxin and specific blocker of MSCs, was monitored for 72 hours using the cell observer. Both motility and velocity of MCF-7 cells were reduced by GsMTx4.

We conclude that hP1 protein acts as a mechanosensor in the plasma membrane of breast cancer cells controlling cellular motility. Possible roles in tumorigenesis and metastasation of breast cancer cells are indicated by the finding that the hazard ratio for

overall survival is substantially increased upon hP1 mRNA overexpression in breast tumors (HR=1.63 (95% confidence interval: 1.26 – 2.09); p<0.00013; N=1115; KM Plotter ("http://www.ncbi.nlm.nih.gov/pubmed/20020197" using the 2014 database), as described by Gyorffy et al., Breast Cancer Res Treatment, 123(3), 725-31, 2010).

INTRODUCTION

People communicate with each other to build up relationship, and then we can live in the society with others smoothly and friendly. While on the cellular level, each single cell, as elementary building block of our human body, needs to "communicate" with other cells to exert their corresponding biological roles.

All organisms are formed by cells: A very simple organism with relatively intact "body", Hydra, is built up by hundreds of cells, while there are over one hundred billion cells in one human body, which is a much more complicate organism than Hydra. Obviously, the single cell, as elementary building block of any living object, steadily encounters physical forces even when certain object is static. Respiratory system, digestive system and circulatory system are always active: Stomach and intestine are wriggling, lung is inflating and deflating, heart is pumping and blood is flowing. Therefore, cells experience different kind of physical forces, such as hydrostatic pressure, osmotic pressure (e.g.: egg cells become more hydrated as they move from the ovary to the uterus) [1], shear stress (vascular endothelial cells), compression (cardiac muscle cell during systolic period) and tension (alveolar cell during exhaling).

How the cells react to those forces? Is there going to be any changes within certain cells due to certain forces? Many studies have demonstrated the reactions of cells against different mechanical cues. Living cells dynamically adapt to and respond to mechanical cues from their living niche by altering their morphological characteristics, behavior or functions, and remodeling the microenvironment surrounding them [2]. The magnitude of forces that cells within tissues encounter varies from nanoscale to macroscale. Cells can respond to alterations of the force from cellular microenvironment in several ways: 1) Secondary messenger signaling alterations due to the activation of mechanosensitive Ca^{2+} permeant channels are indicated to be induced by sensing shear flow. The increase concentration of Ca^{2+} can also be achieved by mechanically stimulating osteoblast [3]; 2) Researchers have speculated that sensing the stiffness of cells' underlying substrate can lead to large-scale mechanosensing mechanism, resulting in stronger traction forces due to remodeling of cytoarchitecture, for instance, the recruitment of more focal adhesion proteins. Moreover, the cytoskeleton also remodels locally over short timescales (seconds to minutes, depending on the physiological state of the cell) in response to local mechanical stimulation. F-actin network, actomyosin etc. can deform, relax or contract, due to nano-Newton forces applied

locally [4, 5]; 3) Nucleus also responds to mechanical cues in the microenvironment. Cytoskeletal elements, such as actomyosin, microtubules (MT) cytoskeleton and chromatin, are essential for the cells' nucleus to keep normal shape and size. On the other hand, changes in nuclear morphology have been found to relate to normal stem cell differentiation and aberrant nuclear morphology and mechanics can be considered as marker for disease detection; 4) At last, gene expression can also be regulated in response to mechanical cues in the microenvironment, which are mostly long-term changes and leads to alterations of cell fate and behavior. Nuclear transcription factors YAP/TAZ has drawn much attention, and it is demonstrated that mechanical cues from the microenvironment, such as substrate stiffness, stress fibers and cytoskeleton tension, can regulate the gene expression of these factors, which also suggests that such mechanosensitive signaling transduction is an independent signaling pathway [4, 6].

When researchers focus on the role of mechanical stress on tissue level, it is increasingly apparent that mechanical cues collaborate with biochemical cues in modulating tissue development and post-natal function [7]. From the beginning of tissue development, forces play fundamental roles in directing how stem cells develop into certain tissue [8~10]. Mechanical properties of the tissue microenvironment influence morphology and even fate of embryonic stem cells. Stem cells develop following lineage selection in response to the stiffness of the matrix substrate [11, 7]. Moreover, it is important for normal tissue development that mechanical stress modulates tissue function and organization, exemplified by the development of lung epithelium and adolescent mammary gland branching [7]. Thereafter, homeostasis of developed tissue requires equilibrium of forces. For instance, we do exercise to train our body not only for shaped and beautiful muscles, but also for increasing our skeletal strength, by which bone matrix deposition is facilitated, proteoglycan content of articular cartilage is increased, and loss of bone mineral is reduced [7]. In addition, blood flow generates shear stress, which gets involved in artery development by directing vascular endothelial cells and the crosslinking of their filamentous cytoskeletal networks [7, 12]. In human mammary gland, the growth behavior is modulated by the stiffness of substrate matrix: mammary cells in a stiffer matrix are more proliferative, while compliant substrate holds mammary cells growth but demonstrates a differentiated behavior when related proteins are expressed and the mammary cells turn to glandular architecture [13]. Furthermore, the mechanical properties of matrices regulate the polarization of the

mammary epithelial cell, which is thought to drive breast epithelial differentiation and further greatly influence breast function like lactation [13~15].

The balance between forces and the consequent cellular responses is pivotal to maintain tissue homeostasis. On the other hand, a lot of findings concerned with distortion of this homeostasis, indicate the role of mechanical factors in pathological changes of tissues, including cancer. The alteration of mechanical microenvironment of artery wall is postulated to modulate progression of atherosclerosis [7, 16]. Besides, mechanical properties change caused by the aberrant proliferation of vascular smooth muscle cells and accompanied ECM stiffness increase involves in the development of vascular occlusive disease [17]. Cancer is demonstrated to be associated with large mechanical properties changes in many studies [7, 18~22]. Tumor palpation is of practical significance because tumors always grow like a bump with much higher collagen fiber density. Richer collagen in ECM can stimulate related signaling pathway and downstream product expression, leading to pro-tumorigenic alterations [13]. Therefore, people with higher mammary density are endangered to have higher risk of generating breast cancer. However, there is not enough evidence that ensure the fact ECM stiffness initially stimulates breast carcinoma. During tumor progression, the thick ECM gets thicker due to thickened collagen fibers and the crosslinking of collagen fibers. The stiffer ECM leads to mechanosensitive signaling pathway and recruit additional stromal cells, facilitating tumor cell invasion and metastasis [13, 23]. Moreover, uncontrolled proliferation of tumor cells contributes to the increase of mechanical stress within ECM, which in turn stimulates tumor progression.

To sense and respond to the changes of mechanical properties in the microenvironment of cells, certain functional components are essential for transferring extracellular mechanical cues inwardly into biochemical signals that are recognized by cells through different signaling pathway cascades. As mentioned above, mechanosensitive signaling pathways do not run solely, but interact or run in parallel with biochemical ones in different ways. For example, the functional site of sensing molecule, talin for instance, is enclosed within the molecule, which is exposed to its ligands when the molecule conformation is altered by external mechanical stress transferred from plasma membrane or cytoskeleton. Moreover, integrins cluster by sensing ECM stiffness, larger focal adhesions form and reactions initiate promoting downstream signaling pathway cascades. Mechanosensitive transmembrane ion channels are involved in this process as their

activation leads to intracellular Ca^{2+} increase, inducing related signaling pathways, which transfers mechanical cues into cellular or further tissue-level response [13, 23, 24]. Mechanosensitive ion channels, also termed as stretch-activated channels (SACs) were first identified by Sachs and his colleagues from chick skeletal myocytes in 1984 [25]. The transient receptor potential (Trp) family ion channel is represented by dozens of genes within the human genome and their members are generally stimulated by numerous environmental stimuli, such as temperature, pH, osmolarity, pheromones and taste compounds, through remarkably diverse mechanisms [26]. Such versatility makes them suitable candidates for different kinds of cellular sensors, and thus the mutation of Trp family genes can lead to many channelopathies, such as focal segmental glomerulosclerosis 2 (TRPC6), congenital stationary night blindness (TRPM1), and familial episodic pain syndrome (TRPA1) and many more [26]. Ion channels formed by particular Trp subunits have been identified to act as stretch-activated channels (SACs), or mechanosensitive ion channels (MSCs) [26, 27]. Widely expressed in the myocytes of the heart, the arteries, the skeletal muscle, and the cardiovascular system, the canonical TRPC1 and TRPC6 channels are found to play essential roles in mammalian muscle mechanotransduction [27~29]. Studies indicate that TRPC1 is not an indispensable component of the SAC complex in vascular smooth muscle cells, while mutation of TRPC6 lead to familial focal segmental glomerulosclerosis in human [12, 30, 31]. There are some other promising candidates for mechanotransduction in mammals, for instance, transmembrane channel-like (TMC) and Piezo family proteins, which represent two recently discovered mechanically gated ion channel families. TMC genes are demonstrated to be essential for the audition in human and mice, while mutation of Piezo proteins is found in several types of human diseases [32~35].

The involvement of ion channels is being demonstrated in all hallmarks of cancer cells: 1) Growth signals for tumor cell proliferation require Ca^{2+} signaling. Ion channels that permeate Ca^{2+} are involved in promoting mitogen secretion, while increased expression of Ca^{2+} and K^{+} channels is demonstrated to enhance sensitivity of cancer cells to mitogen. 2) The function of growth inhibitory factors, such as tumor necrosis factor-alpha (TNF- α) and transforming growth factor-beta (TGF- β), which normally lead cells to proliferation cease and apoptosis and thus is regarded as major tumor suppressors, is modified or even reversed. Tumor cells turn to be insensitive to those antigrowth factors mainly due to disordered Ca^{2+} homeostasis, resulting from disordered expression and functioning of Ca^{2+} permeable ion channels. 3) Disordered ion homeostasis also leads to controlled programmed cell death

(apoptosis) and further to cancer: Ca^{2+} overload abnormality results in prevention of apoptosis triggering, while restraining K^+ efflux by deregulating plasma membrane K^+ channels leads to final apoptosis evasion. 4) Disordered Ca^{2+} homeostasis in tumor cells give rise to upregulated telomerase activity, thus preventing replicative senescence induced by telomere shortening, and further lead to uncontrolled cell proliferation. 5) Various growth factors that have mitogenic or pro-angiogenic effects induce activation of vascular endothelial cells (ECs), which is essential to angiogenesis within tumor. In this case, Ca^{2+} influx through TRP family ion channels facilitates secretion of those factors. Potassium ion channels are also involved in modulating angiogenesis by either enhancing Ca^{2+} influx by facilitating membrane hyperpolarization, or directly by promoting growth factors production. 6) Increase of Na^+ influx alters intracellular ionic content and ion homeostasis dramatically due to overexpression of voltage-gated or non-voltage-gated sodium ion channels. Invasion and metastasis of tumor cells from primary site to other tissues requires enhanced K^+ and Cl^- influx to migrate through extracellular spaces that are quite narrow for normal cell, which is achieved by overexpression of Ca^{2+}-dependent and G-protein-regulated (GIRK) K^+ channels as well as the ClC-3 Cl^- channel [36, 37, 38]. Moreover, periodic changes of inward Ca^{2+} concentration, resulting from periodic Ca^{2+} signaling is implicated in the morphological and adherence changes observed during tumor cell metastasis [39].

As mentioned above, it is crucially important of mechanosensation and ion channels permeating cations for the development and tissue homeostasis of normal mammary gland, as well as for cancerogenesis and subsequent metastasation for breast cancer, thus we have studied MSCs within the plasma membrane of the malignant human MCF-7 breast cancer cellline. Permeation properties of ion channel proteins, i.e. single channel conductance and selectivity for certain kinds of ions, represent highly specific features that can be used to identify peculiar types of ion channels and even to distinguish between orthologs of subtypes from different species (see e.g.: http://www.guidetopharmacology.org/, Figure 1).

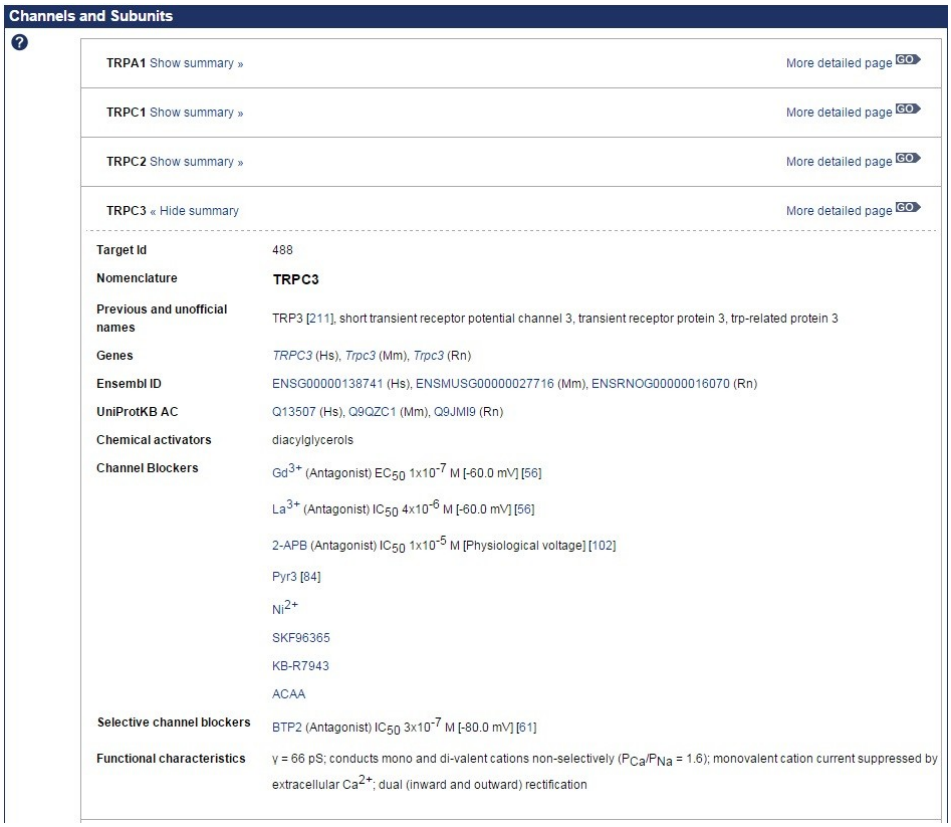

Channels and Subunits

TRPA1 Show summary »	More detailed page GO
TRPC1 Show summary »	More detailed page GO
TRPC2 Show summary »	More detailed page GO
TRPC3 « Hide summary	More detailed page GO
Target Id	488
Nomenclature	**TRPC3**
Previous and unofficial names	TRP3 [211], short transient receptor potential channel 3, transient receptor protein 3, trp-related protein 3
Genes	*TRPC3* (Hs), *Trpc3* (Mm), *Trpc3* (Rn)
Ensembl ID	ENSG00000138741 (Hs), ENSMUSG00000027716 (Mm), ENSRNOG00000016070 (Rn)
UniProtKB AC	Q13507 (Hs), Q9QZC1 (Mm), Q9JMI9 (Rn)
Chemical activators	diacylglycerols
Channel Blockers	Gd^{3+} (Antagonist) EC_{50} $1x10^{-7}$ M [-60.0 mV] [56]
	La^{3+} (Antagonist) IC_{50} $4x10^{-6}$ M [-60.0 mV] [56]
	2-APB (Antagonist) IC_{50} $1x10^{-5}$ M [Physiological voltage] [102]
	Pyr3 [84]
	Ni^{2+}
	SKF96365
	KB-R7943
	ACAA
Selective channel blockers	BTP2 (Antagonist) IC_{50} $3x10^{-7}$ M [-80.0 mV] [61]
Functional characteristics	γ = 66 pS; conducts mono and di-valent cations non-selectively (P_{Ca}/P_{Na} = 1.6); monovalent cation current suppressed by extracellular Ca^{2+}; dual (inward and outward) rectification

Figure 1: Example information for TRPC3 channel, containing mainly electrophysiological and pharmaceutical features.

In our study of screening GIRK channels in MCF-7 cells together with the preliminary study done by V. Wagner [unpublished results], MSCs have been found to be the most abundant ion channels in this wild type cellline. In order to identify the molecular architecture of MSCs in MCF-7 cells, we characterized MSC and compared its biophysical fingerprint to that of recently discovered MSC protein Piezo1. To exclude the contribution of SACs belonging to canonical Trp ion channel subunits we have engineered a control cell line, based on MCF-7 wild type (MCF-7^{WT}), that permanently overexpresses a dominant negative TrpC subunit (MCF-$7^{TrpC\_k.o}$) and studied whether the density of MSCs is affected by knockout of functional TrpC channels, considering widely spread of TRP family ion channels in mammalian cells. We have also prepared a positive control cell line, that scramble sequence is knocked out (MCF-7^{scr}). The benign human MCF-10A mammary epithelial cell (MEC) line was studied in order to investigate whether the existence of MSCs is a peculiar feature of malign MECs or it is a common channel of mammary cells. As mentioned above, Ca^{2+} permeation gets involved in nearly all processes of cancerogenesis and further metastasis, and Ca^{2+} transient influx induced by Ca^{2+} permeable MSCs has been

shown to play an important role in cell motility and migration [40], we investigated whether block by the tarantula toxin GsMTx-4 influenced motility of the two MEC lines studied. Finally we have analyzed whether expression levels for the mRNA encoding the MSC of MCF-7 cells in primary tumors has an influence on prognosis for patients suffering from breast cancer.

MATERIALS AND METHODS

1 Materials

1.1 Solutions

Firstly, stock solutions were prepared in advance. The solid chemicals were from ROTH ($MgCl_2$, Cat.#: 2189.1; NaCl, Cat.#: 3957.1; HEPES Cat.#: 9105.3), MERCK ($CaCl_2$, Cat.#: 1.02382.0250; Aspartic Acid, Cat.#: 1.00129.1000; KCl, Cat.#: 1.02382.0250; KOH Cat.#: 1.04936.1000; NaOH Cat.#: 1.05033.1000; $BaCl_2$ Cat.#: 2489126; CsCl Cat.#: 2038.0100), CALBIOCHEM (LiCl, Cat.#: 438002) and SIGMA (EGTA, Cat.#: E4378100G; RbCl Cat.#: 83979-25G; $GdCl_3$, Cat.#: G7532-5G).

KOH, NaOH, KCl and NaCl were dissolved in deionized water at a concentration of 3 mole/L, $MgCl_2$, $CaCl_2$,$BaCl_2$, LiCl, RbCl, CsCl, $GdCl_3$ and K^+/Asp (The molar ratio of KOH and Aspartic Acid is 1:1, pH was adjusted to 7.4 using KOH) 1 mole/L, $HEPES^-/K^+$ (pH was adjusted to 7.4 using KOH) and $HEPES^-/Na^+$ (pH was adjusted to 7.4 using NaOH) 0.5 mol/L and $EGTA^-/K^+$ (pH was adjusted to 7.4 using KOH) 0.1 mole/L, respectively. KOH, NaOH, KCl, NaCl, $CaCl_2$, and $MgCl_2$ were prepared freshly every month and stored in 50 mL falcon tubes and stored at 4ºC. The final volume of those solutions was 50 mL, which was more than enough for one month's usage. K^+/Asp, $HEPES^-/K^+$, $HEPES^-/Na^+$ and $EGTA^-/K^+$ were prepared in larger stock (200 mL or 500 mL), aliquoted into 15 mL or 50 mL falcon tubes and stored in -20 °C freezer. Those smaller stocks of solutions were preserved in +4 °C fridge together with all the alkaline and chlorine salt solutions and were ready for preparing solutions used in electrophysiological experiments.

Using the solution stocks, the zeroing bathing solution (ZBS) and pipette filling solution (PFS) could be prepared earlier in the day before electrophysiological experiments were performed. If both of the solutions were kept sealed within the containers or syringes and preserved in +4 °C fridge after the experiments, they could be available for two to three days. Nonetheless, fresh solution could help achieving the optimum experimental conditions during the sealing process. Therefore, preparing fresh solutions was necessary when other factors were not good enough, such as the cells were not healthy enough or the glass pipettes were not well fabricated.

1.1.1 Zeroing Bath Solution (ZBS)

ZBS was prepared following the recipe (final con. in mmole/L): K^+/Asp (120), KCl (20), $MgCl_2$ (4), NaCl (10), $EGTA^-/K^+$ (10), $HEPES^-$ (10). 100 mL ZBS was enough for two day's experiments. Therefore, 12 mL K^+/Asp, 0.667 mL KCl, 0.4 mL $MgCl_2$, 0.333 mL NaCl, 1 mL $EGTA^-/K^+$ and 2 mL $HEPES^-$ were pipetted into an 100 mL volumetric flask respectively from their own stock, deionized water was filled in the flask till 100 mL. Then, the flask was sealed using parafilm and the solution was mixed by inverting the flask. After mixing, the solution's pH was examined using pH test strips and the 3 mole/L KOH stock solution was added to buffer the solution pH to 7.4. If outside-out mode was performed during the experiment, then more ZBS was needed.

1.1.2 Pipette Filling Solution (PFS)

Less PFS was needed for the whole week than ZBS, as PFS was only injected to fill glass pipettes, not used for perfusion. This time, only 25 mL volumetric flask was occupied and here was the recipe (final con. in mmole/L): *PFS/K^+:* KCl (153), $MgCl_2$ (4), $CaCl_2$ (1), $GdCl_3$ (0.02), $HEPES^-$ (10). *PFS/Li^+ (PFS/Na^+; PFS/Rb^+; PFS/Cs^+; PFS/(K^+:Na^+)):* similar as PFS, but K^+ was replaced by the appropriate cation or mixture of K^+ and Na^+ at 3:1, 1:1 or 1:3 ratio. *PFS/Ca^{2+} (PFS/Ba^{2+}):* $CaCl_2$ (or $BaCl_2$; 100), $MgCl_2$ (4), $CaCl_2$ (1), $GdCl_3$ (0.02), $HEPES^-$ (10). All kinds of PFSs were buffered with the 3 mole/L KOH stock solution to pH 7.4.

The content of PFS was altered when ion selectivity and permeability of certain channel was studied. Therefore, more than one kind of PFS could be prepared for one single experimental day. Potential agonists or antagonists of target channel could also be added to PFS to study the characteristics of the channel or to identify it. Lyophilized GsMTx-4 was obtained from Alomone Labs (Cat.#: STG-100, Jerusalem, Israel) and reconstituted at a concentration of 90 mole/L. Aliquots were shock frozen in liquid N_2 and stored at -30 °C until use. During the day when outside-out mode was performed, the GsMTx-4 aliquots were thawed up and pipetted into the bath with independent pipette to study the effect of this tarantula toxin on MSC channels. To facilitate screening GIRK channels, Angiotensin II (Sigma, Cat. #: A9525) were added into PFS trying to stimulate membrane GIRK channel. All reagents used were of reagent grade unless stated otherwise.

1.1.3 Polylysine solution

The stock solution was prepared by dissolving 100 mg polylysine in 100 mL water (either poly-L-lysine or poly-D-lysine can be used) and filter sterilize through a 0.22-micron filter.

The prepared solution was pipetted into 15-mL falcon tubes, sealed with parafilm, and stored at -20 °C. Every time for coating glass plate, the solution was thawed up and mixed thoroughly, and after coating the falcon tube should be sealed with parafilm again and stored at -20 °C for further usage.

1.2 Medium

Additives: Fetal Bovine Serum (FBS Gold: PAA, Cat. #: A15-151-500mL; FBS HL1: SAFC Biosciences, Cat. #: 12103-500M), Penicillin-Streptomycin (Pen/Strep, Sigma, Cat. #: P0781), L-glutamine (Sigma, Cat. #: G7513), HEPES buffer (PAA, Cat. #: S11-001), Sodium pyruvate (Sigma, Cat. #: S11-003), MEBM SingleQuot (Lonza, Cat. #: CC-4136)

Basal medium (500 mL bottle): MEM (Life Technology, REF #: 31095-029), DMEM (Low Glucose) (Sigma, Cat. #: D6046), DMEM (High Glucose) (Life Technology, REF #: 11960-044), MEBM (Lonza, Cat. #: CC-3151).

1.2.1 Normal medium recipe

MCF-7 medium: 50 mL MEM medium was pipetted out from the bottle into a fresh falcon tube, then 50 mL FBS, 5 mL Sodium Pyruvate, 5.81 mL Pen/Strep were given into the bottle. After mixing all the ingredients by shaking gently, the medium were filtered through a filtering system (Millipore, Cat. #: SCGPT01RE) which was screw onto an autoclaved 500 mL glass bottle. The bottle was screwed up with an autoclaved lid;

HEK-293 medium: Stocks of FBS, Pen/Strep, and L-glutamine were thawed up in water bath before preparation medium. 50 mL DMEM medium (High Glucose) was pipetted out of the original bottle into a sterile falcon tube. Then, 50 mL FBS, 5 mL Pen/Strep, 5.5 mL L-glutamine and 5.5 mL HEPES buffer (stored in 4 °C fridge) were given into the bottle. Then filtering process was the same as filtering MCF-7 medium;

MCF-10A medium: 5.81 mL Pen/Strep and ingredients within SingleQuot tubes except the EGF tube were poured into MEBM bottle before filtration, and ingredient in the EGF tube was pipetted into the bottle after filtration;

MDA-231 medium: 50 mL FBS was pipetted into 450 mL DMEM (Low Glucose) basal medium. Then 5.81 mL Pen/Strep was added and the whole mixture was filtered.

All media were preserved in +4 °C fridge.

1.2.2 Stable medium

Based on the kill curve for each stable cellline, the antibiotics were added to normal medium. Stable transfected celllines were cultured in this stable medium to "stablilize" the alteration induced by permanently overexpression.

Two kinds of antibiotics were used in my experiments according to the vectors applied for stable transfection, Geneticin (G418; an aminoglycoside antibiotic that blocks translation; LifeTech Company; Order No.: 11811-031; 3 mg/mL) and Zeocin (Invivogen, Cat. #: ant-zn-5p). Both antibiotics were in powder form, and were dissolved in water (Roth, Cat. #: T143) with the concentration of 1 g/mL (G418) and 100 mg/mL (Zeocin). The G418 stock could be kept in +4 °C fridge and the zeocin one should be preserved in eppendorf tube wrapped up with aluminum paper in -20 °C freezer.

MCF-7 stable medium (G418): 30 µL G418 diluent was given to every 10 mL normal MCF-7 medium.

MDA-231 stable medium (G418): 140 µL G418 diluent was given to every 10 mL normal MDA-231 medium.

MCF-7 stable medium (Zeocin): 3 mL Zeocin diluent was given to every 50 mL normal MCF-7 medium.

1.3 Plastic culturing flask and plates

Cell culturing flask (Roth, Cat #: CE 48.1);

6-well culturing plate (Roth, Cat #: CE 54.1), 12-well culturing plate (Roth, Cat #: CE 55.1); 24-well culturing plate (Roth, Cat #: CE 56.1).

1.4 Buffers

Hank's Balanced Salt Solution (HBSS, Gibco, Cat #: 14175-095) and Phosphate-Buffered Saline (PBS, Gibco, Cat #: 10010-015)

1.5 Transfection reagents

Two transfection reagents were frequently used for transiently transfecting target constructs. TransFast (Promega, Cat. #: E2431) was utilized for the transfection of HEK-293^{WT} and MCF-7^{WT} celllines, and Lipofectamine (Life Technology, Cat. #:11668-019) for MCF-10A^{WT} only.

The transfection protocol is shown in Methods part.

1.6 Kits

Midi prep (Promega, Cat. #: A1460); Ligation (Qiagen, Cat. #:231124); Wizard Genomic DNA Purification (Promega, Cat. #: A1125); RT-PCR (Qiagen, Cat. #: 204054); Reverse Transcription (Qiagen, Cat. #: 205311)

1.7 Glass plates

All glass plates were bought from Thermo Scientific (12mm: Art. # CB00120RA1, 6mm: Lot. # 2330983).

The 6mm plates were not fabricated industrially and therefore should be ordered quite in advance, two to three months for instance.

Both kinds of glass plates can be autoclaved and dried in 60 °C drier (in plastic box), or incubated in 180 °C oven for four hours (in glass culture dish and wrapped with aluminum paper). The container of sterilized glass plates should be closed after seeding cells.

Both kinds of glass plates could be used for seeding any cellline. One can screen more cells using bigger glass plate, which would take more time. Therefore, if one cellline could keep healthy in the bath for longer time, like MCF-10A cells, then bigger glass plates can be used for seeding the cells. If not, smaller but more plates in each well can be used.

1.8 Other materials for patch clamp

1.8.1 Metal electrode

Ag wire from ÖGUSSA.

1.8.2 Glass pipettes

Hydrophobic chemical interaction between plasma membrane and inner wall of glass pipette leads to giga-ohm seal resistance, which is the eligible status for cell-attached recording.

Properties of the glass tube may impact the sealing process: The diameter of glass tube may affect recording noise caused by the tube; the minor components in glass tube are noteworthy, as they may dissolve into pipette filling solution and affect channel activity.

The tubes we used are from Assistant, Micro-Haematocrit-tubes, Lot # 1201473 (outer diameter: 1.6 mm, inner diameter: 1.0 mm).

1.8.3 Containers for culturing

Petri dishes (nunc, Cat. #: 153066)

1.8.4 Solution filtering system

Syringe (B|Braun, Ref. #: 4606205V); Needle (B|Braun, Ref. #: 4665600); Filter (GE Healthcare, Ref. #: 10462200);

1.8.5 Silica coating materials

The silicone base and catalyst were from DOW CORNING, Sylgard® 184 Silicone Elastomer. The ratio of silicone base to catalyst was 10: 1.

2 Methods

2.1 Genetic engineering

GIRKs construct: mRNA was isolated, cDNA was synthesized, cDNAs encoding different know splice variants following protocols done by Wagner et al (2010). Maps of splice variants were demonstrated in Figure 2 [38]. The names of vector used are: MCF-7 peYFPC1-hG1a, hG1c, hG1d and hG1e, respectively, among which hG1e construct was permanently transfected into MCF-7 cell but not included in my thesis project.

Piezo1 construct: RNA was isolated from MCF-7, HEK-293 and MCF-10A cells (wild type ones and transfected ones), respectively, and cDNA synthesis was performed (PolyATtract System 1000; ImProm-II Reverse Transcription System; both from Promega, Madison, WI) [41]. Six ng cDNA were subjected to PCR for gene quantification (QuantiFast SYBER Green PCR kit, Qiagen GmbH) using Light Cycler 480 system (40 Cycles; Roche Diagnostics). The following primer pairs were used: Piezo1: f*orward: 5'-CATCTTGGTGGTCTCCTCTGTCT-3'; reverse: 5'-CTGGCATCCACATCCCTCTCATC-3'*. GAPDH: *forward: 5'-ATGGGGAAGGTGAAGGTCG-3'; reverse: 5'-GGGGTCATTCATGGCAACAATA-3'*. Relative mRNA expression levels of Piezo1 gene compared to the housekeeping gene (GAPDH) were calculated using $2^{-\Delta\Delta C_\tau}$ method [42].

a

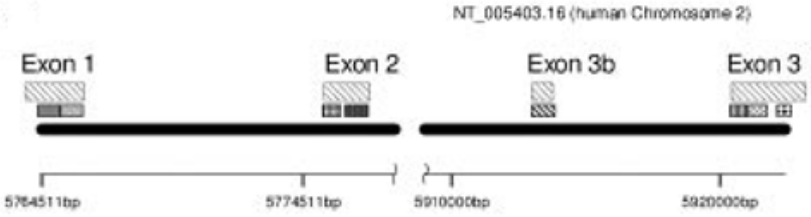

b

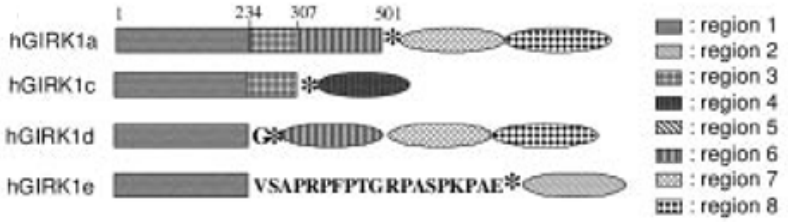

c

```
          1                                                  50
hGIRK1a MSALRRKFGD DYQVVTTSSS GSGLQPQGPG QDPQQQLVPK KKRQRFVDKN
hGIRK1c MSALRRKFGD DYQVVTTSSS GSGLQPQGPG QDPQQQLVPK KKRQRFVDKN
hGIRK1d MSALRRKFGD DYQVVTTSSS GSGLQPQGPG QDPQQQLVPK KKRQRFVDKN
hGIRK1e MSALRRKFGD DYQVVTTSSS GSGLQPQGPG QDPQQQLVPK KKRQRFVDKN

                                                    TM1
          51                                         100
hGIRK1a GRCNVQHGNL GSETSRYLSD LFTTLVDLKW RWNLFIFILT YTVAWLFMAS
hGIRK1c GRCNVQHGNL GSETSRYLSD LFTTLVDLKW RWNLFIFILT YTVAWLFMAS
hGIRK1d GRCNVQHGNL GSETSRYLSD LFTTLVDLKW RWNLFIFILT YTVAWLFMAS
hGIRK1e GRCNVQHGNL GSETSRYLSD LFTTLVDLKW RWNLFIFILT YTVAWLFMAS

                                                    P
          101                                        150
hGIRK1a MWWVIAYTRG DLNKAHVGNY TPCVANVYNF PSAFLFFIET EATIGYGYRY
hGIRK1c MWWVIAYTRG DLNKAHVGNY TPCVANVYNF PSAFLFFIET EATIGYGYRY
hGIRK1d MWWVIAYTRG DLNKAHVGNY TPCVANVYNF PSAFLFFIET EATIGYGYRY
hGIRK1e MWWVIAYTRG DLNKAHVGNY TPCVANVYNF PSAFLFFIET EATIGYGYRY

                    TM2
          151                                        200
hGIRK1a ITDKCPEGII LFLFQSILGS IVDAFLIGCM FIKMSQPKKR AETLMFSEHA
hGIRK1c ITDKCPEGII LFLFQSILGS IVDAFLIGCM FIKMSQPKKR AETLMFSEHA
hGIRK1d ITDKCPEGII LFLFQSILGS IVDAFLIGCM FIKMSQPKKR AETLMFSEHA
hGIRK1e ITDKCPEGII LFLFQSILGS IVDAFLIGCM FIKMSQPKKR AETLMFSEHA

          201                                 234
hGIRK1a VISMRDGKLT LMFRVGNLRN SHMVSAQIRC KLLK...... ..........
hGIRK1c VISMRDGKLT LMFRVGNLRN SHMVSAQIRC KLLK...... ..........
hGIRK1d VISMRDGKLT LMFRVGNLRN SHMVSAQIRC KLLKG----- ----------
hGIRK1e VISMRDGKLT LMFRVGNLRN SHMVSAQIRC KLLK.VSAPR PFPTGRPASP

             235                                         280
hGIRK1a ....SRQTPE GEFLPLDQLE LDVGFSTGAD QLFLVSPLTI CHVIDAKSPF
hGIRK1c ....SRQTPE GEFLPLDQLE LDVGFSTGAD QLFLVSPLTI CHVIDAKSPF
hGIRK1e KPAE------ ---------- ---------- ---------- ----------

          281                                         330
hGIRK1a YDLSQRSMQT EQFEIVVILE GIVETTGMIC QARTSYTEDE VLWGHRFFPV
hGIRK1c YDLSQRSMQT EQFEIVVILE GI-------- ---------- ----------

          331                                         380
hGIRK1a ISLEEGFFKV DYSQFHATFE VPTPPYSVKE QEEMLLMSSP LIAPAITNSK

          381                                         430
hGIRK1a ERHNSVECLD GLDDITTKLP SKLQKITGRE DFPKKLLRMS STTSEKAYSL

          431                                         480
hGIRK1a GDLPMKLQRI SSVPGNSEEK LVSKTTKMLS DPMSQSVADL PPKLQKMAGG

          481                 501
hGIRK1a AARMEGNLPA KLRKMNSDRF T
```

Figure 2.: Nucleotide and protein sequence of the different GIRK1 variants and chromosomal localization of exons [41].

2a (Up): Localization of the different exons of the KCNJ3 gene, the coding gene of GRIK1 protein, on chromosome 2. 2b (Up): Splice variants of hGIRK1 protein identified in the MCF-7 cell line. The origin of the RNA from the different exons of the chromosome are shown (regions 1, 3 and 6 correspond to exons 1, 2 and 3, respectively). Rectangles denote open reading frames, ellipsoids untranslated regions. Single amino acids preceding the stop codon (marked by asterisks) are also shown. 2c (Below): Alignment of the deduced amino acid sequence of the splice variants. TM1, TM2 and P denote the two transmembrane regions and the pore region, respectively.

E_coli strain with hPiezo1 plasmid (hPiezo1-pIRES-EGFP) was cultured in 5 mL LB medium with 2.5 μL Kanamycin (Final Conc.: 25 μg/mL) in 15 mL falcon tube. After 3 to 4 hours culturing, bacteria suspension was transferred into big culturing flask with 30 - 50 mL medium in it. Culturing overnight, plasmid could be extracted following protocol from Promega (midi or maxi prep kit). After the elution step, the concentration of DNA was evaluated using Nanodrop 2000. According to the concentration, the DNA solution was diluted to 1μg/μL in 1.5 mL Eppendorf tube and preserved in -20 °C freezer.

HEK-293 cells were transfected with the biscistronic pIRES2 plasmid containing human Piezo1 construct and a variant of the green fluorescence protein (eGFP) using the Transfast™ reagent (Promega) and MCF-10A cells with Lipofectamine™ 2000 (Invitrogen) according to the manufacturers' protocols. Transfected HEK-293 cells were used within 24 to 48h and MCF-10A within 24h after transfection, as the total number transfected HEK-293 cells were high enough and only a limited number of MCF-10A were successfully transfected, therefore there were enough transfected HEK-293 cells but not enough MCF-10A cells left for recording at the second day.

2.2 Celllines fabrication

2.2.1 Transient transfected cellline preparation

Optimization for the best transfection reagent content ratio:

Every time new transfection reagent was applied for transient transfection, an optimization trial was done before to get the suitable ratio of reagent solution and DNA for the best transfection result. The optimization was performed following the protocol for each reagent.

In the optimization for TransFast reagent, for instance, a serial test was performed to test the transfection results using different amount of DNA, which was 0.25 μg, 0.5 μg, 0.75 μg and 1 μg. The reagent:DNA ratios were set to 2:1 and 1:1. The incubation time as the third variable varied from 1 h, 2 h to 4 h. This serial tests were performed both in 6-well plate, with final volume of 1400 μL, or in 24-well plate, with final volume of 200 μL. The exact protocols were shown in Figure 3, Table 1, and Table 2 [Protocol from Promega], taking transfection in 24-well plate as an example.

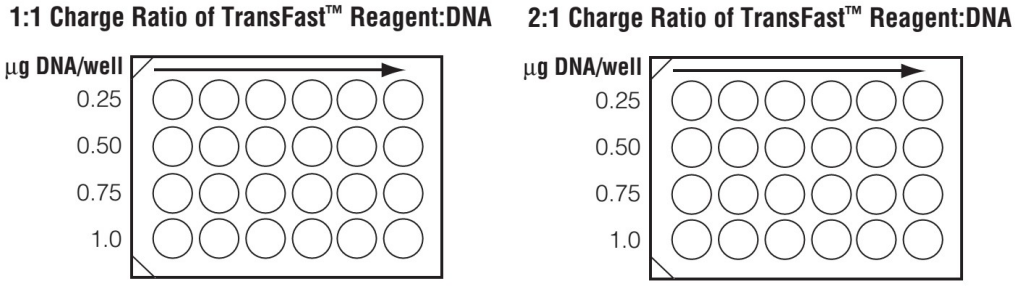

Figure 3: Arrangement of 24-well plate for transfection optimization

Cells were seeded in six duplicate wells for each DNA quantity, and the amount of reagent was calculated for each row of wells according to the reagent:DNA ratio for either plate. Six duplicates were prepared for assessing the effect of incubation time on transfection efficiency. The incubation time for the first two columns was 1 hour, the second two was 2 hours and the last two 4 hours. The exact amount of reagent and DNA added to each well was demonstrated in Table 1&2.

Table 1. Total volume of medium, DNA and TransFast™ reagent for multiwell plates.

Plate Size	*Total Transfection Volume (per well)*	*Amount of DNA (per well)*
6-well plate	*1.4mL*	*1.8–7μg*
24-well plate	*200μL*	*0.25–1μg*

Table 2a. Optimization protocol for transfection in 24-well plate using a 1:1 Ratio of TransFast™ reagent to DNA.

Amount of DNA per Well	*0.25μg*	*0.5μg*	*0.75μg*	*1μg*
*Volume of master mix**	*1,400μL*	*1,400μL*	*1,400μL*	*1,400μL*
DNA	*1.8μg*	*3.5μg*	*5.3μg*	*7.0μg*
*TransFast™ reagent***	*5.4μL*	*10.5μL*	*15.9μL*	*21μL*

**: The volumes given were calculated for 7 wells, which was for 6 replicates for each well.*
***: Volumes calculated were for use with TransFast™ reagent suspended in 400μl/vial.*

Table 2b. Optimization protocol for transfection in 24-well plate using a 2:1 Ratio of TransFast™ reagent to DNA.

Amount of DNA per Well	*0.25μg*	*0.5μg*	*0.75μg*	*1μg*
*Volume of master mix**	*1,400μL*	*1,400μL*	*1,400μL*	*1,400μL*
DNA	*1.8μg*	*3.5μg*	*5.3μg*	*7.0μg*
*TransFast™ reagent***	*10.8μL*	*21μL*	*31.8μL*	*42μL*

**: The volumes given were calculated for 7 wells, which was for 6 replicates for each well.*
***: Volumes calculated were for use with TransFast™ reagent suspended in 400μLvial.*

Kill curve preparation:

Transfected celllines were cultured using stable medium during experimental period. The concentration of antibiotics within stable medium was determined by drawing a kill curve for certain antibiotics against certain cellline.

Kill curve plotting for G418 was taken for example. Cells were grown in 6-well plates till 80% confluence, when different concentration of G418 was given to each slot: Slot 1, native cells; Slot 2, 0.5mg/mL G418; Slot 3, 1.0 mg/mL G418; Slot 4, 1.5 mg/mL G418; Slot 5, 2.0 mg/mL G418; Slot 6, 2.5 mg/mL G418; Slot 7, 3.0 mg/mL G418, and so on, if necessary. More concentrated G418 might be required for certain cells, thus more slots were needed for plotting kill curve, when a new 6-well plates of cells was necessary. The proper

G418 concentration for certain stable celllines was the lowest concentration where all the cells in the slot are dead after 5 days (Figure 4).

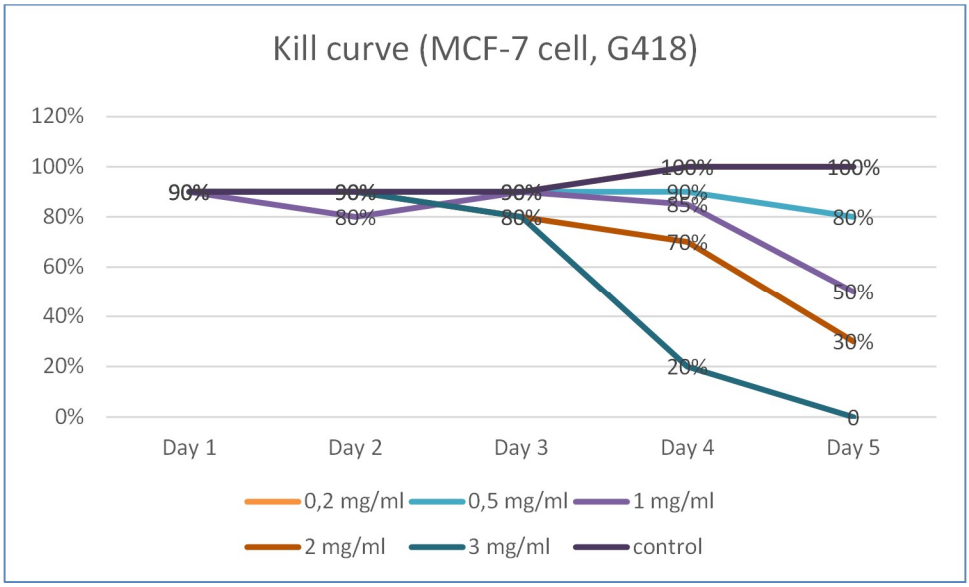

Figure 4: Kill curve example.

The confluency increased or decreased due to cell proliferation or being killed by different concentration of antibiotics, respectively, which was indicated by lines with different colors. The corresponding percentages of confluency was written on the lines, indicating the time points when cells were examined. The line that demonstrated the confluency change of cells cultured with 0.2 mg/mL G418 was overlapping with the control line, indicating that the concentration was too little for killing MCF-7 cells.

HEK-293 transfection:

Two to three days before transfection, HEK-293WT cells should be seeded and cultured in six-well plate. Before seeding HEK-293^{WT} cells, the glass plates should be first coated with polylysine solution, since HEK-293^{WT} cells were easy to get detached from glass plates. The final confluency should be around 80%. Too much confluency would make the cells hard to be taken record, while if there were too little cells within one cell colony before transfection could not survive during the transfection procedure.

Based on the results of optimization, the amount of transfection reagent (Transfast, Promega) and DNA was 9 µL and 4 µL, respectively. Reagent and DNA were pipetted into

a sterilized eppendorf tube filled with 700 μL base medium (In this case, DMEM high glucose medium, no FBS or Pen/Strp), and the mixture was vortexed for 5 to 10 seconds to mix thoroughly and placed in room temperature for 10 to 15 minutes.

MCF-10A transfection:

MCF-10A WT cells grow much slower than HEK-293 WT cells. Therefore, cells for Wednesday and Thursday's recording were prepared on the previous Friday. No extra solution was needed to treat the glass plates for MCF-10A WT cells.

hP1 construct was much bigger than other constructs (vector, hG1a, etc.). Several transfection reagents were used (Promega: TransFast, FuGene, ViaFect; Life Technologies: Lipofectamine.) to transfect hP1 construct into MCF-10A WT cells and only Lipofectamine could gave a satisfactory transfection result.

Before preparing transfection mixture, old medium was changed and 750 μL new base medium (In this case, MEBM medium, no FBS or Pen/Strp) was given to the cells. Based on the optimization results, the amount of transfection reagent (Lipofectamine) and DNA was 9 μL and 4 μL, respectively. The reagent and DNA were pipetted into two different sterilized eppendorf tubes filled with 240 μL and 246 μL opti medium (GIBCO, Lot # 386619), respectively, and the mixture was vortexed to mix thoroughly and was placed in room temperature for 5 minutes. Then, the mixtures in two tubes were mixed , vortexed thoroughly and placed at room temperature for 20 minutes. Finally, 250 μL of the mixture was given to one well of cells and the rest 250 μL the other (Therefore, if one need more transfected cells, more mixture should be prepared.).

2.2.2 Stable transfected cellline fabrication

Many stable transfected celllines were used in this project. In the GIRK study, MCF-$7^{hG1a\#6}$, MCF-$7^{hG1c\#9}$, MCF-$7^{hG1c\#4}$, MCF-$7^{G\beta\gamma}$, and MCF-$7^{hG1d\#7}$ were studied, and in the Piezo project, MCF-$7^{TrpC\_k.o.}$, MCF-$7^{scr\_k.o.}$, and MCF-$7^{hP1\_k.o.}$ were assessed.

Stable transfection starts from normal transient transfection. Taking the fabrication of MCF-$7^{hG1d\#7}$ cellline as an example, MCF-7 cells were grew in one slot of 6 well plate till 70%~80% confluency for transient transfection. Transfection was performed on Thursday, and the first fluorescence control was performed on Friday under Leica Confocal Microscope

(LSM) by checking the fluorescence of chimeric subunit that was fused to a blue fluorescence protein (CFP) or a yellow variant of the green fluorescence protein (eYFP). Transfected cells were cultivated with normal MCF-7 medium over weekend. The cells were examined under light microscope during weekend, and their medium should be changed after being examined if they were not in good condition. The cells were given with stable medium (G418) on Monday, starting stabling the transfected construct. Stable medium should be changed every day for maintaining extraneous construct and keeping the culturing environment fresh to get rid of cell debris, resulting from transfection, until no more cell death was observed, when most of untransfected cells were killed by antibiotics (G418, in this case). As the cultivation went on, cells fluorescence was control once per week. Cells were removed by trypsin when the flask reached to 50% confluent, and centrifuged at 500 rpm for 5 minutes. Then, the cell pellet was resuspended with 1 mL normal medium, preserved in 15 mL falcon tube, and went for cell sorting. A new 48 well plate was also prepared for cell sorting to sorts only cells with fluorescence.

In our study, 50 cells were seeded into one single well of 48-well plate to get faster growing speed (One single cell could also be seeded for each well, with much slower growing speed.) The growing status as well as the fluorescence of the cells in 48-well plate was monitored every day. If certain well was full, cells in that well were trypsinized and transferred to bigger wells, from wells in 24-well plate, 12-well plate, 6-well plate, and at last to culturing flask. The whole growing process might last for months, depending on growing speed and would be much faster when growing in flasks. Until then, cells were split into several flasks, of which could be freezed and preserved in liquid nitrogen (mentioned below) or cultured in incubator for following experiment.

The MCF-7$^{TrpC_k.o.}$ cell line, stably expressing a dominant negative TrpC construct [43], was generated by adding G418 72h after Transfast^{TM} transfection. Successful expression was monitored by fluorescence of the chimeric k.o subunit that was fused to a yellow variant of the green fluorescence protein (eYFP). The cells were kept in culture for 14 days, prior to selecting stable clones were selected. G418 was removed 48h before experimentation was started.

2.3 Cell culturing

2.3.1 Incubation and splitting cells

The splitting methods for different celllines were slightly different due to different tightness that cells attach to culturing flask. The first step of splitting for all celllines was removing old medium together with death cell debris by vacuum pipetting and washing with buffering (FBSS or PBS) solution. After buffering solution was gently pipette in to wash MCF-7 and MCF-10A celllines (WT and transfected), the culturing flask was slightly shaken for more efficiently washing, while the HEK-293 flask was only left standing for several minutes as HEK-293 cells were easy to be detached. The buffering solution was also sucked out and the cells were ready for detaching.

No trypsin was required during the detaching of HEK-293 celllines (WT and transfected) and the cells could be detached only by pipetting medium for several times. The cell suspension was transferred to a sterilized 15 mL falcon tube and centrifuged with the speed of 500 rpm for 5 minutes. The supernatant was removed carefully by vacuum pipetting device and 5 mL new medium was pipetted into the tube to resuspended the cell pellet. At last, this cell suspension was diluted with fresh medium to reach to a certain ratio.

HEK-293 WT cells grow with the fastest speed among all celllines, and splitting should be performed every five days with the splitting ratio of 1:10. MCF-7 WT cells grow slower than HEK-293 WT cells with splitting period of one week to ten days and the splitting ratio of 3:10. MCF-10A WT cells grow with the slowest with splitting period of no less than ten days and splitting ratio of 2:5 to 1:2. The volume of final diluted cell suspension for routine culturing was 5 mL, and the volume of 15 mL suspension was chosen for large scale culturing in bigger culturing flask.

Trypsin was necessary for splitting MCF-7 and MCF-10A celllines (WT and transfected). After removing old medium and washing the cells, one milliliter 0.25% Trypsin-EDTA (Sigma, Cat #: T4049) was pipetted to the cells, after which the cells was incubated in 37 °C for 10 minutes or 15 minutes for MCF-7 or MCF-10A, respectively. After incubation, MCF-7 cells had been already detached and several strong knocks were required for MCF-10A cells to finally detach them. When most of the cells were detached, which was ensured under light microscope, four milliliter corresponding normal medium

was pipetted in the flask to neutralize trypsin, and all the cell suspension was transferred to a fresh falcon tube. The following steps were the same as splitting HEK-293 cells.

2.3.2 Cell freezing and thawing

Freezing

Cell freezing starts from trypsinization. Similar to splitting, after 10 minutes trypsinization and 5 minutes centrifuge, cell pellet were resuspended in 1 mL freezing medium (5 mL freezing medium was prepared using 4.5 mL normal medium and 0.5 mL DMSO (Dimethyl sulfoxide, Sigma, Cat #: D2438), and transferred into marked freezing tube. The tube with cells was placed into the slot of freezing container with isopropanol in the inside layer, which should immerse the tube slots partially, to achieve 1 °C/min rate of cooling when they were put into -70 °C fridge for overnight. In the following morning, the cells were transferred from the container to liquid nitrogen.

Thawing

Frozen cells were took out from liquid nitrogen and thaw up at room temperature or were held by hand. Then the cells were given to 5 mL HBSS buffer in a sterile 15 mL falcon tube and centrifuged at 500 rpm for 5 minutes. The cell pellet was resuspended using normal medium, transferred in culturing flask, and cultured in 37 °C incubator.

To get a suitable confluency for electrophysiological assessment, cell counter was used at the beginning to calculate the approximate volume needed from the re-suspended cells. Then the average volume could be estimated under the similar condition (cellline, confluency, volume of re-suspension medium), which could be used for preparing cells for patch clamp without cell counter.

2.4 Electrophysiology: Single channel recording

2.4.1 Preparation of patch clamp experiments

The air-conditioner in the recording room was turned on at the beginning of the experimental day to keep the temperature of the working environment stable at around 20 °C where cells can stay healthy longer than in the temperature variable environment.

2.4.1.1 Calibration of negative pressure

During recording, negative pressure was applied by extracting air through thin plastic tube connected to a 1 mL syringe. Therefore, a calibration was required to convert the volume of syringe to corresponding mbar value. A pressure sensor was connected to the plastic tube instead of the pipette holder. When different amounts of negative pressure, applied by pulling out syringe piston, the corresponding mbar values for each volume were measured by the sensor. The mbar value when no pressure was applied was also measured. The actual negative value produced by syringe in mbar was calculated by subtracting this "zero" value from the value for each volume. For each volume, three parallel tests were performed, and the average value was calculated. Calibration results are shown in Table 3, and data are shown in Mean value ± SEM.

Table 3: Negative pressure calibration results

Volume of syringe (μL)	50	100	150	200	250	300	350	400
actual pressure (mbar) ± S.E.M.	-21.6 ± 1.8	-35.6 ± 3.5	-56.1 ± 2.0	-72.8 ± 0.9	-90.3 ± 0.4	-107.5 ± 2.2	-122.9 ± 0.7	-137.9 ± 0.4

2.4.1.2 Solutions

The stock solutions could be used for recording within one month, and the PFS and ZBS should be prepared freshly every week.

2.4.1.3 Silver electrodes coating

The silver wires were first polished with sand paper to get rid of the old coating. Then, wash the wires consecutively with excessive normal water and distill water and make sure there was no tiny particle like dust or metal filings on them, leave them on clean absorbent paper, keep the wires off dust and air dry.

Put the dried wires in a clean Eppendorf tube filled with chloric detergent (DanKlorix hygiene cleaners, Reg. #: N-11648) and immerge the silver part into the surface. The coating process would take about 15 to 30 minutes. Then wash the coated wires consecutively with excessive normal water and distill water and make sure there was no chloride solution left, leave them on clean absorbent paper, keep the wires off dust and air dry.

2.4.1.4 Glass pipettes preparation

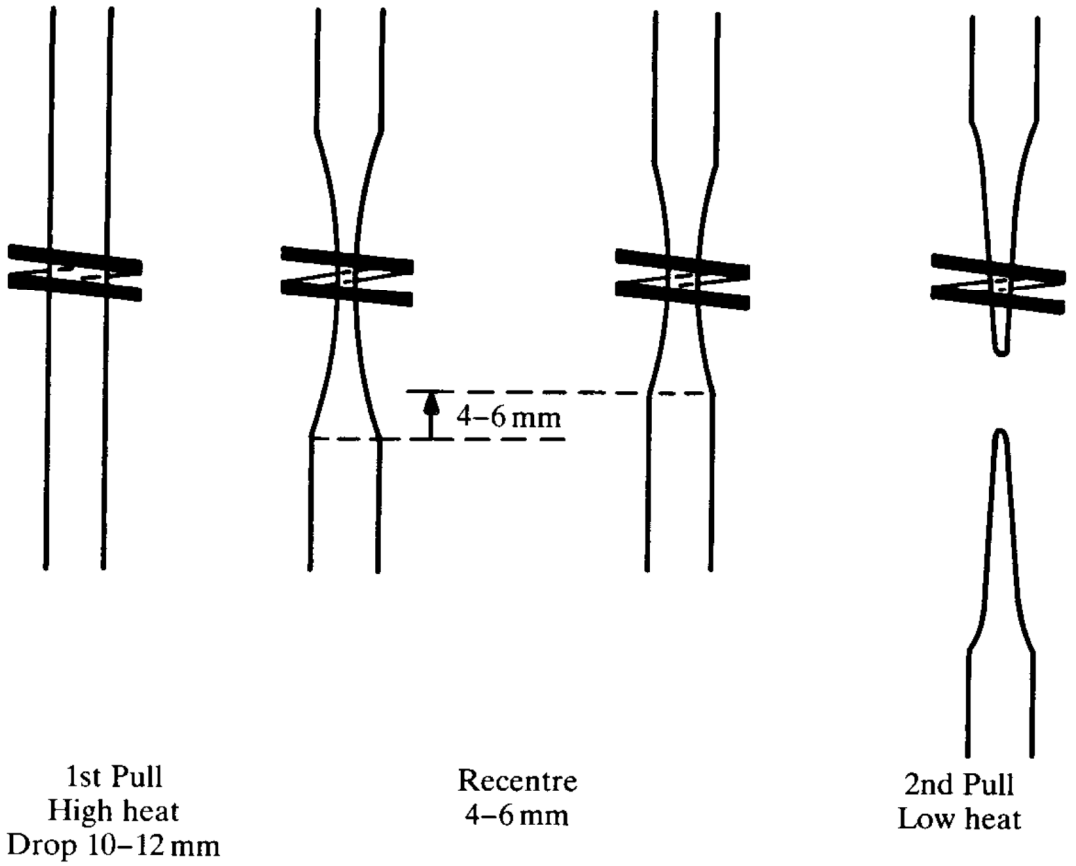

Figure 5a. Two-stage pull of patch pipettes.

Figure 5a illustrates how to produce patch pipettes from glass tubes with the double pull procedure using a vertical pipette puller (L/M-3P-A, List-Medical, Stock # 57761-1) [44]. With that conventional upright puller, the two tips of glass tube were fixed and centered the middle of the tube within the solenoid. When the puller was switched on, the solenoid was heated to orange-hot temperature by higher current (17.90A) and the tube within it was heated melt. Then gravity only provides the pull and the current was disconnected as soon as the pull started. After the elongated tube cooled down, it was re-centered and the second

stage of pulling started. This time the solenoid was heated to red-hot by a lower current (11.85 A~12.05A) and finally the tube was melt into two pre-pipettes.

The ideal resistance of pipette for our experiment would be 1.0 MΩ to 1.5 MΩ.

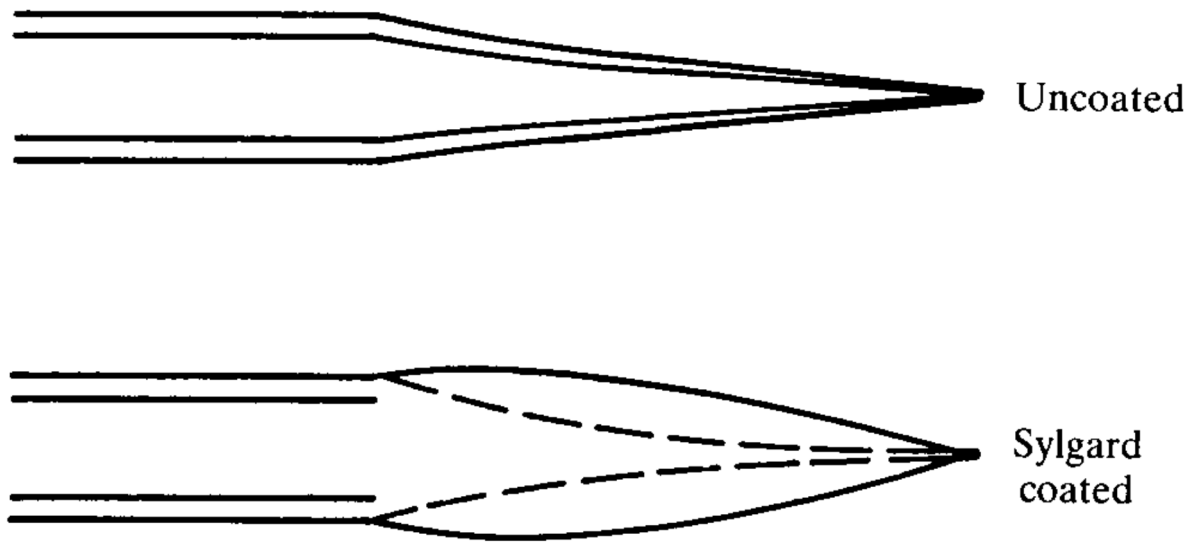

Figure 5b. Patch pipette before and after coating with Sylgard and curing.

The pipettes were ready for recording after being coated with Sylgard 184, an inert, hydrophobic, translucent elastomer resin which could be rapidly cured by heating, which could significantly reduce noise level during single channel recording. The Sylgard mixture (base to catalyst ratio was 10: 1) was kept in -20 °C fridge.

As shown in Figure 5b, one should not coat Sylgard till the very tip of pipette, which could disturb the sealing process. Leaving visible uncoated part under 2× microscope would give one a perfect pipette.

After being Sylgard coated, pipette was mounted to the 2× microscope again for heat polishing. A small heating wire with approaching device was placed right towards the tip of pipette. The tip of pipette was shown clearly under the microscope and the heating wire was moved to the edge of field before the heat was turned on. A small blower was started first to make sure the glass pipette was heated evenly when the air was blew towards the approaching point. When the heat was turned on, the wire was observed moving closer to the middle of the microscope field, and only a small approaching was needed and a very little shrink was observed to the tip of pipette, indicating it was successfully heat polished, which was enough

for polishing, while visible change of width lead to difficulties in getting rid of air from pipette tip when one tries to get successfully filled pipette.

Both uncoated and coated pipette should be kept off dust before recording. Pipettes were fresh only for one day and should be prepared again for the other experimental day, giving better sealing status.

2.5.1 Assembling the recording set

Firstly, ZBS should be filtered into the perfusion system and filled half of bath well, which should be changed to a new petri well to start the experiment day. Then, the computer and the recording devices (Axopatch 200A) were turned on and the recording software (Clampex10.3). Figure 6 showed the main interface of Clampex.

Pipette was filled with filtered PFS and mounted to the headstage after selecting suitable cell for recording.

2.5.2 Cell attach mode

2.5.2.1 Introduction

The cell-attached configuration can be used to record single-channel activity. This configuration is noninvasive to the cell membrane, and the pipette is sealed onto the cell membrane to obtain a gigaseal, leaving the ion channel in its intact physiological environment. Also, the disturbance from the cell inner structure is very low as the pipette only attaches to the exterior of the cell membrane [45]. Therefore, the function and characteristics of ion channel enclosed by the pipette could still be affected by the intracellular mechanism. The initial aim of our study was to seek GIRK channels among different breast cancer celllines. Therefore, we studied breast cancer cells under cell-attach mode to acquire properties of single, or a few, ion channels captured by the pipette. Moreover, the channels within the patch could not be directly gated by the receptor agonist, we could only study whether the target channel could be affected by cytosolic diffusible second messenger, neurotransmitter, and so on that could interact with the channels from outside plasma membrane, or content change of PFS.

2.5.2.2 Obtaining a giga-sealed patch

To obtain a successful recording patch, one should first make sure that all the solutions, cell culturing well plates, silver electrode coated with chloride and glass pipettes coated with silica were all prepared freshly. After assembling the setup, turning on power for the vacuum pump, computer and recording devices, ZBS was filtered with 0.2um Syringe filter and added to the storage container of perfusion system. Perfusion was started until the bath well was filled with 5 mL ZBS. Then, glass plate with cells was took out and the culturing well plate should be put back immediately. The cells were perfused with 5 mL ZBS, and the glass pipette was filled with filtered PFS and loaded to the recording headstage. The headstage was manipulated downwardly, until the tip of the pipette was submerged by ZBS in the bath when seal resistance of the pipette was measured, before which around 30 mbar positive pressure was applied to the system to generate outward stream through tip of the pipette, keeping small particles away from pipette tip. There should be no air within the tip of pipette, whose ohmic resistance ranged from 1.0 MΩ to 2.0 MΩ. If the pipette was not successfully filled, it should be demounted and snapped with finger hardly to get rid of the air until its seal resistance fell into normal range. If the seal resistance was still in MΩ range, but significantly higher (around 50%), then there was dust or cell debris attaching to pipette tip and a strong pulse of positive pressure was needed to blow the particle away. If the resistance was lower than normal (around 50%) or even in kΩ range, the pipette was broken and a new one was required.

MCF-7 and HEK-293 cells (including transfected ones) could be kept in the recording chamber for 15 to 20 minutes, while MCF-10A cells (including transfected ones) 40 minutes average. Therefore, less than half of fresh time could be used for searching cells for recording. Cells with clear plasma membrane, enough space for pipette tip between plasma membrane and nucleus, medium size and not round-up morphology were selected for single channel recording. In the recording of MCF-7 cells transfected with dominant negative hPiezo1 construct, only round-up cells were observed to have moderate fluorescence and could be selected for recording. The pipette continued to be moved downwardly and paused just before touching the cell when the positive pressure was released. After releasing pressure, the manipulator was geared down for finer approaching. The seal resistance would increase by 0.1 MΩ to 0.2 MΩ as soon as the pipette tip touched the target plasma membrane, and pressing continued until the resistance increased by around 50%.

The last step for obtaining a recording patch was applying negative pressure after the pipette was pressed appropriately. Less than 26.2 mbar negative pressure was applied to suck the plasma membrane up into the pipette. When the membrane spontaneously crept up, seal resistance increased fast till GΩ range, a stable patch was achieved and was ready for recording.

2.5.2.3 Patch clamp data acquisition and analysis

Data acquisition (Clampex)

The Clampex software was started and membrane test was first performed to check the status of glass electrode when its tip was just submerged by the bath. As mentioned above, the resistance of most of the glass electrodes used in our project ranged from 1.0 MΩ to 2.0 MΩ (Figure 7), and less than 500 KΩ or more than GΩ during membrane indicated broken electrode or air embolus within electrode, respectively.

After obtaining a giga-seal, the faraday cage where patch clamp setup was located was closed gently, and the negative pressure for starting giga-seal formation was released before starting recording. An edited Gap-free protocol was acquired for checking status of patch and for starting a recording, during which researcher could apply negative pressure or start other events. Episodic stimulation protocol could also be created to perform quick screening of membrane potentials only for recording openings (Figure 7).

By pressing the recording button (red dot in the second row from top), status of patch was recorded, during which every action to the patch as well as the action time was written down for documentation and for further analysis. Recording file was saved and analyzed using Clampfit.

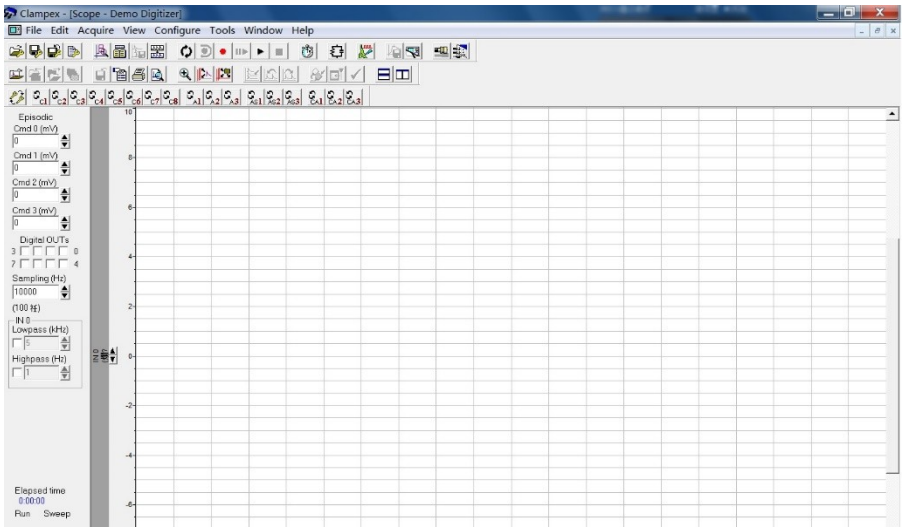

Figure 6: Main interface of Clampex.

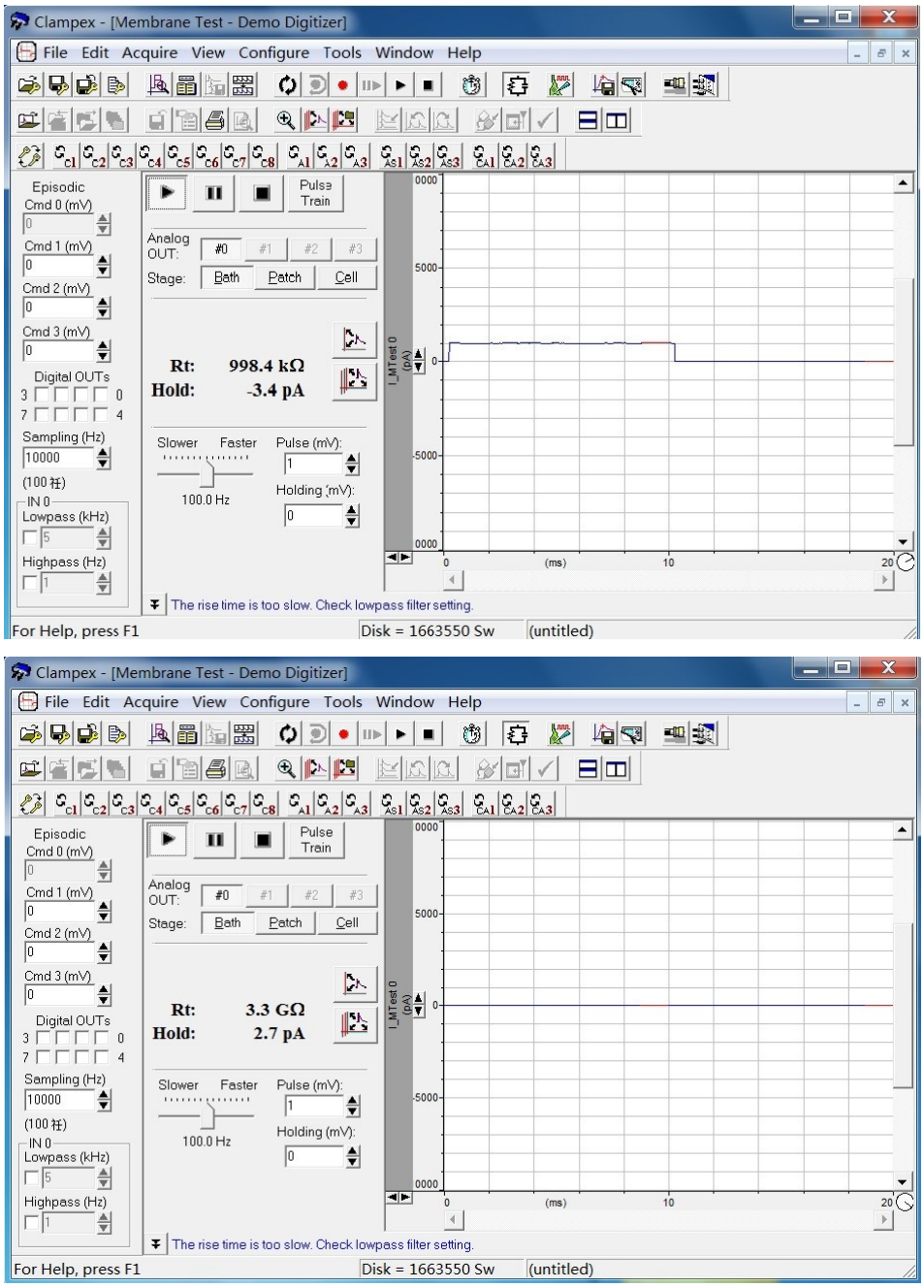

Figure 7: Demo membrane test showing resistance of electrode (up) and giga-seal (down).

When the tip of a perfectly filled glass pipette was just submerged into the bath solution, the resistance of the pipette was calculated, as shown by the upper figure. After the pipette was pressed onto cell membrane and negative pressure was applied, cell membrane was sucked into the pipette and seal resistance increased with very high speed to GΩ scale, as shown in the lower figure, indicating stable recordable patch.

Data analysis (Clampfit)

Recording file from Clampex using all protocol was readable to Clampfit. A gap-free data file was opened and demonstrated in Figure 8, in which the action of applying negative pressure was shown both inwardly and outwardly.

Data was lowpass filtered before being analyzed, aiming to filter out noise (Figure 9 & 10). The type of filter was Gaussian and the cutoff value was 1500 Hz for all analyzed data, which could filter out most of noise and not filter out too much signals from opening channels. Figure 11 (left and right) indicated the difference before and after lowpass filtering. After filtering, single channel data was ready to be analyzed.

Measuring the amplitude of single opening channel is shown in Figure 12. Current through channel was measured using in-built cursor function at different membrane potentials. At most ten opening channels were measured and the average amplitude was calculated at corresponding potential. At last, current-voltage relation of this patch was plotted and single channel conductance was calculated using Sigmaplot.

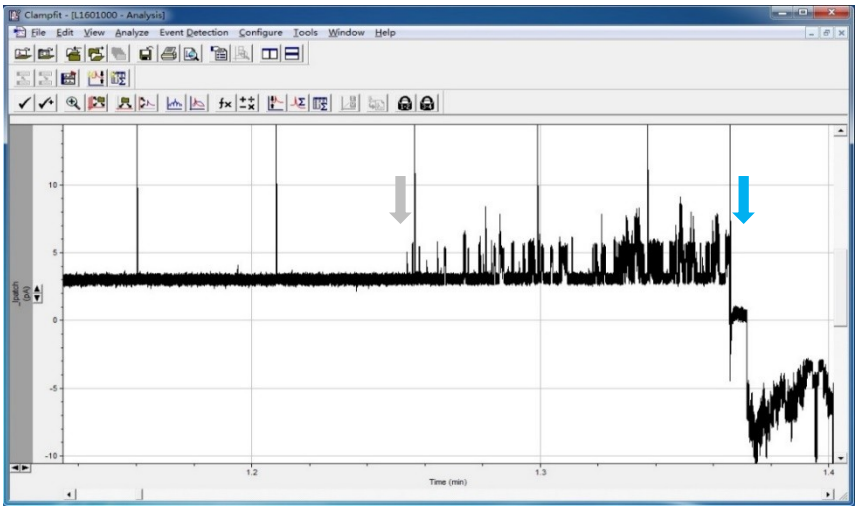

Figure 8: Data analyzing interface of Clampfit.

This example of data analyzing demonstrated one patch of MCF-7 WT cell, during which negative pressure was applied (grey arrow) and MSCs were activated. The recording was done in 01.06.2011, therefore named L1601000 (L stands for Li Chouyang, who performed the experiment.), which was under cell attach mode, with glass pipette resistance of 4.2 MΩ, analog Bessel TP filter frequency of 2 kHz, and gain of 0.2 V/pA. The membrane potential was -80 mV when 35.6 mbar negative was applied (grey arrow). At the end of shown

recording, membrane potential was shifted to 80 mV, showing MSC was still activated by negative pressure when the direction of ion flow was changed to the opposite (blue arrow).

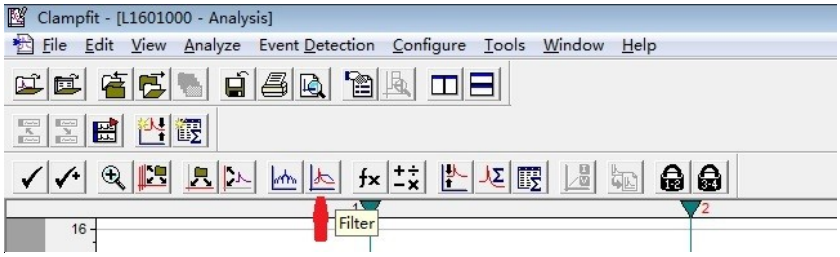

Figure 9: Control panel of Clampfit.

The filter button was indicated by red arrow. All data were lowpass filtered out background noise for ease of better data quality.

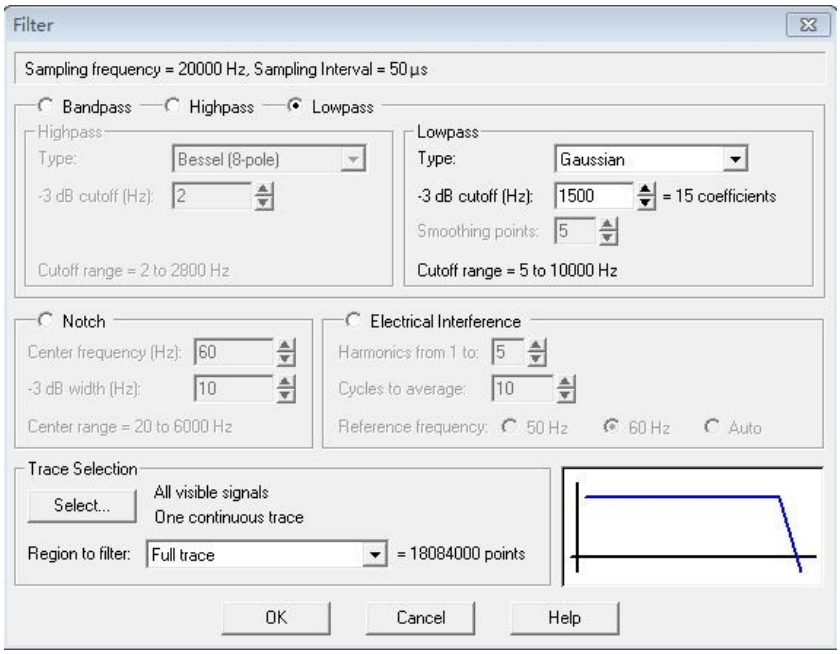

Figure 10: Filter interface.

The type of filter could be changed by checking boxes (Bandpass, Highpass, Lowpass). The cutoff frequency ranged from 5 to 10000 Hz.

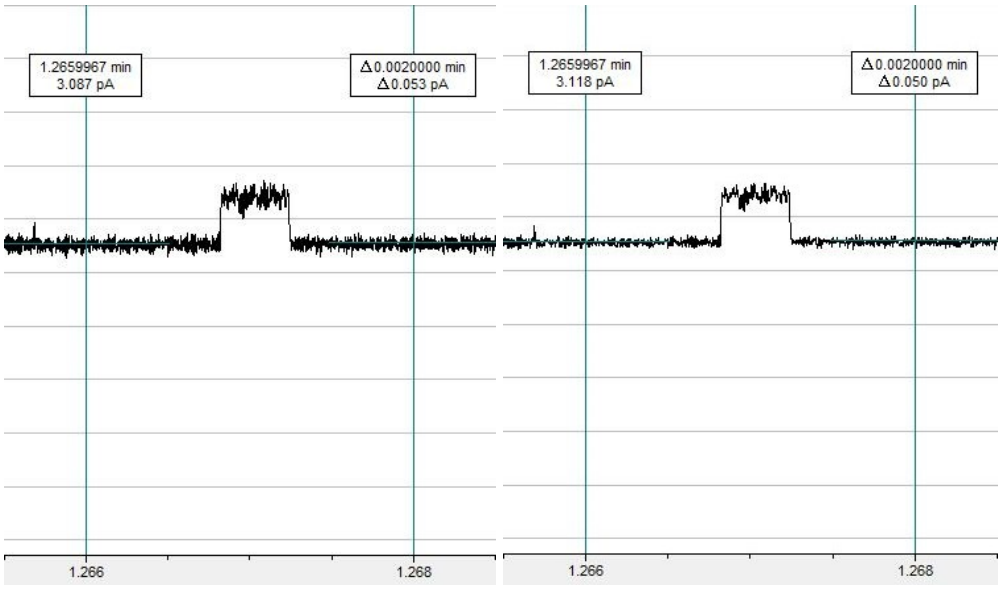

Figure 11: Data before and after lowpass filtering.

This recording was all from L1601000, with much higher resolution. The unit of time cursor was minute. The membrane potential was -80 mV when 35.6 mbar negative was applied.

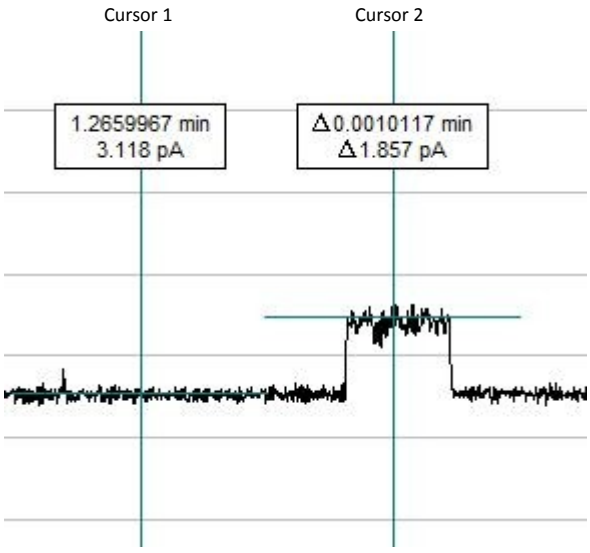

Figure 12: Measuring amplitude of single channel opening.

After filtering was done in Figure 11, cursors were brought in and measuring was done to the opening current demonstrated in Figure 11. The difference between the horizontal line of cursor 1 and 2, or 3 and 4 demonstrated the amplitude of selected channel.

2.5.2.4 Electrophysiological characterization of channels (MSC, BC)

To characterize and identify different channels observed in our recording, the single channel conductance G_Λ, ion selectivity, cations permeability, and dose response to negative pressure for all the channels.

Ion selectivity of K^+

We screened different celllines that were stably transfected with GIRK variants for GIRK channels by applying negative pressure within the recording patches.

Since GIRK channels selectively permeate to potassium ion, the content of PFS was altered to assess the permeability profile of channels observed. In normal PFS, the concentration of K^+ was 153 mM. To study the ion selectivity of observed channels, PFS50, PFS25 or PFS0 were also prepared together with PFS, where K^+ was replaced by 50%, 75% and 100% Na^+ in pipette filling solution, respectively and the total concentration of K^+ and Na^+ was 150 mM.

G_Λs of observed channel using different PFS were calculated and compared, and current-voltage relations were plotted, by which permeability for K^+ of channels (MSC, BC, etc.) was evaluated.

Cations permeability

Similar as mentioned above, K^+ was replaced by other monovalent cations, Li^+, Rb^+, and Cs^+, and divalent cations, Ca^{2+}, and Ba^{2+}. The concentration of monovalent cations in pipette filling solution were all 150 mM, and that of divalent cations were 100 mM (The osmotic pressure were the same in PFS with monovalent cation and PFS with divalent cation, so that the patch could last longer.).

G_Λs of observed channel using different PFS were calculated and compared to create the permeability profile for channels observed, which could be used to identify them as it is unique for certain channel.

Dose response

The dose response demonstrates the quantitative reaction of certain channel to mechanical stress. In a stable patch, different amount of negative pressure was applied to the patch from around 21 mbar to over 120 mbar (Upper limit uncertain, depending on status of patch; Figure 13).

The recording traces could be considered as millions of data point corresponding to the transient current under the same membrane potential. When the frequency of current amplitude of the data points was plotted against the transient current, we can get the Gaussian function amplitude histogram, which was acquired by in-built function of Clampfit and was plotted for each action of applying and releasing negative pressure (Figure 14~16).

Then the integration of each Gaussian curve gave the average current at each np value. This integration value was plotted against the np dose. Then the new plot can reflect the quantitative reaction of the channel to the mechanical stress.

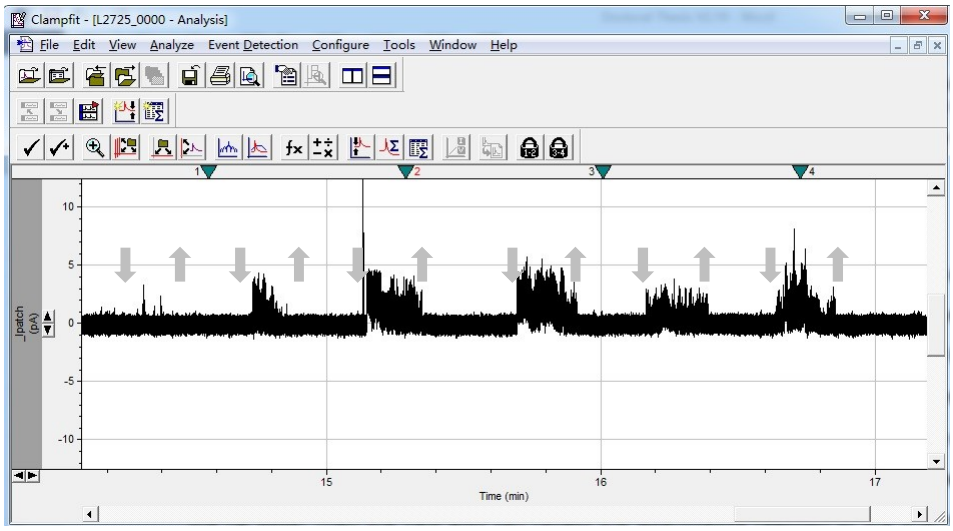

Figure 13: Overview of dose response recording data.

The recording was done in 25.07.2012, named L2725000, which was under cell attach mode, with glass pipette resistance of 1.2 MΩ, analog Bessel TP filter frequency of 2 kHz, and gain of 0.2 V/pA. Time points of applying and releasing negative pressure were indicated by downward and upward gray arrows, respectively. From left to right, 21.6 mbar, 35.6 mbar, 56.1 mbar, 72.8 mbar, 90.3 mbar, and 107.5 mbar were applied, successively.

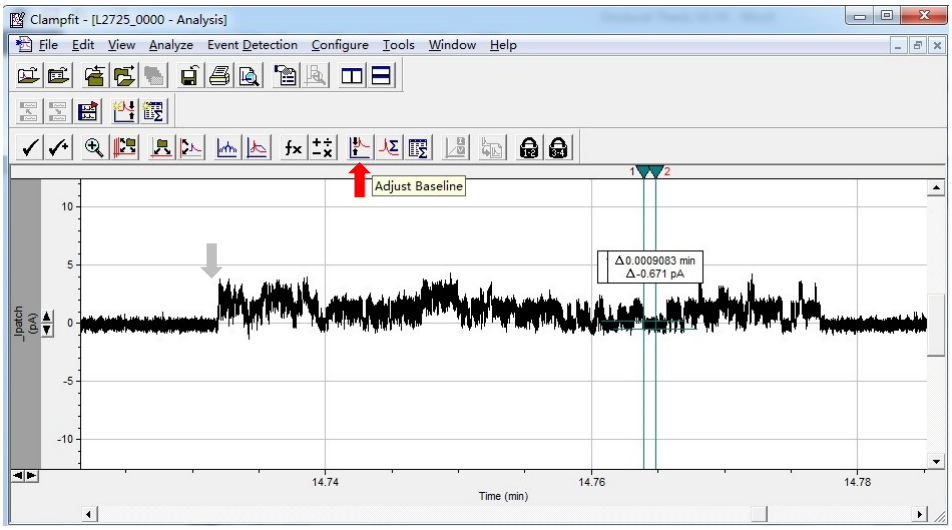

Figure 14: Dose response analysis-adjusting baseline.

The baseline was adjusted to zero for plotting amplitude histogram according to the baseline between selected cursor pair, which was moved within the negative pressure applied region, as negative pressure might alter the baseline level. Gray arrow indicated that 35.6 mbar negative pressure was applied, and the releasing of negative pressure was not included in this recording range. The recording was done in 25.07.2012, named L2725000, which was under cell attach mode, with glass pipette resistance of 1.2 MΩ, analog Bessel TP filter frequency of 2 kHz, and gain of 0.2 V/pA.

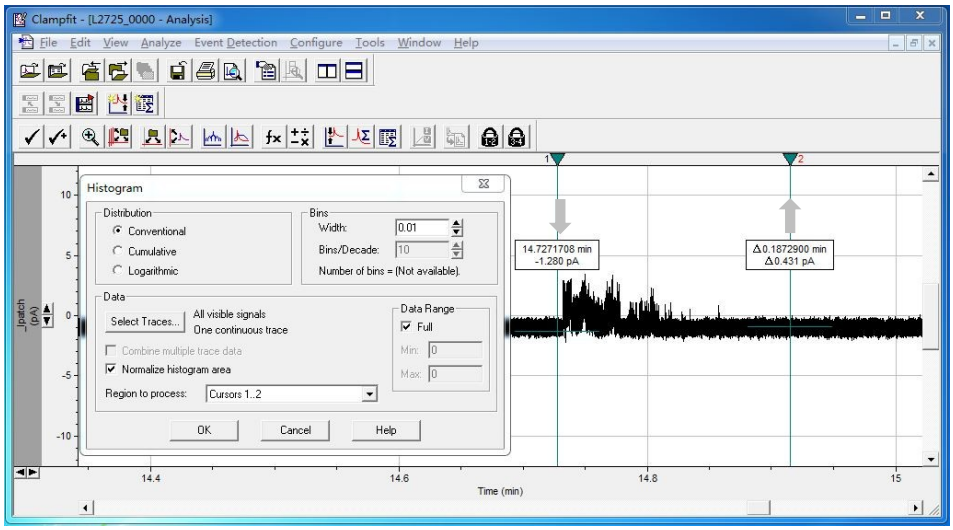

Figure 15: Amplitude histogram setup.

Conventional distribution was chosen and bin width was set to 0.01 pA, indicating moderate sensitivity of data sampling. Histogram was plotted between Cursor 1 and Cursor 2, which

is shown in the following figures, where 35.6 mbar negative pressure was applied and released, indicated by downward and upward gray arrows, respectively. The recording was done in 25.07.2012, named L2725000, which was under cell attached mode, with glass pipette resistance of 1.2 MΩ, analog Bessel TP filter frequency of 2 kHz, and gain of 0.2 V/pA.

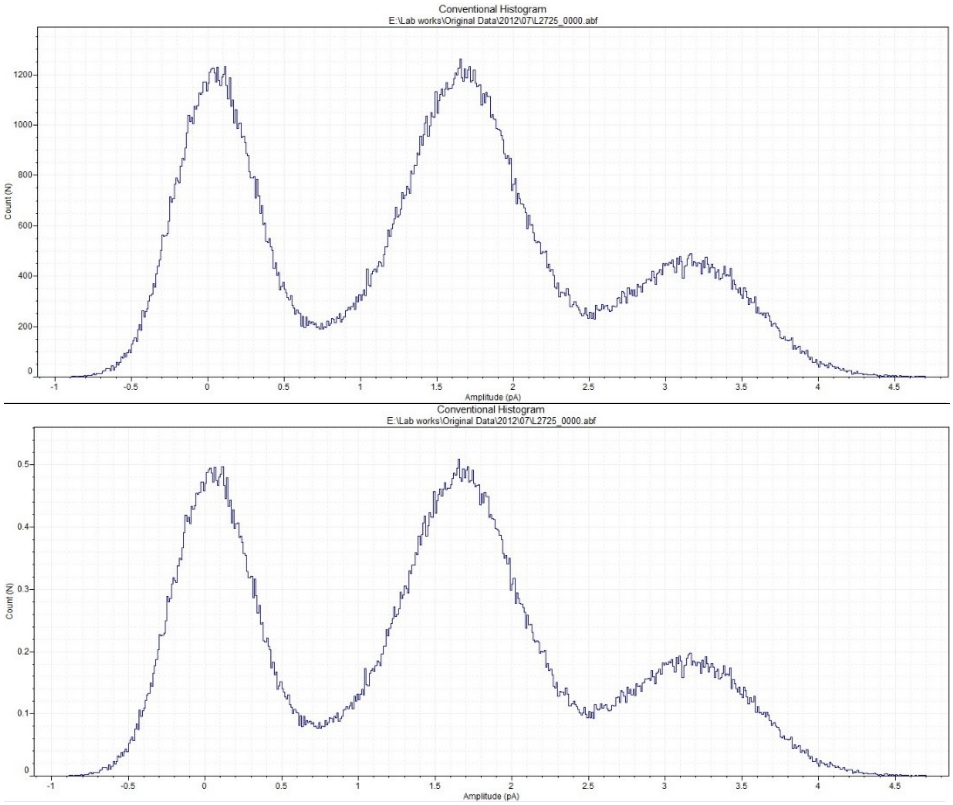

Figure 16: Amplitude histogram example.

These two histograms were plotted from the selected region showing in Figure 15. The lower histogram was normalized to 1, showing the frequency of each data point with different amplitude.

2.5.3 Outside-out mode

This configuration allows one to change the microenvironment of the extracellular side of the patch freely, for instance, perfusing with receptor agonist or antagonist. Therefore, it is often used to study receptor-operated ion channels, in this case, we tried to operate the channel we observed in MCF-7 cell with specific blocker.

Obtaining an outside-out patch began with forming giga-sealed patch in cell-attached mode. After a successful giga-seal formation, the patch was broken by a strong pulse of negative pressure (usually done by a sudden mouth suction) to get a successful whole-cell recording patch. After the whole-cell configuration was formed, the electrode was slowly withdrawn from the cell following the same way as approaching, allowing formation of a bulb of plasma membrane separated from the cell and reform as an intact convex membrane on the end of the pipette tip. Since this moment, the original outside of the membrane faced the outward bath of the pipette instead of facing pipette solution, when pipette solution was mimicking cytosol, while we could change perfusion content in the bath freely during the time the patch was still alive.

2.6 Microscopy

2.6.1 Fluorescent microscopy

Each time after transient transfection or before performing recording of transient transfected cells, cells were examined under fluorescent microscopy for transfection efficiency, or they were screened for cells with healthy morphology and moderate fluorescence. Different filters were applied depending on what fluorescent protein was combined with the induced construct.

One minute or two was required for HBO lamp we used to heat up before getting a clear view. Since switching the HBO lamp, on and off, would cause severe damage to the lamp, it was turned off only after we managed a successful cell-attached patch or experiments were completely done for the day.

2.6.2 Confocal fluorescence microscopy

During stable transfected cellline fabrication, cells were examined under confocal microscope once per week for checking the fluorescence of the cells and photographed for documentation.

The localization of induced protein can be visualized using confocal microscope. With higher magnification, researcher can get photo about where exactly the induced proteins are expressed within the cell. Using co-localization study with certain organelle markers, we can

even get the information that whether the induced protein co-localize with certain organelle, such as endoplasmic reticulum.

2.7 Western blot to detect hPiezo1 protein expression

2.7.1 Cell lysis and protein estimation

Cells were collected by centrifugation (500 rpm, 4 °C, 5 minutes), washed in ice cold PBS, pelleted and stored at -20 °C until use. The cell pellets were lysed with 100-400 µL RIPA buffer (Thermo Scientific, Cat. #89901, volume depending on pellet size) containing a protease inhibitor cocktail (PIC, Sigma-Aldrich, Cat. #P8340). The mixture was incubated for 20 minutes on ice and vortexed thoroughly. The lysates were sonicated (2 cycles, 10 seconds on and 30 seconds off, amplitude 20%) on ice and centrifuged in a pre-cooled Eppendorf centrifuge (13000 rpm, 4 °C, 20 minutes) to remove the debris. The supernatant was collected, aliquoted in fresh tubes and stored at -20 °C until use. Protein concentrations of the lysates were estimated using a BCA protein assay kit (Thermo Scientific, Cat. #23225) according to manufacturer's instructions.

2.7.2 Western blots

Cell lysates were diluted to the desired protein concentration with RIPA buffer, mixed 1:5 with 5x Laemmli sample buffer containing 10% SDS (Promega, #H5113), 300 mM Tris-HCl (pH 6.8), 25% glycerol (Sigma-Aldrich, #G5516), traces of bromphenol blue (Merck, #1081220005) and 5% β-mercaptoethanol (Sigma-Aldrich, #M3148). The samples were heat-denaturated at 95 °C for 5 minutes and subjected to sodium dodecyl sulfate-polyacrylamide gel electrophoresis (SDS-PAGE; 8% gels) together with a protein marker (PageRuler Prestained Protein Ladder, Thermo Scientific, #26616). Gels were run at 80 V for 20 minutes (stacking gel) and then at 120 V (separation gel). After 1.5 hours electro transfer (150 mA, on ice) on a nitrocellulose membrane (GE Healthcare Life Sciences, #RPN203D), the membranes were stained with Ponceau S solution (Sigma-Aldrich, #P7170) to check the protein transfer. Membranes were blocked with PBST (PBS 0.05% Tween, Merck, #8221840500) containing 5% non-fat dry milk (Bio-Rad, #170-6404) for 1 hour at room temperature on a shaker. The membranes were washed with PBST and incubated with

the primary antibody (Proteintech #15939-1-AP or Abcam #ab82336) diluted 1:1000 in PBST containing 1% non-fat dry milk over night at 4 °C on a shaker. The membranes were washed 3 x 10 minutes with PBST before incubation with the secondary antibody (1 hour at room temperature on a shaker). As secondary antibody a sheep anti-rabbit/HRP (kindly provided by Amir Zarnani, Teheran, Iran) was used in PBST containing 1% non-fat dry milk. The membranes were washed 3 x 10 minutes with PBST, incubated for 1 minute with ECL Select detection solution (GE Healthcare, #RPN2235) and then exposed to a CCD camera using the ChemiDoc™ MP System (Bio-Rad, #170-8280).

2.8 Cancer cell motility study

Cells were split and seeded to 24 well plates at densities of $1*10^4$ cells/well and $2.5*10^3$ cells/well for MCF-7 and MCF-10A, respectively, approximately 24h before observation by the cell observer (Axiovert200M, Zeiss, Germany). The total medium volume in each well was 2 mL. In control wells, 2 mL normal medium was filled in directly, while in toxic wells, half of normal medium was filled in first and then the other half medium with certain amount of GsMTx-4 (final concentration: 300 nmol/L and 1.5 μmol/L) was added to the wells before frame acquisition was started. Frames were acquired every 20 minutes for a total time period of 72 h. Frame files were analyzed after being stabilized and individual cells were tracked using the ImageJ software (v1.47; Wayne Rasband, NIH, http://imageJ.NIH.gov/) using the manual tracking plugin.

2.8.1 Single cell tracking

Figure 17a shows the main control panel of ImageJ. Images for one position within certain well were saved in the same file, which were imported to ImageJ by pressing 'Image Sequence' (Figure 17b). As image stabilization using the Lucas-Kanade algorithm is a time and computer power consuming work, it was performed two days before manual tracking. After stabilization, jittery images sequence was stabled, giving us the correct and stable coordinates of cell movement [46] (Figure 17c). After stabilization, the stabilized images stacks were used for further analysis. Before acquiring cell coordinates, the brightness and contrast were adjusted using 'Auto' mode (Figure 17d). Manual tracking then was performed to get the track of individual cell during 72 hours (Figure 17 e - g).

a

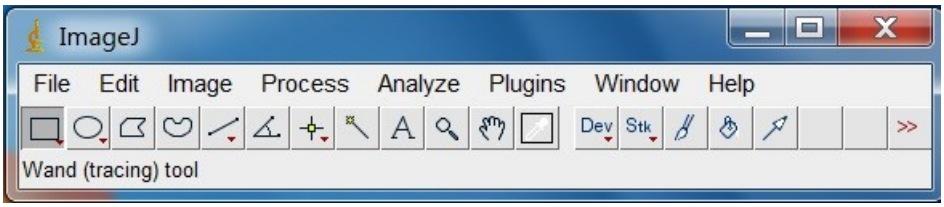

Figure 17a: Main panel of ImageJ.

b

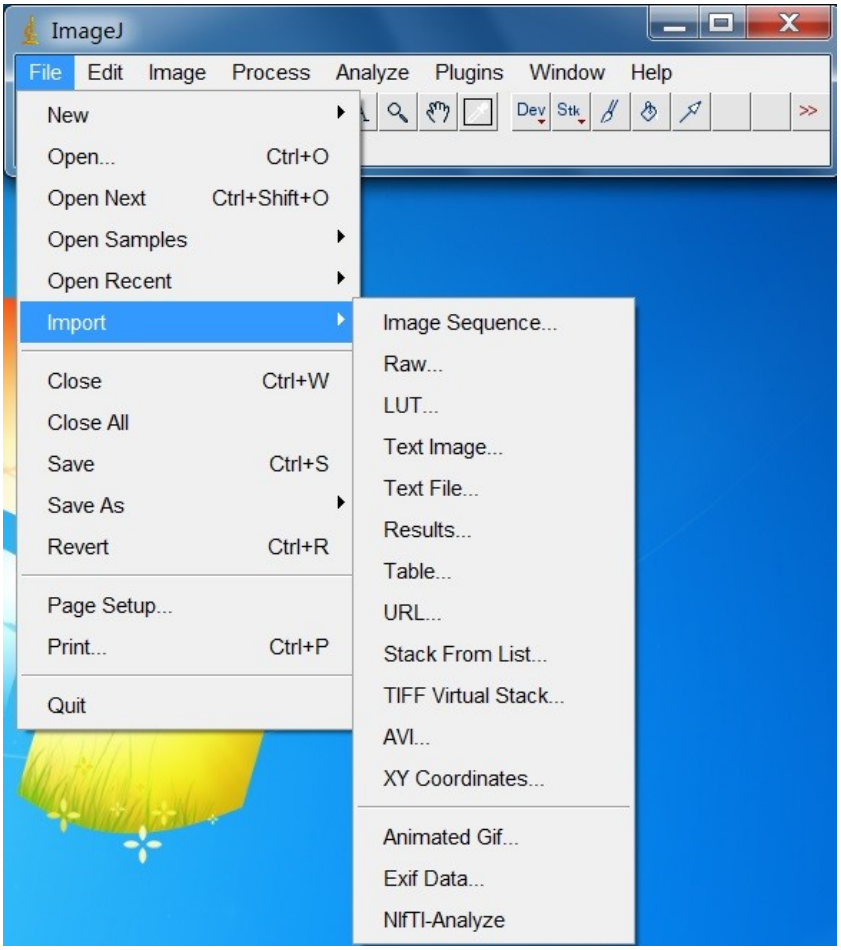

Figure 17b: Importing image sequence using ImageJ.

By pressing "Image Sequence", a series of images in one folder can be imported and analyzed.

c

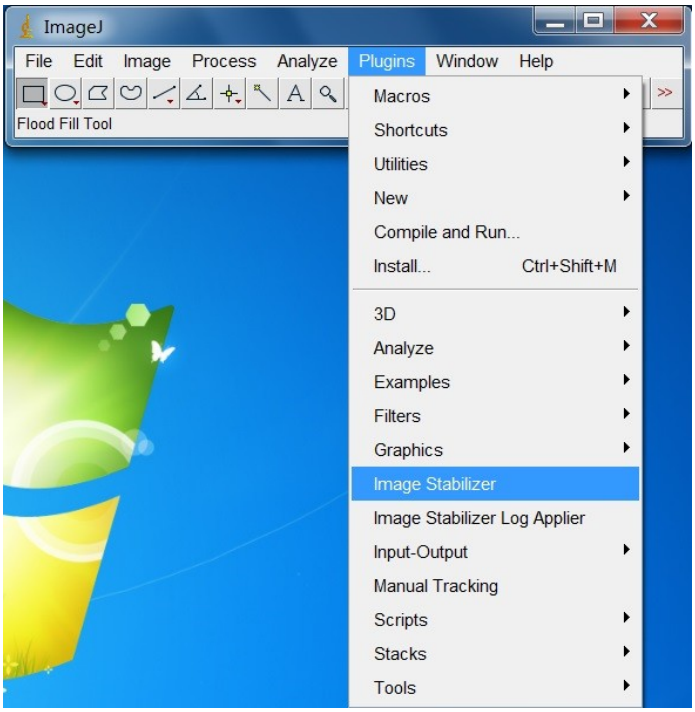

Figure 17c: Stabilizing the image sequence.

By using this foreign plugin, the imported image sequence can be stabilized, by which photographing error was minimized.

d

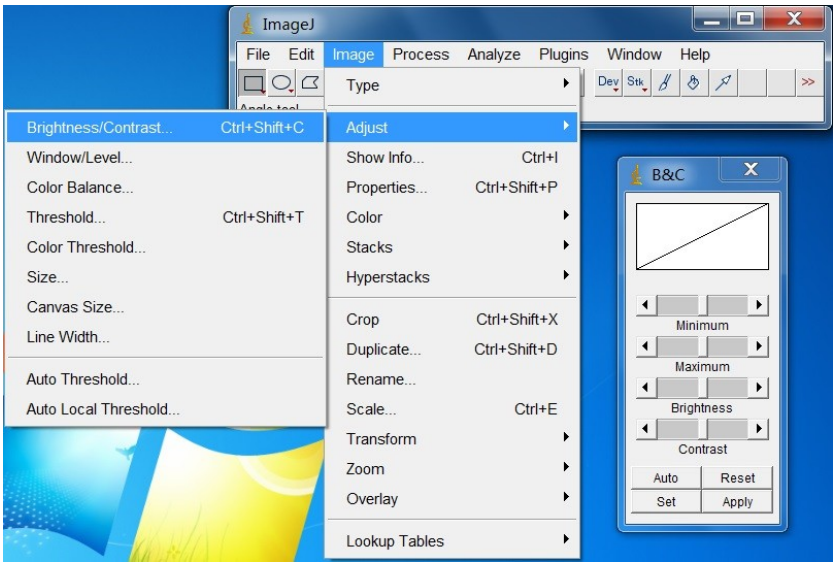

Figure 17d: Adjusting image properties.

The brightness and contrast were adjusted to get better image quality. In the sub panel, auto adjust was enough (Press "Auto") for adjusting image quality and the adjustment can be applied by pressing "Apply" or reversed by pressing "Reset".

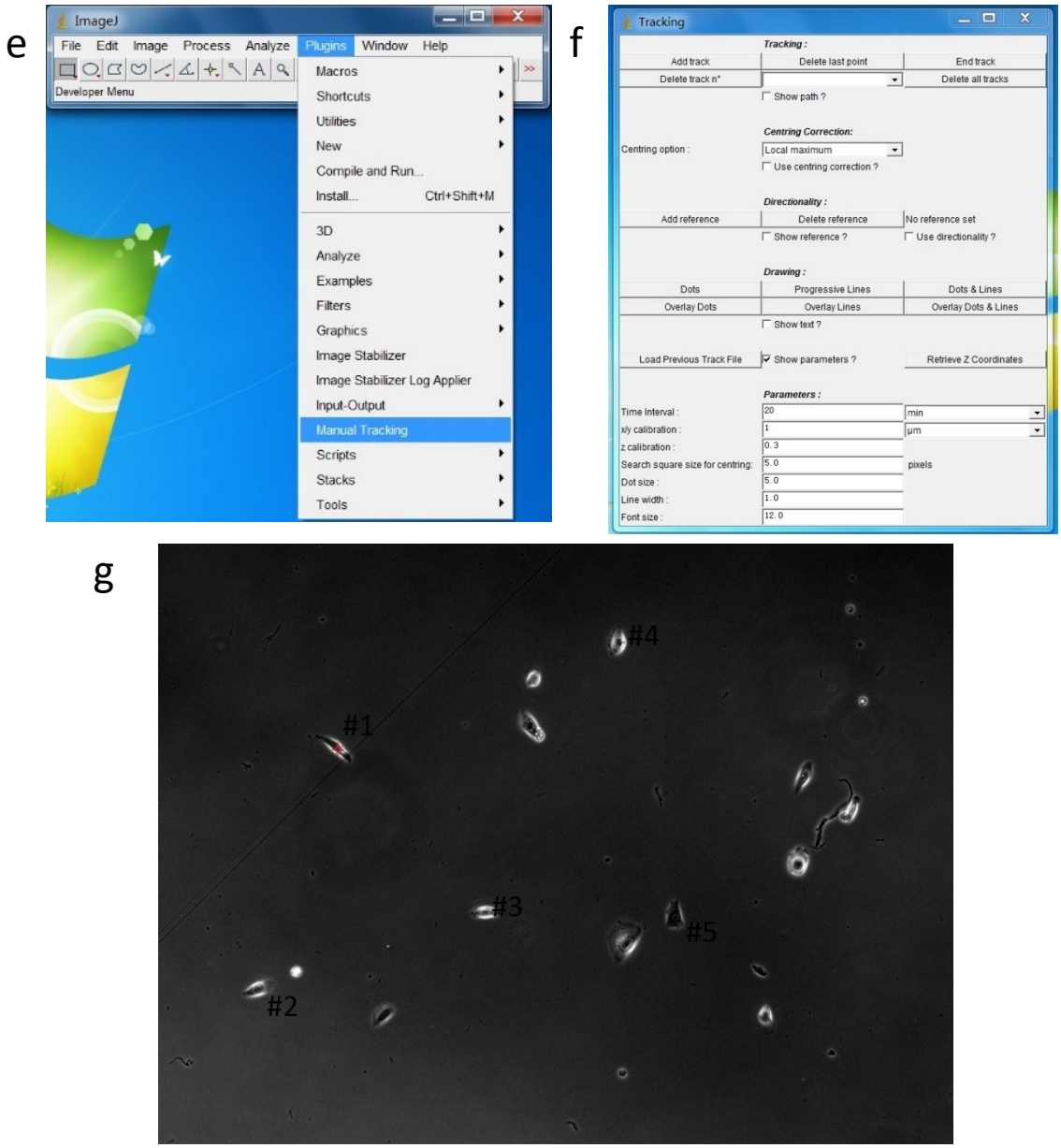

Figure 17e~g: Manual Tracking.

To study the motility properties of cultured cells, the exact coordinates of selected cells were tracted using this plugin. Pressing "Manual Tracking" in Figure 17e can activate the control panel in Figure 17f. Time interval between each image can be set from the beginning of tracking, and tracking for each new cell was started after pressing "Add track" and was ended by pressing "End track", which would mark the start and end points for tracking each single cell in the summary excel file when all selected cells were manually tracked in the imported folder. Figure 17g was an example for manual tracking. Five or more cells, which stay within the field all along the images, were selected and marked. Then the position of nucleus center of certain cell was tracked, indicated by red star on cell #1, and division and encirclement activities were recorded.

2.8.2 Motility data analysis

Cell coordinates were recorded and analyzed using Microsoft Excel 2010 and routines written in Visual Basic for Applications (version 7.0). The 2D motility coefficient (MC ($\mu m^2.min^{-1}$)) was calculated from the slope ($D^2/\Delta t$) of the linear regression of the squared distance (D^2) as a function of time interval Δt (Δt_{max}=10h) according to equation (1) as described [47]:

$$(1)\quad MC = \frac{D^2}{4.\Delta t}$$

2.9 Statistics and bioinformatics

Statistical analysis was performed using SigmaPlot/SigmaStat (version 12.5, Systat Software, USA). Experimental parameters were first tested for normal distribution. Subsequently, tests for statistical significance were performed (One Way ANOVA or Kruskal-Wallis test), followed by the appropriate pairwise multiple comparison procedures.

The overall survival curves based on Piezo1 (Fam38A; affymetrix ID: 202771_at) mRNA expression was calculated by an internet Kaplan–Meier plotter (http://kmplot.com/analysis/; [48]) using the breast cancer database (version 2014; N=1115) (Figure 18). Using this on-line plotter, information of relation between certain marker gene and cancer prognostic can be visualized based on PostgreSQL server, which contains data of the effect of 22,277 genes on patient's survival using 10,188 cancer samples (breast, ovarian, lung and gastric).

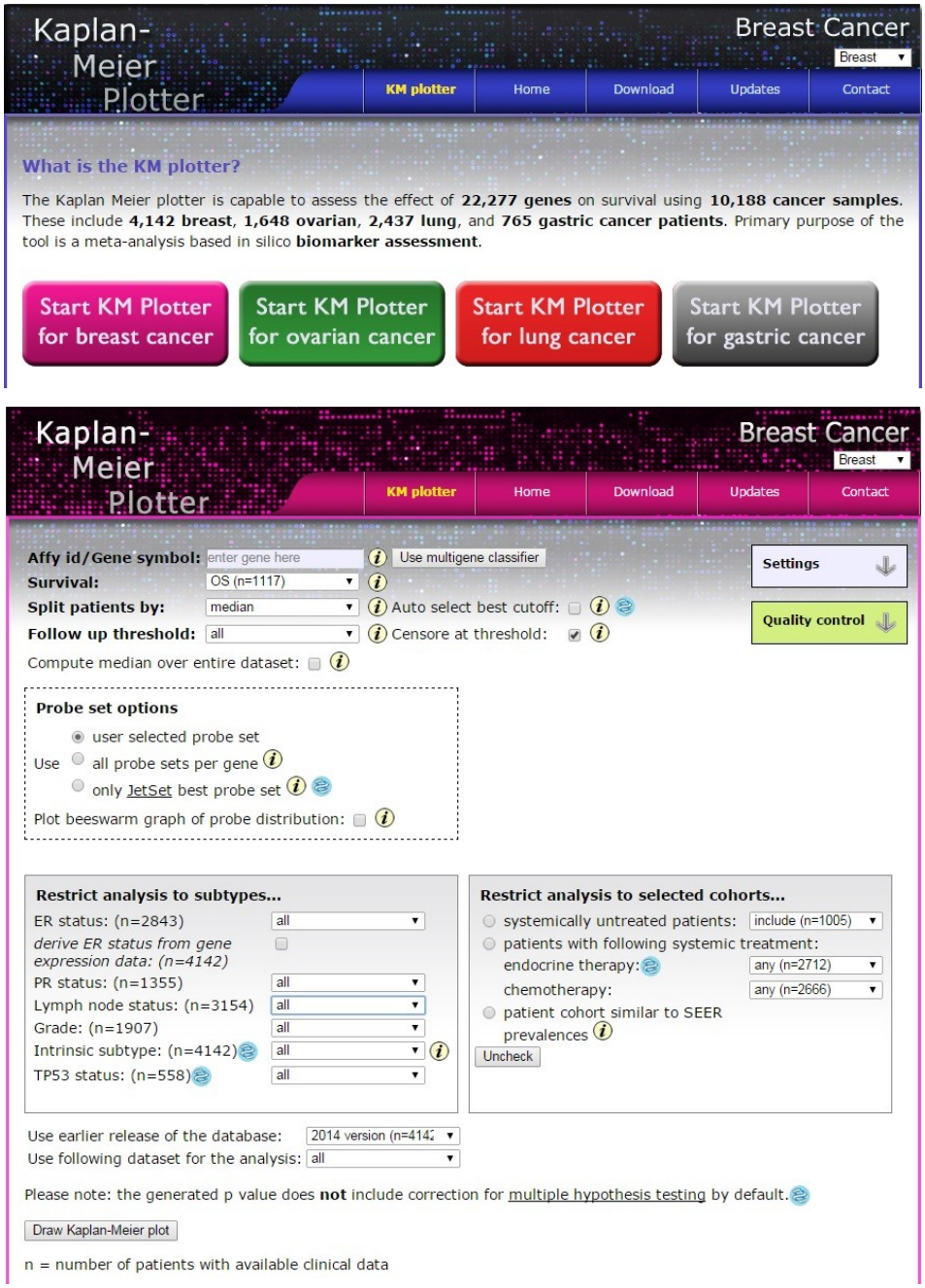

Figure 18: Internet Kaplan–Meier plotter.

The upper figure demonstrated the starting panel of this online plotter, in which databases of patients with four different kinds of cancer were included and could be related to expression of certain gene, respectively. The lower figure showed the parameters for plotting Kaplan–Meier plot. The databases were updated annually and the 2014 version one was used in this research.

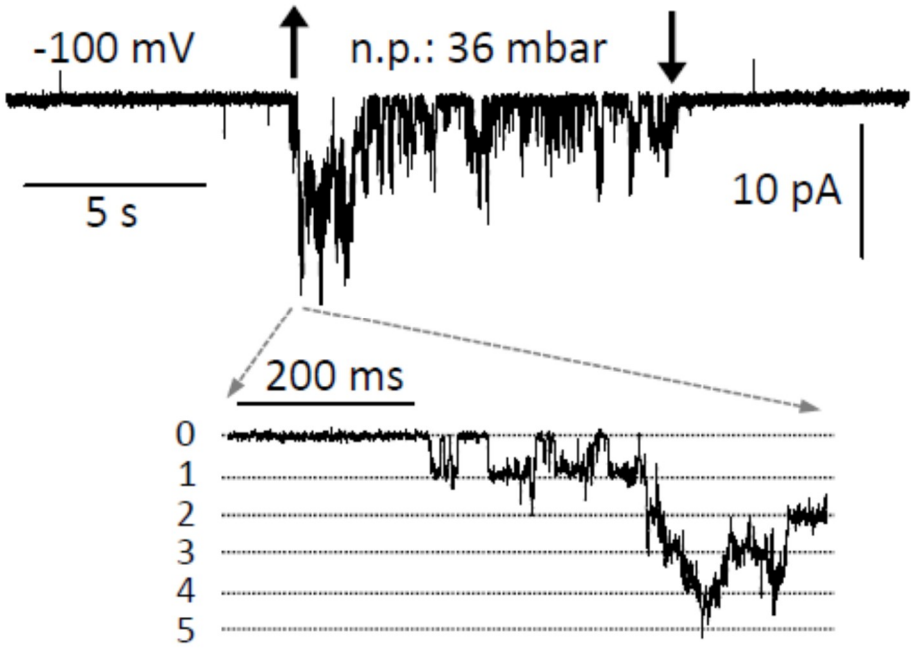

Figure 19.: Example recording of MSC patch. [49]

In this recording, 36 mbar was applied at -100 mV membrane potential. Black arrows indicated the time range when negative pressure was applied (Upwards: On; Downwards: Off). Bottom part of the figure demonstrates the activation with higher resolution. Numbers with dotted lines indicate numbers of openings activated by negative pressure.

Table 4.: Frequency of occurrence of MSCs in different cell lines.

	Total number of patches	*Number of patches with MSCs*	*% of patches with MSCs*
MCF-7^{WT}	291*	157	54%
MCF-7$^{hG1d\#7}$	31	18	58%
MCF-7$^{hG1c\#9}$	37	20	54%
MCF-7$^{hG1c\#4}$	8	5	63%
MCF-7$^{hG1a\#6}$	16	10	63%
MCF-7$^{G\beta\gamma}$	41	35	85%
MCF-10A^{WT}	30	0	0%
HEK-293^{WT}	16	0	0%

*****: *Numbers includes patches using all kinds of pipette filling solution.*

After applying mechanical stress, functional mechano-sensitive ion channels (MSCs) were detected in 54% of cell attached membrane patches derived from MCF-7^{WT} cells (Figure 19, Table 4), indicating its strong sensitivity to the application and release of negative pressure. The next frequently observed ion channel within the plasma membrane of MCF-7 cells was a constitutively active, highly K^+ selective, inward rectifying ion channel (Figure 20 a~f, Table 5) with an inward single channel conductance in PFS of approximately 72±3.7pS (Figure 20b), which was well characterized during the pilot study and named as Big Channel (BC). Since this ion channel, in comparison to MSCs, was observed in only 8 out of 96 patches (≈8%) and other species of ion channels were only detected as in quite limited observations, we conclude that MSCs represent a major ion channel population of the malignant MCF-7 breast cancer cell line. (Table 6)

Table 5.: Frequency of occurrence of BCs in different MCF-7 cell lines.

	Total No. Patches	*BC*	*%*
MCF-7$^{hG1d\#7}$	31	3	10%
MCF-7^{WT}	96*	8	8%
MCF-7$^{hG1c\#9}$	37	10	27%
MCF-7$^{hG1c\#4}$	8	3	38%
MCF-7$^{G\beta\gamma}$	41	4	10%
MCF-7$^{hG1a\#6}$	16	2	13%

**: Number includes patches only using PFS (100% K^+).*

Table 6.: Summary of channels detected in different cell lines permeating K^+ or Na^+.

	Total Patches No.	*No channel*	*MSC*	*nMSC*	*MTC*	*BC*	*DR*	*others*
MCF-7$^{hG1d\#7}$	31	4	18	6	3	3	0	0
MCF-7^{WT}	96*	9	75	0	2	8	1	1
MCF-7$^{hG1c\#9}$	37	2	20	1	3	10	1	0
MCF-7$^{hG1c\#4}$	8	1	5	0	0	3	0	0
MCF-7$^{G\beta\gamma}$	41	3	35	0	0	4	1	1
MCF-7$^{hG1a\#6}$	16	1	10	0	0	2	0	1
MDA-231^{WT}	34	4	15	2	0	0	0	0

**: Number includes patches only using PFS (100% K^+).*

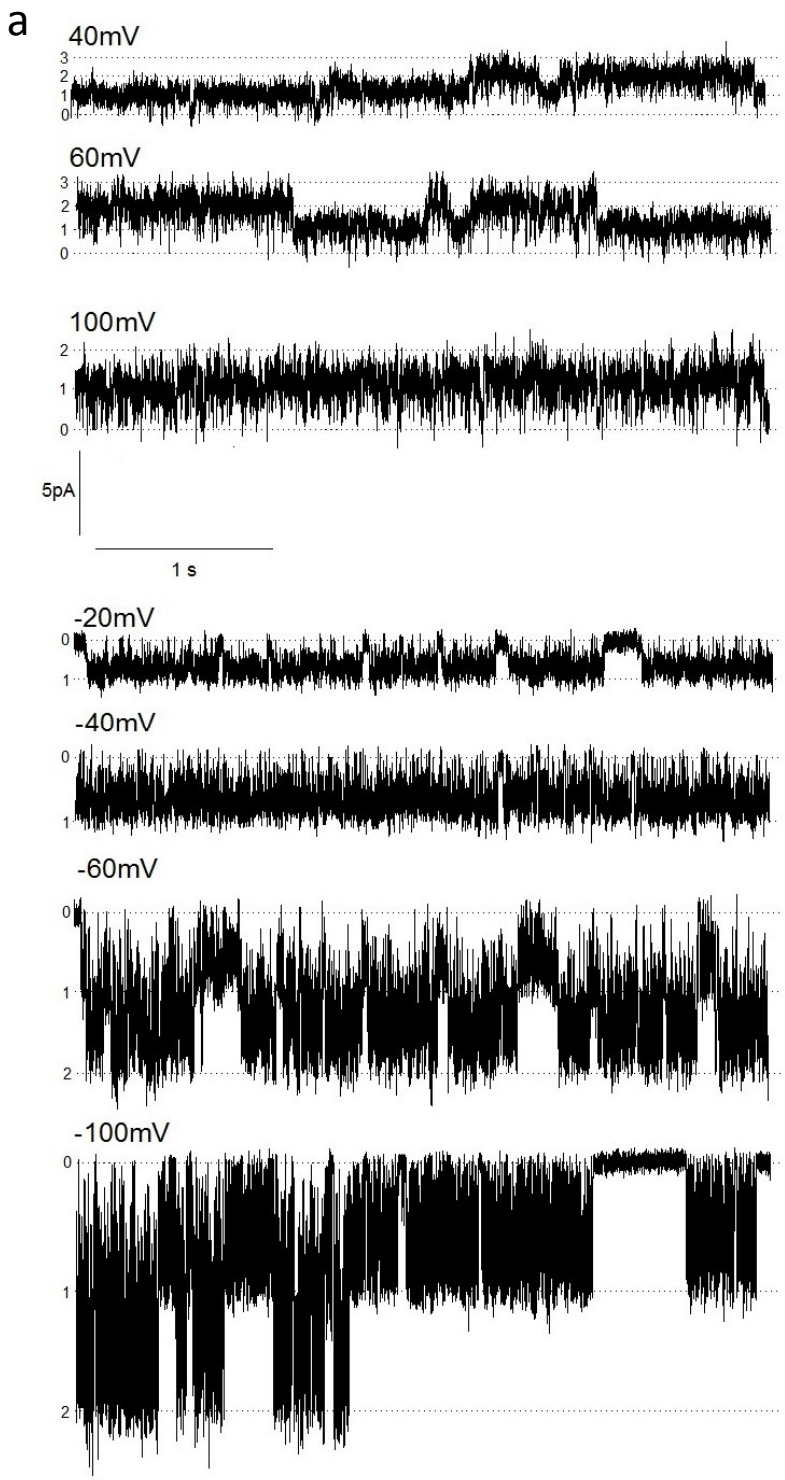

Figure 20a.: Recording traces of BC in the MCF-7cell line using normal pipette filling solution.

This figure shows the constitutively active BC currents both inwardly and outwardly at different membrane potentials. The pipette filling solution was PFS, containing 153 mM K^+ as permeating cation. The size of opening currents and the number of channel were indicated by dotted straight line with numbers on the left.

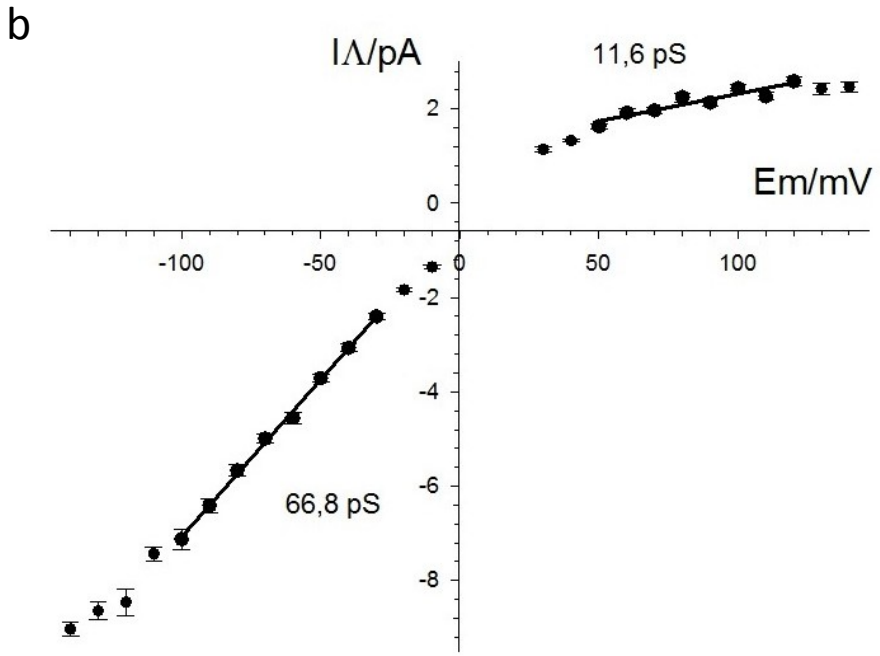

Figure 20b.: Current-voltage relations of BC in the MCF-7cell line using normal pipette filling solution.

Data points for different membrane potentials were demonstrated by black points, which was the average amplitude of ten opening channels sampled at the same membrane potential. The regression regions for this patch from which G_{Λ} was calculated were indicated by black straight lines, ranging from 40 mV to 110 mV, outwardly, and -40 mV to -110 mV, inwardly, which will shift according to E_{rev} (reverse potential), for example, E_{rev}=10 mV indicates that the regression region shift outward for 10 mV. Single channel conductance for both direction was calculated and demonstrated.

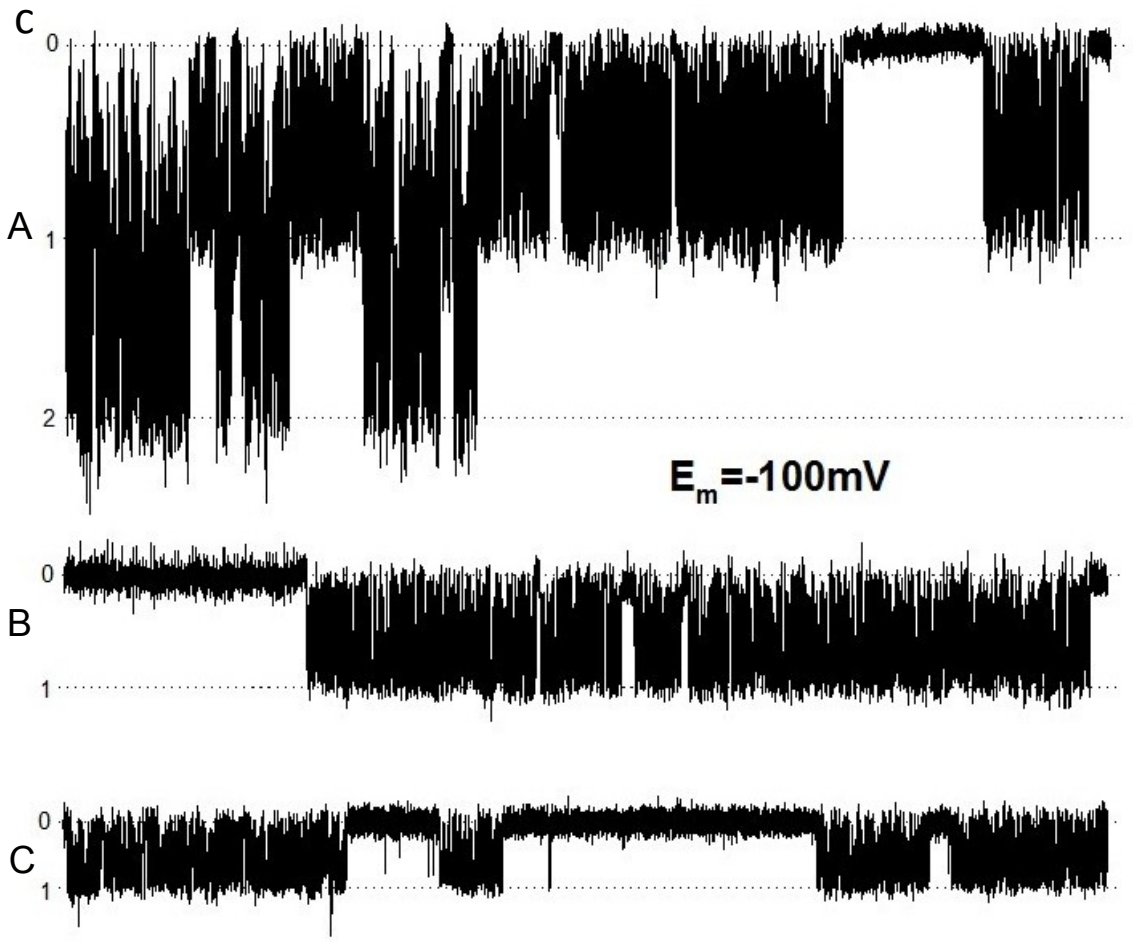

Figure 20c.: Recording traces of BC in the MCF-7 cell line using different pipette filling solution.

At the same membrane potential (-100 mV in this case), pipette filling solution with different concentration of K^+ were used within patches. The size of opening channels was indicated by dotted straight lines with numbers on the left indicating the channel number. Figure 20cA indicated recording in which 153mM K^+ was dominant in pipette filling solution, while Figure 20cB demonstrated the size of constitutively active opening channels when half of K^+ was replaced with Na^+, that is 75mM K^+,75mM Na^+ within the patch, and in Figure 20cC, 75% of K^+ was replaced with Na^+ ,that is 37.5mM K^+,112.5mM Na^+.

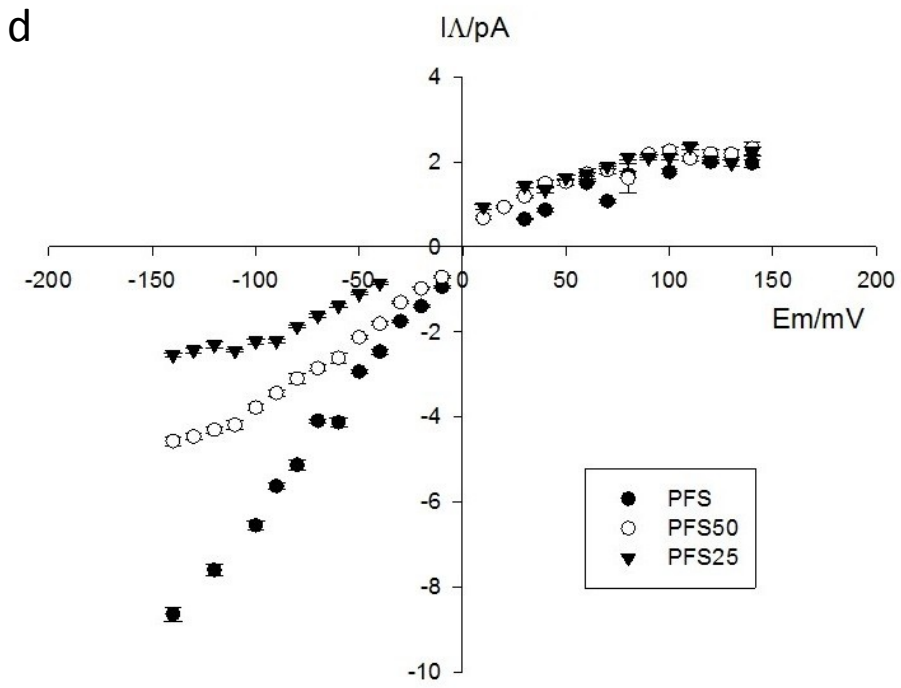

Figure 20d.: Current-voltage relations of BC in the MCF-7 cell line using different pipette filling solution.

Data points from different recordings were demonstrated by different graphic symbols. Solid cycles demonstrated the current-voltage relations of BC when 153mM K^+ was dominant in pipette filling solution, hollow ones showed those when permeating 75mM K^+,75mM Na^+, and solid triangles indicated those when 37.5mM K^+,112.5mM Na^+ was in pipette filling solution, which only 25% K^+.

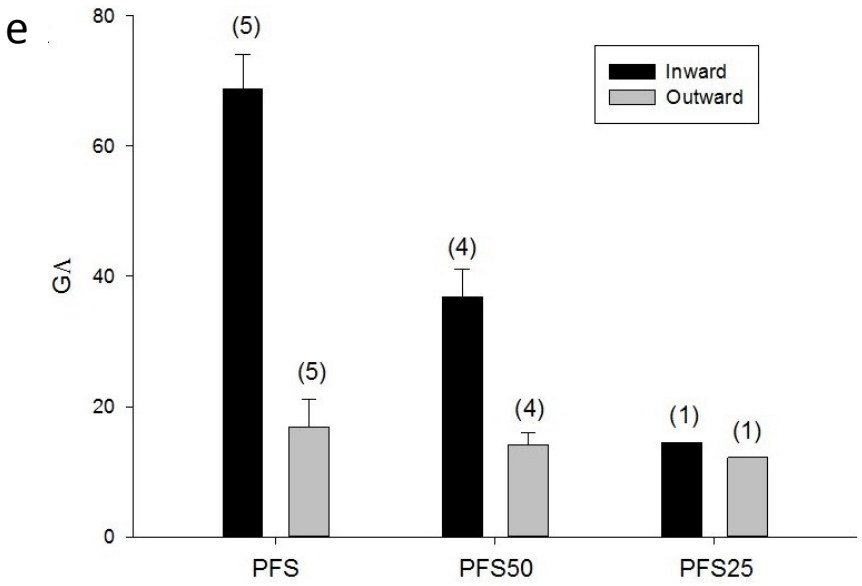

Figure 20e.: Summary of G_{Λ} of BC in the MCF-7 cell line using different pipette filling solution.

Single channel conductance, G_{Λ}, of BC in the MCF-7 cell line using different pipette filling solution were calculated as Figure 20b indicated and summarized using bar graph. Patch number using each kind of pipette filling solution was indicated on top of corresponding bar. Mean values ± SEM are shown.

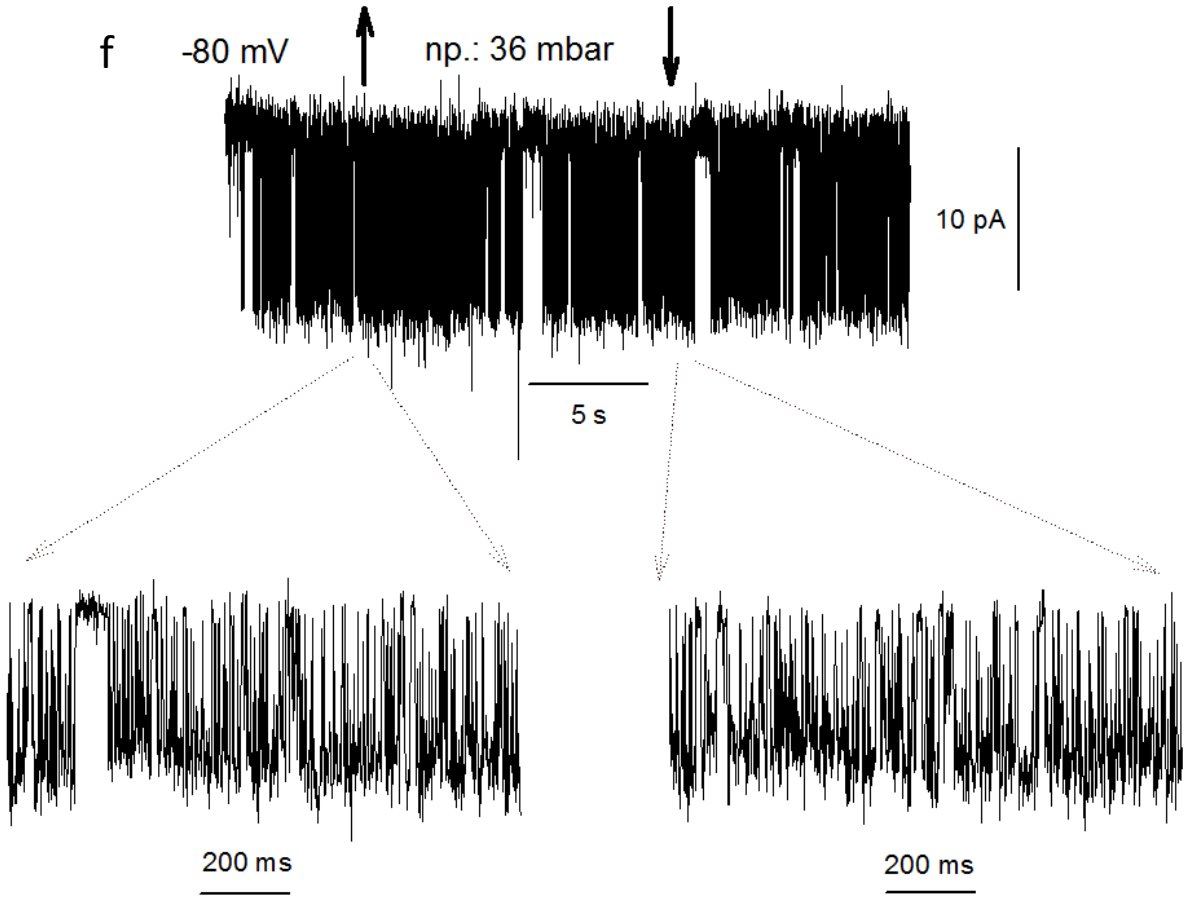

Figure 20f.: Recording trace of BC in the MCF-7 cell line when negative pressure was applied.

In this recording, only BC was observed and no MSC found.36 mbar negative pressure, which is sufficient for activating MSCs, was applied to this patch. As shown both in the overview recording and in traces with higher magnification, no activity change could be observed for BC, indicating BCs are not mechanosensitive.

MSC activity depended on the strength of negative pressure (n.p.) applied within the patch in a saturable manner (Figure 21). The property of activating MSC by negative pressure was assessed by dose response study. Figure 21a showed the data acquisition when different amount of n.p. was applied and the amplitude histograms of corresponding recording. The product of relative frequency and transient current value indicated the total current activated by corresponding amount of negative pressure. Then the total current value was plotted against the amount of negative pressure, and the activation of corresponding patch by different amount of negative pressure was demonstrated by regressing a sigmoid curve based on this plot. The relative activation percentage was also calculated for each X-

Y pair by dividing the actual total current value by the value on the curve with the same negative pressure value, which demonstrated how much exactly those channels within certain patch were stimulated by different amount of negative pressure. Those percentage values for all 18 successful dose response patches were recorded and the mean activation percentage when the same amount of negative pressure was applied was calculated. Then Figure 21b was plotted using these mean percentage values to demonstrate the average dose response against different amount of negative pressure of MSC in MCF-7^{WT} cells. Half maximal n.p. for activation ($EP_{50:}$ 40.8 ± 1.1 mbar (N=18)) in MCF-7 cells was similar to EP_{50} values observed for Piezo1, a recently discovered MSC subunit, overexpressed in HEK-293 cells [32, 34].

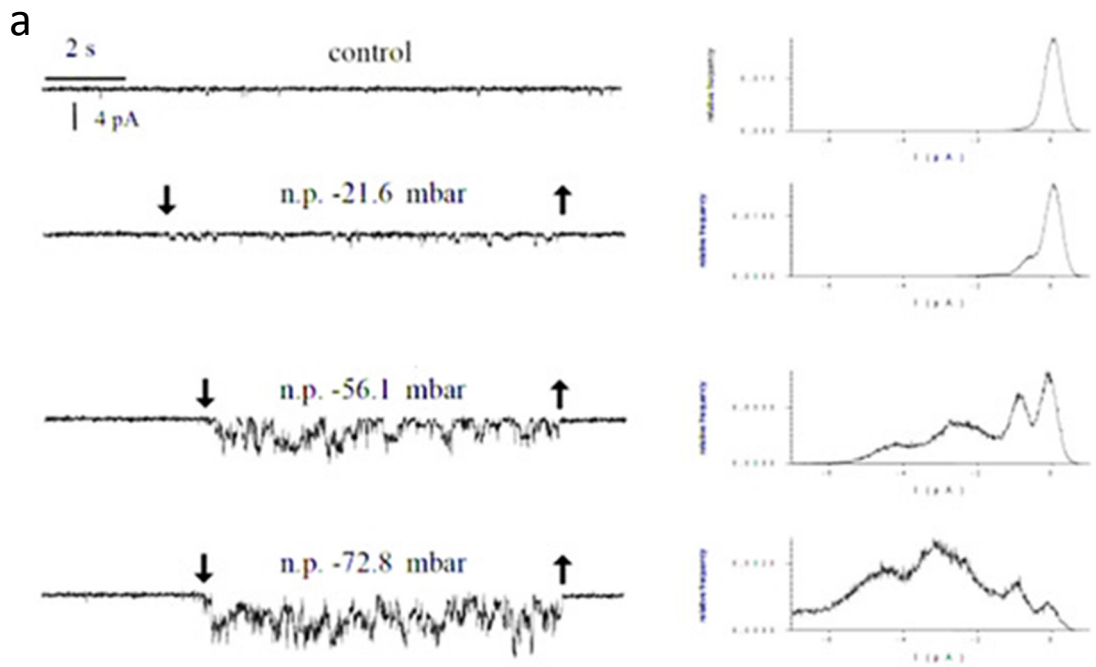

Figure 21a.: Original recording (left column) at different amount of negative pressure and the corresponding amplitude histograms(right column).

When negative pressure was applied, the current was recorded and represented by thousands of data points with different transient current value. More data points with higher current values demonstrates that channels captured within certain patch have higher activity, which was reflected by the amplitude histograms on the right. The x-axis was the frequency of data points and the y-axis was the transient current value of them. Thus, the histograms showed that when no negative pressure was applied, most of the data points were close to zero ampere, indicating static state of the channels, while histograms below showed that as

negative pressure applied within the patch grew, more and more data points with higher current value were observed. In the last histogram, most of the data points were found around -3 pA, indicating very strong activity after applying over 70 mbar negative pressure within the patch. The real negative value was calibrated for each patch clamp set. There were three parallel test during calibration, and the value was stated as Mean ± SEM.

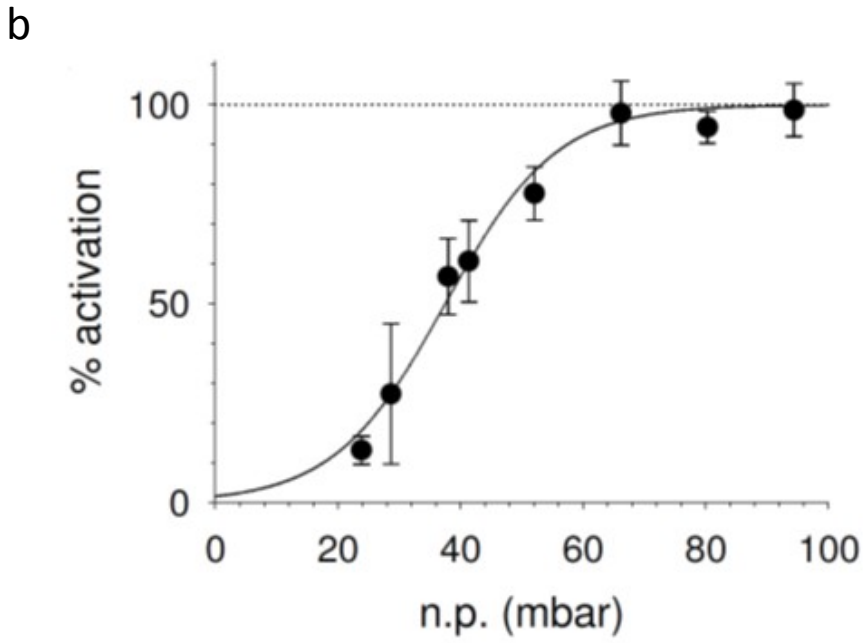

Figure 21b.: Open probability (in % of maximum activation) as a function of negative pressure applied. [49]

Y-axis was the average open probability calculated from 18 dose response patches, and there were over 15 values for each data point in this plot. Mean values ± SEM are shown for each point. The exact negative pressure values in X-axis were calibrated for each patch clamp setup. The sigmoid curve was regressed and EP_{50} value was calculated.

Single MSC conductance (G_Λ) was measured for cation flux across the plasma membrane from the extracellular compartment into the cytosol and in the opposite direction. Figure 22 shows the single channel conductance properties of MSC observed in MCF-7^{WT} cells under different membrane potential. Figure 22a indicates the linear relation between membrane potential and the size of channel currents. The figure only shows parts of the entire trace. The amplitude of currents was measured, current-voltage curve was plotted, and single channel conductance (G_Λ) was calculated (Figure 22b). The G_Λ calculated for inward currents carried predominantly by K^+ ions was 25.6 ± 0.4 pS, and for outward ones 20.6 ± 2.1 pS (Table 7, N=8).At the same absolute value of pipette potential (V_p) (40 mV to 110

mV) applied, I_{Λ}s were greater in the inward than in the outward direction (Figure 22b). The inward G_{Λ} is close to that reported for murinePiezo1 (mPiezo1) overexpressed in HEK-293 cells [32].

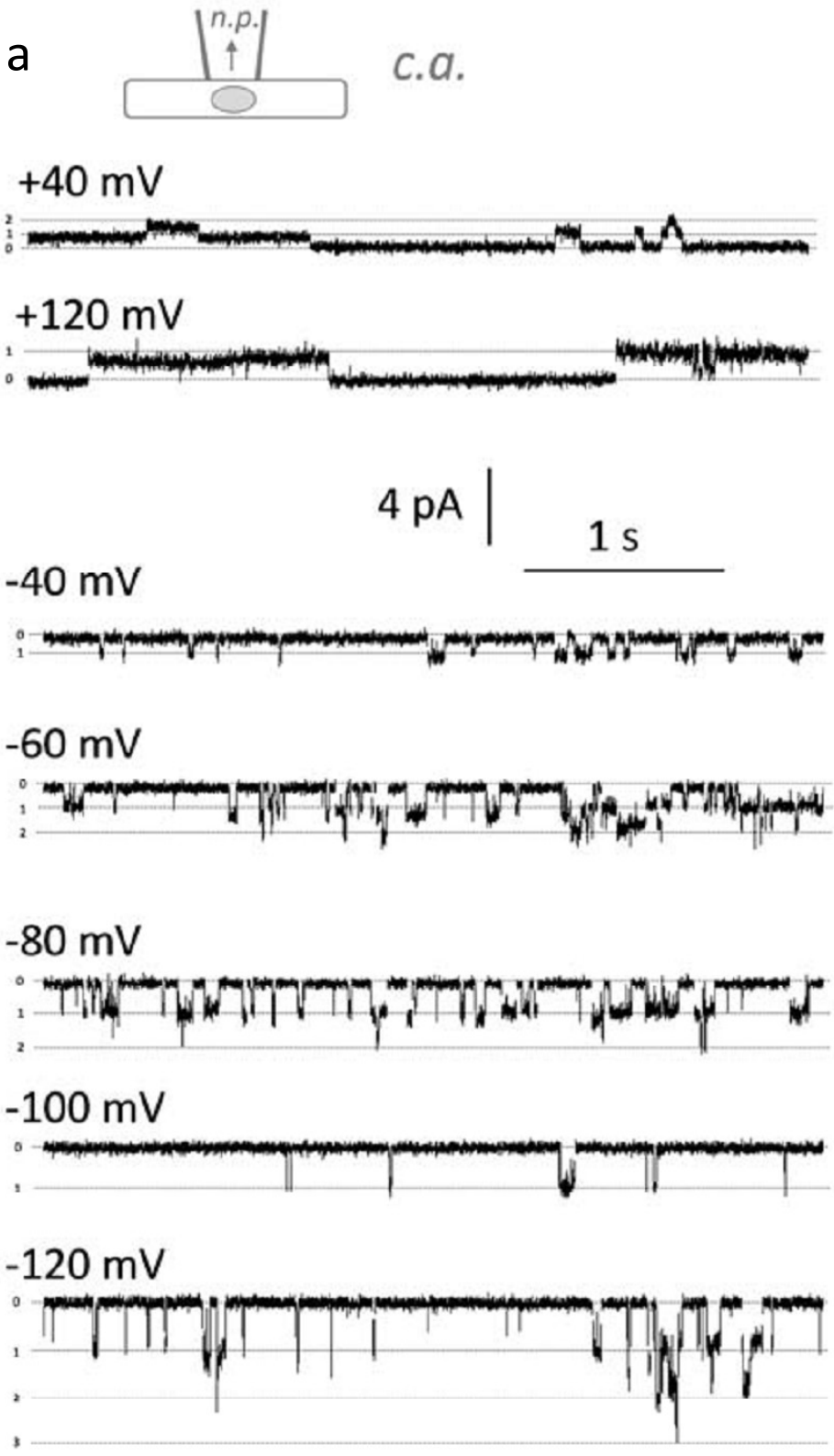
a
n.p.
c.a.
+40 mV
+120 mV
4 pA
1 s
-40 mV
-60 mV
-80 mV
-100 mV
-120 mV

b

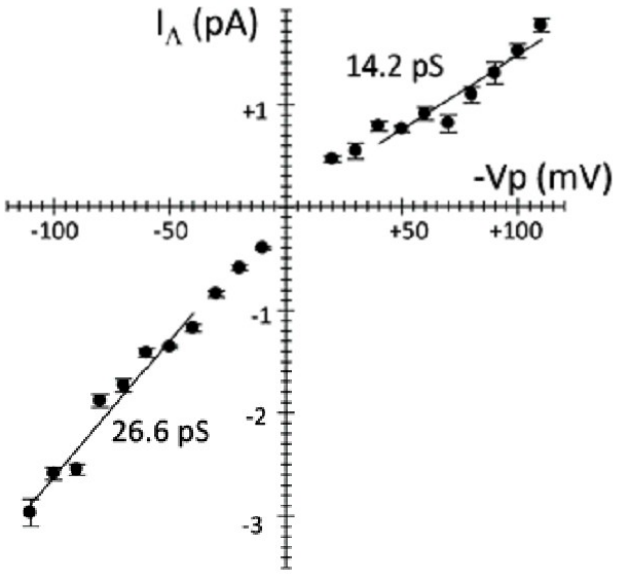

Figure 22.: Single channel conductance properties of MSC in the MCF-7 cellline. [49]

22a.: Original registrations recorded at different potentials during mechanical stress (configuration shown schematically at top). K^+ ions (153 mmole/L) were carrying the inward single channel currents at negative potentials. The size of opening channels was indicated by dotted straight lines with numbers on the left indicating the channel number. 22b.: I/V relation for the single channel currents shown in 22a. Regression region was indicated by black straight line and single channel conductance G_Λ for both inward and outward currents were demonstrated on the graph.

Table 7.: Single channel properties of MSCs in the MCF-7^{WT}cell line (*PFS*). [49]

	Mean ± SEM	*N*
E_{rev} *(mV)*	7.3 ± 1.2	8
G_Λ *(pS); inward*	25.6 ± 0.4	8
G_Λ *(pS); outward*	20.6 ± 2.1	8

Although both EP_{50} and G_Λ values, respectively, are indicative that Piezo1 protein may be the key component of MSCs in MCF-7 cells, members of other ion channel families

have also to be considered as possible candidates for MSCs formation in mammalian cells [24]. Moreover, G_Λ of mPiezo1 has been reported to be variable, since it is blocked by divalent cations, such as Mg^{2+}, Ca^{2+} and Zn^{2+} and hence the close similarity in G_Λ's observed may be misleading [50].

In order to gather additional biophysical distinguishing marks that may help us to identify the molecular nature of MSCs in MCF-7 cells, we evaluated the ion selectivity of MSC in MCF-7 cells by assessing G_Λ for different monovalent and divalent cations under standardized conditions (Figure 23 & Figure 24). Such ion selectivity assessment has been included in nearly all studies of ion channels. For instance, to identify GIRK channels, K^+ specificity was assessed in the beginning of our study. Besides, the permeability profile was evaluated during study of Piezo channels, facilitating the identification of our MSC channel in MCF-7 cells. Figure 23a and Figure 24a shows the original traces using different pipette filling solutions, where the size of channel openings depends on permeability for certain cations. In our study, five monovalent cations and the divalent Ca^{2+} and Ba^{2+} were assessed for ion permeability. Figure 23b and Figure 24b show current-voltage relation comparison of recordings using different pipette filling solutions. Based on each I/V curve, each G_Λ was calculated and summarized in Figure 24c.Among monovalent cations, G_Λ was significantly reduced when Li^+ or Na^+ were used as permeant cations with the succession $Li^+ < Na^+ < K^+ \approx Rb^+ \approx Cs^+$. Divalent cations also permeated considerably, but at significantly reduced G_Λ's, when compared to K^+ under the experimental conditions used. G_Λ was also significantly smaller for Ca^{2+} compared to Ba^{2+} (see Figure 24c showing G_Λ's for different cations). In summary, both distinct and significant differences in G_Λ, the rate of ion permeation across an open MSC, were observed. Ion selectivity of MSCs (measured by the quotient of permeability coefficients (P_{X^+} / P_{K^+}) of the respective ion (P_{X^+}), normalized to the permeability coefficient for K^+ (P_{K^+})), was calculated from the observed reversal potential of single channel currents (I_Λ's). The ratio $P_{Ca^{2+}} / P_{K^+}$ (0.40 ± 0.04; N=4) was significantly lower for Ca^{2+} when compared to K^+, but Ca^{2+} permeation was still substantial as indicated by G_Λ. Ion permeability ratios were close to 1 for the other cations tested (Figure 24d).

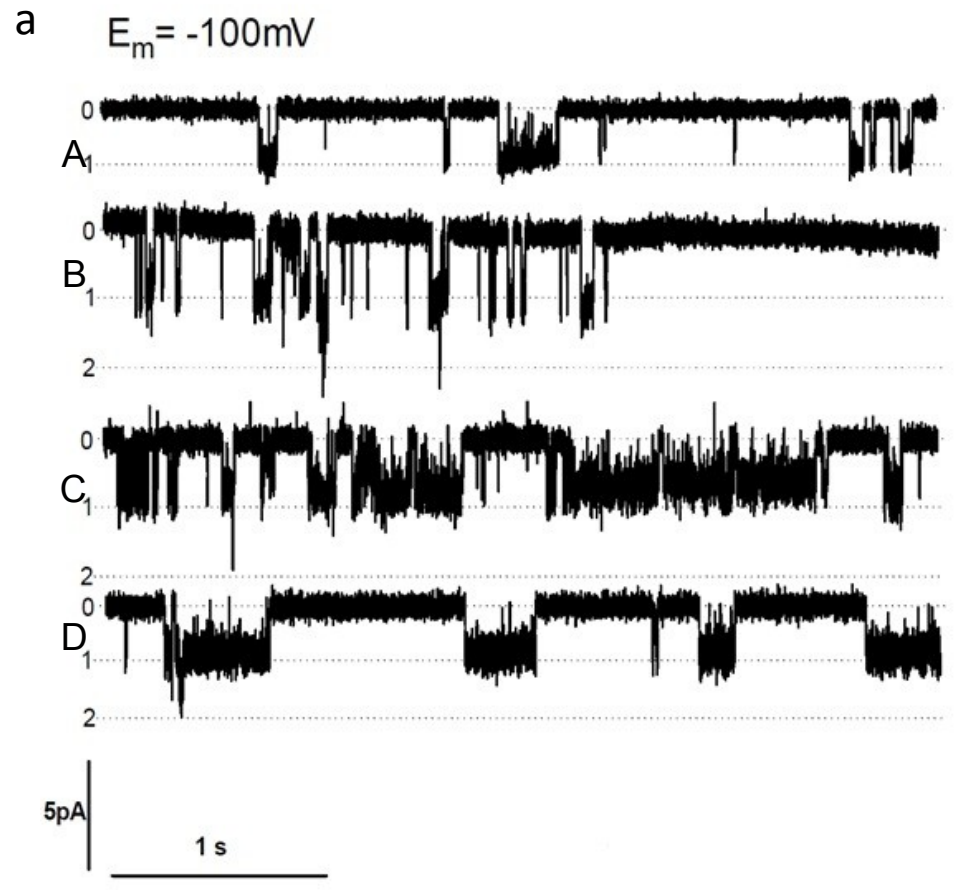

Figure 23a.: Recording traces of MSC in the MCF-7 cellline using different pipette filling solution..

The size of opening channels was indicated by dotted straight lines with numbers on the left indicating the channel number. 5aA.: MSC, 153mM K^+; 5aB.: MSC, 75mM K^+,75mM Na^+; 5aC.:MSC, 37.5mM K^+,112.5mM Na^+;5aD.:MSC, 150mM Na^+.

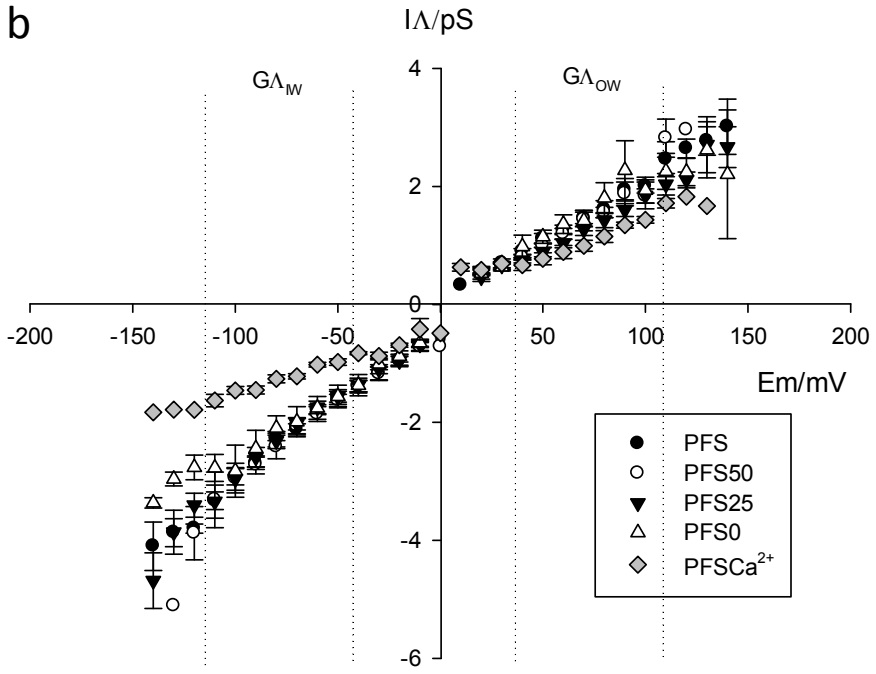

Figure 23b.: Current-voltage relations of MSC in the MCF-7 cell line using different pipette filling solution.

Data points from different recordings were demonstrated by different graphic symbols. The regression regions from which G_Λ (Inward and outward) was calculated were indicated by dotted lines.

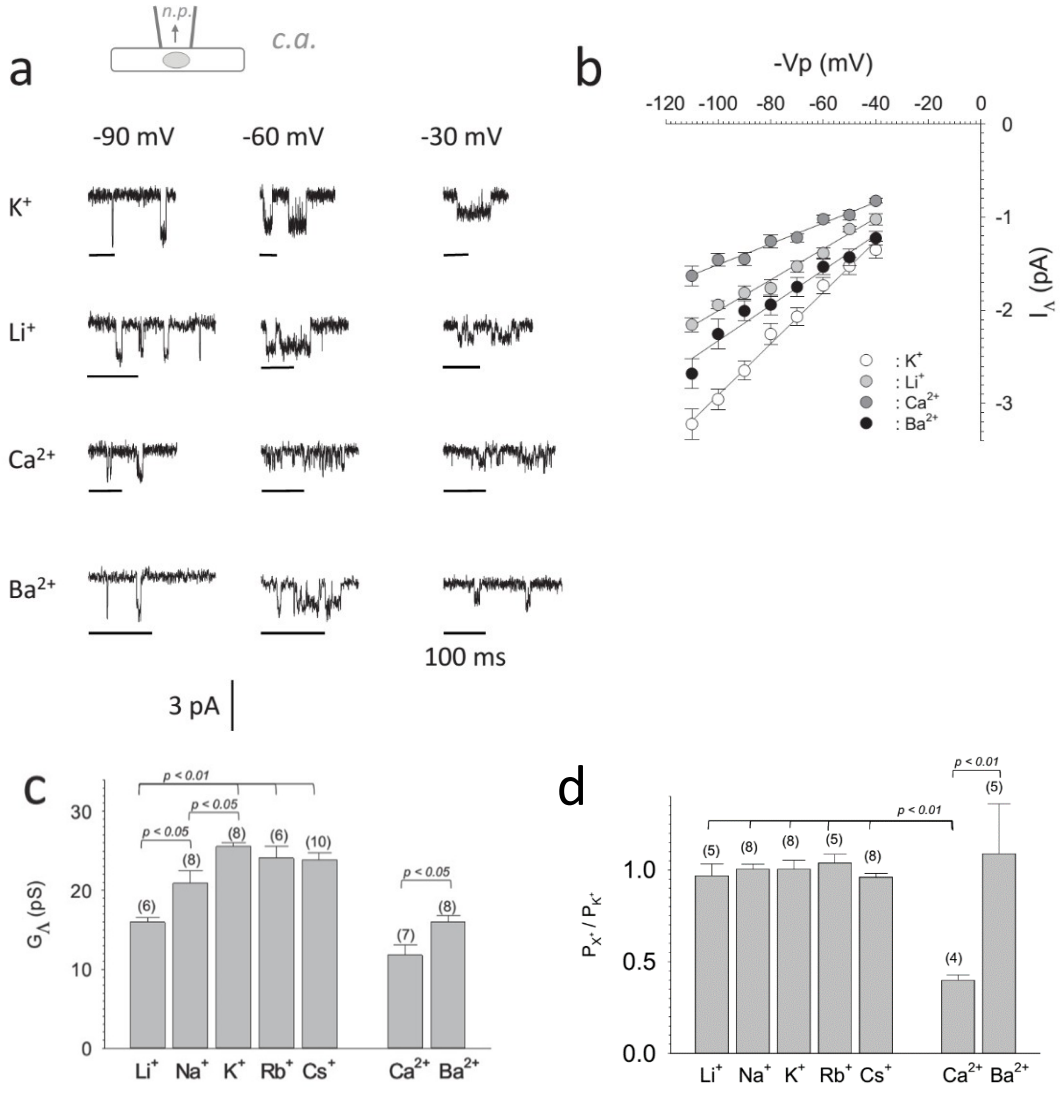

Figure 24.: Ion Selectivity profile of MSC in MCF-7cell line. [49]

24a.: Original registrations recorded in the cell attached configuration at three different potentials during mechanical stress. Different ions were used as charge carriers for the inward currents (153 mmole/L were used in case of monovalent cations and 100 mmole/L in case of divalent cations). 24b.: Average I/V relations for single I_Λ inward currents carried by different cations (N= 6 – 10). Symbols denote mean values ± SEM, line denotes linear regression through the data. 24c.: Ion selectivity profile of inward single channel conductance carried by different mono- and divalent cations. Number of individual experiments is shown at the top of each bar in parenthesis. Mean values ± SEM is shown. 24d.: Bars represent permeability ratios (P_{X+}/P_{K+}), relative to the permeability coefficient for K^+ ions (P_{K+}). Bars represent SEMs. N of experiments is given above each bar in

parenthesis. P_{Ca2+}/P_{K+} is statistically significantly smaller when compared to other P_{X+}/P_{K+}'s ($p<0.01$). First, using the Nernst equation and E_{rev} measured with PFS within the patch clamp pipette, the intracellular K_I^+ concentration was calculated to be 113 mmole/L. Subsequently, P_{X+}/P_{K+} ratios were calculated as described in reference [51].

To further study MSC observed in MCF-7 cell and correlate our MSC and hPiezo1, we overexpressed hPiezo1 in HEK-293 cells and to characterize MSCs, as no MSC can be observed in wildtype HEK-293 cells, being an negative control for further MSC study (Figure 25) [34]. q-PCR technique revealed that mRNA encoding Piezo1 was overexpressed by more than 100 fold in transiently transfected HEK-293 cells, when compared to HEK-293^{WT} (Figure 25E). Accordingly, MSCs that were not observed by us in HEK-293^{WT} cells were frequently recorded from transfected HEK^{hP1} ones (Figure 25a&b; Table 8). Next, G_Λ 's of the resulting MSCs at chosen ion compositions were characterized (Figure 25c&d). Single channel conductance was significantly smaller ($p<0.001$) when Li^+ was used as charge carrier. Ca^{2+} alike MSCs recorded from MCF-7^{WT}, permeated also. G_Λ's assessed for Li^+, K^+, Ca^{2+} and Na^+: K^+ (at a 1:1 molar ratio) were indistinguishable from those of MSCs recorded from MCF-7 cells (Figure 25d). The peculiar G_Λ's profile for different cations observed by us strongly suggest that MSCs in MCF-7 are composed of Piezo1 protein.

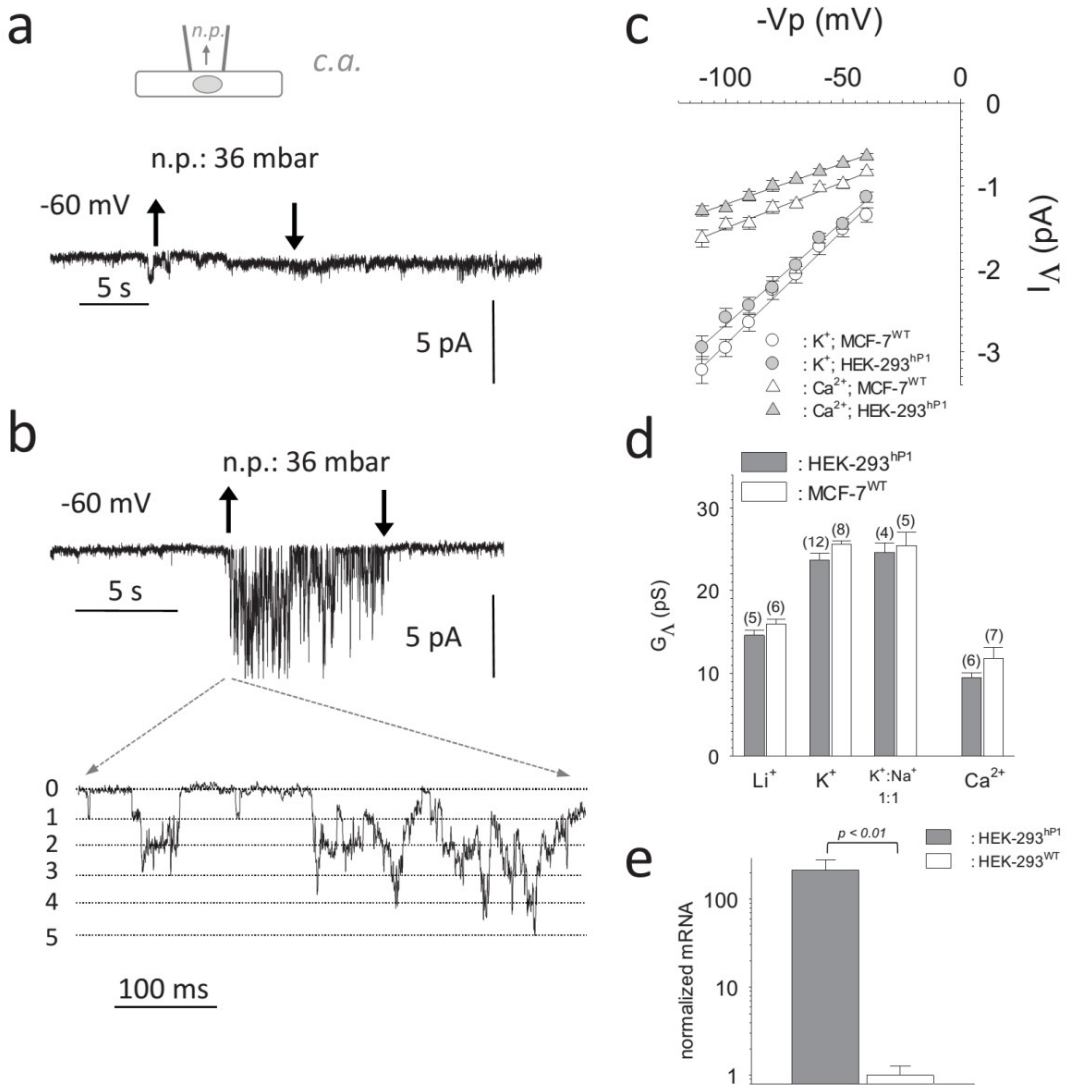

Figure 25.: Heterologous overexpression of hPiezo1 in the HEK cell line. [49]

25a.: Original registration from untransfected HEK-293 cell (configuration shown schematically at top). 25b.: same as 4A, but cell was transfected with biscistronic pIRES2 containing hPiezo1 and eGFP as inserts. 25c.: Average I/V relations for single I_Λ inward currents carried by 153 mmole/L K^+ (grey circles) and 100 mmole/L Ca^{2+} (grey triangles). White symbols denote I_Λ's recorded from MCF-7 cells, lines represent a linear regression through the data (N = 5 – 8). 25d.: Ion selectivity profile of inward single channel conductance carried by different mono- and divalent cations and by Na^+:K^+ at a 1:1 ratio. Number of individual experiments is shown at the top of each bar in parenthesis. Mean values ± SEM is shown. 25e.: Quantitative RT-PCR assessing the fold increase in the number

of hPiezo1 mRNA transcripts upon transient transfection of HEK-293 cells with the pIRES2 construct (data were derived from 3 individual transfection experiments). Mean values ± SEM is shown.

Table 8.: Frequency of occurrence of MSCs in the cell lines used. [49]

	Total number of patches	*Number of patches with MSCs*	*% of patches with MSCs*
MCF-7^{WT}	291*	157	54%
*MCF-7$^{TrpC_k.o}$***	39	22	56%
HEK-293^{WT}	16	0	0%
HEK-293^{hP1}	44	27	61%
MCF-10A^{WT}	30	0	0%
MCF-10A^{hP1}	45	28	62%

**: Numbers included patches using all kinds of pipette filling solution.*

***: stably expressing cell line.*

In order to generate additional data that would contribute to MSC identification, further cell line fabrication and patch clamp experiment screening were performed. To exclude the possibility of MSC forming by other ion channel families, we have engineered a MCF-7 based cell line overexpressing a dominant negative TrpC subunit (MCF-7$^{TrpC_k.o}$). Overexpression of the ion permeation deficient subunit is expected to eliminate currents through channels formed by TrpC proteins that are known homo- or heteromerization partners, for instance, TrpC1, TrpC3, TrpC4, TrpC6 and TrpC7 [40]. If TrpC subunits involve in MSC formation in MCF-7 cells, a significant reduction in the number of functional ion channels would be expected in the MCF-7$^{TrpC_k.o}$cell line. After all, the frequency of occurrence of functional MSCs in both cell lines was similar, suggesting that TrpC subunits are not involved (Table 8).

Table 9.: Activation of MSCs by negative pressure in the different breast cancer cell lines studied. [49]

	EP_{50}± SEM (mm Hg)	b± SEM(mm Hg^{-1})*	N
MCF-7^{WT}	40.8 ± 1.1	9.1 ± 1.0	18
MCF-10A^{hP1}	38.7 ± 1.1	5.9 ± 1.1	4

**.: b represented the slope of the sigmoid curve.*

MCF-7 cells have been cultivated from invasive ductal carcinoma and exert the luminal gene cluster subtype signature [52]. Subsequently we investigated whether non-cancerous breast cells do also possess functional MSCs at the surface. Accordingly, the MCF-10A line, derived from human fibrocystic mammary tissue and representing an immortal non neoplastic MEC line [53] was used as a model for normal mammary gland cells. Under our standardized experimental conditions we could not detect functional MSCs in MCF-10A cells (Figure 26a; Table 8).

Western blot assay was performed by my colleague Sarah Kammerer to check the existence of possible hPiezo1 protein in wild type or transfected celllines. Several commercial antibodies targeting hPiezo1 protein were applied, but no one gave specific band as the product sheet claims. Two antibodies were found from internet, one from Abcam (Name: Anti-FAM38A antibody; Rabbit polyclonal to FAM38A; # ab82336) and the other from Proteintech (Source: Rabbit; Isotype: IgG; Cat. #: 15939-1-AP). As shown in Figure 26, no band appeared near the top edge of gel, indicating no specific band for hPiezo1, which is 286kDa, while only unspecific bands were observed. Therefore, q-PCR was applied to acquire indirect evidence of the existence of hPiezo1 amongst celllines.

a

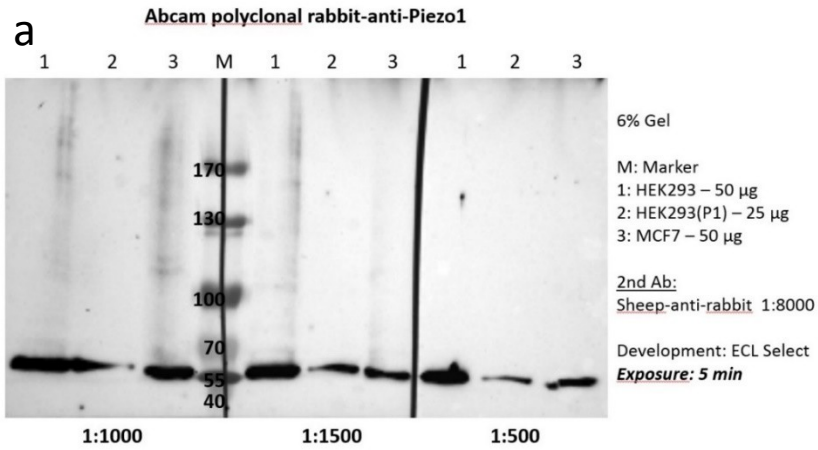
Abcam polyclonal rabbit-anti-Piezo1
1 2 3 M 1 2 3 1 2 3
170
130
100
70
55
40
1:1000
1:1500
1:500
6% Gel
M: Marker
1: HEK293 – 50 µg
2: HEK293(P1) – 25 µg
3: MCF7 – 50 µg
2nd Ab:
Sheep-anti-rabbit 1:8000
Development: ECL Select
Exposure: 5 min

b

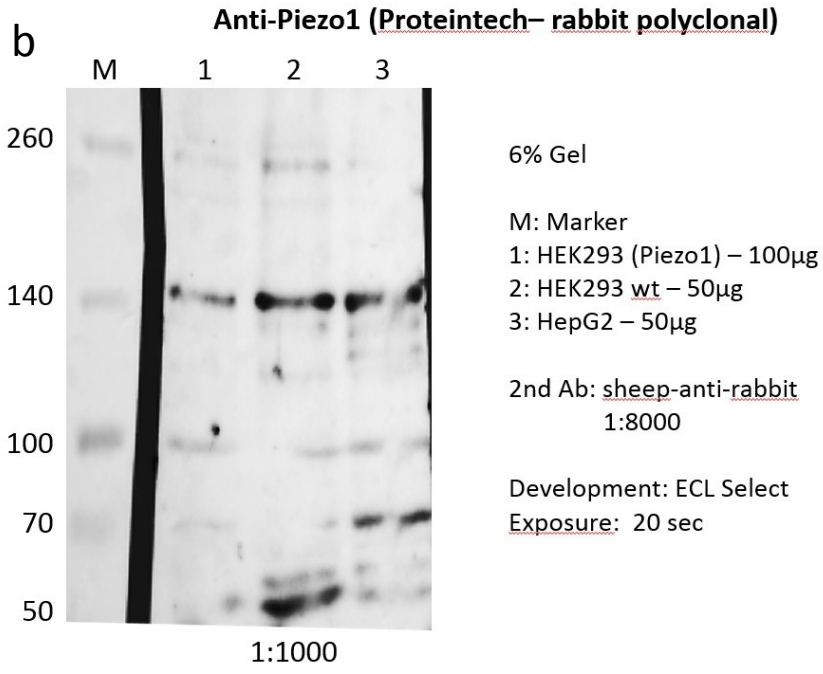
Anti-Piezo1 (Proteintech– rabbit polyclonal)
M 1 2 3
260
140
100
70
50
1:1000
6% Gel
M: Marker
1: HEK293 (Piezo1) – 100µg
2: HEK293 wt – 50µg
3: HepG2 – 50µg
2nd Ab: sheep-anti-rabbit
1:8000
Development: ECL Select
Exposure: 20 sec

c

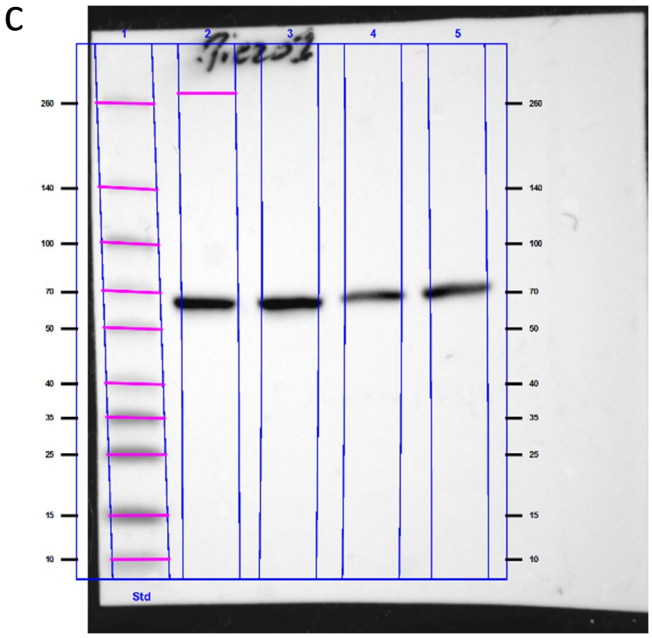
1 2 3 4 5
260
140
100
70
50
40
35
25
15
10
Std

Figure 26: Western blot assay for checking hPiezo1 protein expression amongst celllines.

Figure 26a demonstrated results using antibody form Abcam, while in Figure 26b, antibody from Proteintech was applied. In both figures, marker was on the left side, ratio on the bottom was the antibody dilution ratio, and the experiment detail was on the right side. Figure 26c demonstrated the exact position where Piezo1 band located (The pink line in the second column).

q-PCR revealed that mRNA encoding Piezo1 is substantially reduced in MCF-10A compared to MCF-7 cells, but not entirely absent (Figure 27d, right). When cDNA encoding human Piezo1 was overexpressed transiently in MCF-10A cells, endogenous Piezo1 mRNA levels increased by over 10 fold (Figure 27d, left). Consequently MSCs with single channel conductance for K^+ indistinguishable from those obtained from wildtype MCF-7 and transfected HEK-293 cells were observed (Figure 27c&e, Table 9). The results indicate that MCF-10A cells are able to express MSCs formed by Piezo1 protein, but endogenous expression is not sufficient to form functional channels.

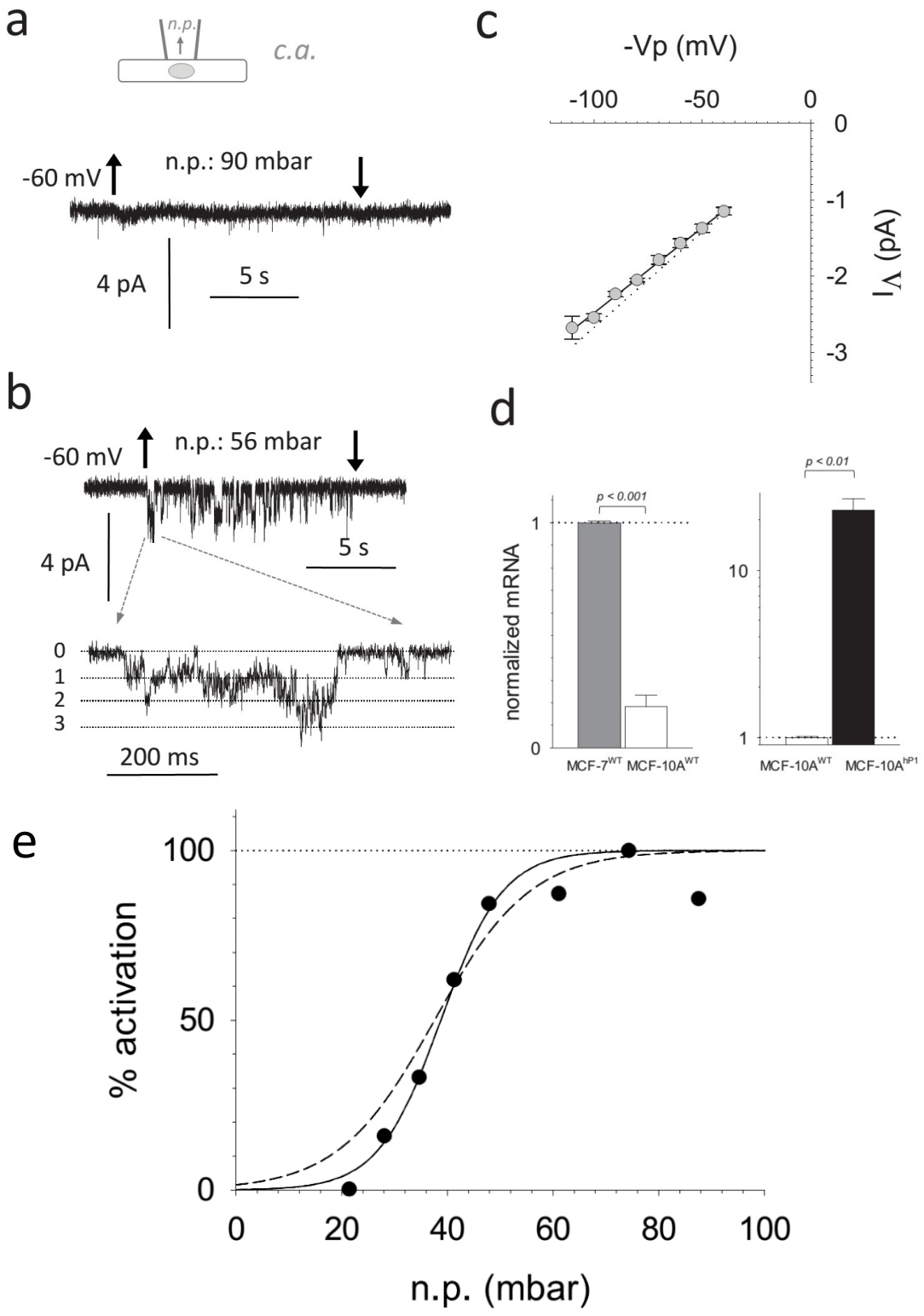

Figure 27.: Single channel conductance properties of hPiezo1 expressed in the MCF-10A cell line. [49]

27a.: Original registration from untransfected MCF-10A cell (configuration shown schematically at top). 27b.: same as 9a, but cell was transfected with biscistronic pIRES2

containing hPiezo1 and eGFP as inserts. 27c.: Average I/V relation for single I_{Λ} inward currents carried by 153 mmole/L K^+. Lines represents a linear regression through the data (N = 5), dotted line represents I_{Λ} recorded from HEK-293 cells under identical conditions. 27d.: left: Quantitative RT-PCR assessing the relative amount of hPiezo1 mRNA transcripts of MCF-10A^{WT} cells compared to MCF-7^{WT}. Mean values ± SEM is shown (N = 3). Right: the fold increase in the number of hPiezo1 mRNA transcripts upon transient transfection of MCF-10A with the pIRES2 construct. Mean values ± SEM is shown (N = 3). 27e.: Filled circles represent mean values derived from 4 individual patches. Solid line represents fit through the data. Dashed line represents activation curve of MSCs in MCF-7^{WT} as shown in Figure 21b.

Migration, motility and invasion represent an essential hallmark of cancer cells, essential for malignancy and metastasation [54]. Moreover, Ca^{2+} permeable MSCs have been mentioned above to be pivotal for cell motility and migration [39]. Subsequently we investigated whether MSCs formed by Piezo1 may regulate these cellular properties. Motility and velocity of MCF-7^{WT} cells were studied in the absence and in the presence of GsMTx-4 (Figure 28a&b) in the standardized culturing medium, a peptide toxin from Chilean rose tarantula venom, known to block functional Piezo1 channels [55]. Both cellular velocity and motility of MCF-7^{WT} cells were reduced by the presence of GsMTx-4 (Figure 28c&d). On the contrary, GsMTx-4 did not affect velocity or motility of MCF-10A^{WT} cells (Figure 28e&f). This observation further supports a role of Piezo1 in motility of the cancerous MCF-7 cell line.

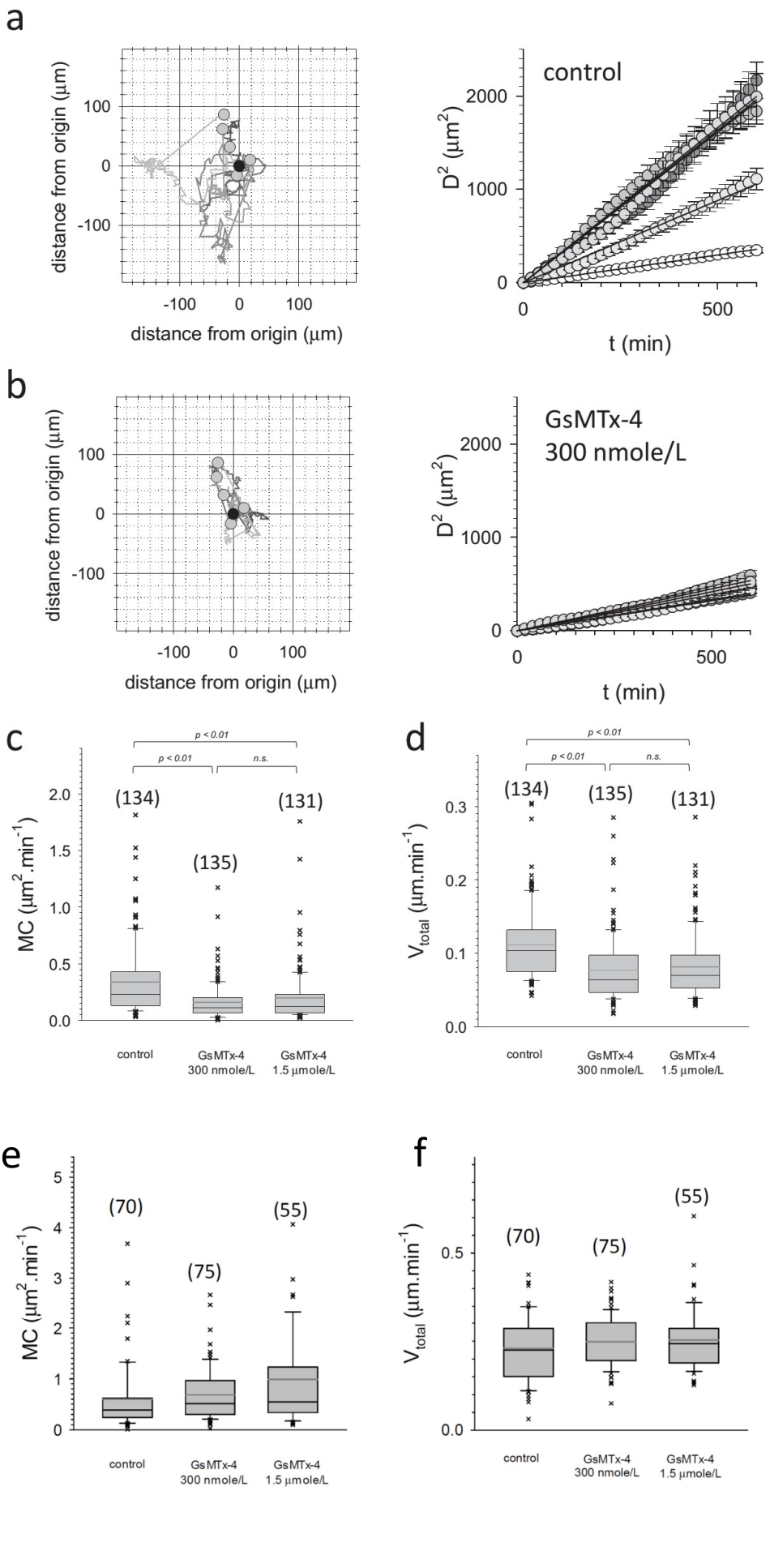
a
distance from origin (µm)
100
0
-100
-100
0
100
distance from origin (µm)
control
D² (µm²)
2000
1000
0
0
500
t (min)
b
distance from origin (µm)
100
0
-100
-100
0
100
distance from origin (µm)
GsMTx-4
300 nmole/L
D² (µm²)
2000
1000
0
0
500
t (min)
c
p < 0.01
p < 0.01
n.s.
MC (µm².min⁻¹)
2.0
1.5
1.0
0.5
0.0
(134)
(135)
(131)
control
GsMTx-4
300 nmole/L
GsMTx-4
1.5 µmole/L
d
p < 0.01
p < 0.01
n.s.
V_total (µm.min⁻¹)
0.3
0.2
0.1
0.0
(134)
(135)
(131)
control
GsMTx-4
300 nmole/L
GsMTx-4
1.5 µmole/L
e
MC (µm².min⁻¹)
5
4
3
2
1
0
(70)
(75)
(55)
control
GsMTx-4
300 nmole/L
GsMTx-4
1.5 µmole/L
f
V_total (µm.min⁻¹)
0.5
0.0
(70)
(75)
(55)
control
GsMTx-4
300 nmole/L
GsMTx-4
1.5 µmole/L

Figure 28.: Effect of GsMTx-4 on migration and velocity of MCF-7 cells. [49]

28a.: left: Migration trajectories of five single MCF-7^{WT} cells over the entire observation interval of 72h. Right: Squared distance as a function of time for the five cells shown to the left. 28b.: similar to 6A but in the presence of 300 nmol/L GsMTx-4. 28c.: statistical analysis of motility coefficients. Black line in box marks median, upper and lower borders of box mark 25% and 75% percentiles, error bars mark 10% and 90% percentiles, respectively; black crosses mark individual single cell velocities below and above the 10% and 90% percentiles. Grey line marks mean value. Number of individual cells studied is shown in parenthesis above each box. The dataset was checked for statistical significant differences using ANOVA based on ranks. 28d.: similar to 9c but cellular velocities are shown. 28e&f.: similar to 10c&d, respectively, but the statistics for MCF-10A cells.

The observations derived from models of benign and malign MECs prompted us to investigate whether overexpression of mRNA encoding Piezo1 in the primary tumor may be related to clinical outcome in breast cancer patients. A dataset generated from GEO and comprising overall survival data for 1115 patients (version 2014) was used [48]. Overall survival times of breast cancer patients with low mRNA expression for Piezo1 in the primary tumor turned out to be significantly longer when compared to patients with high expression levels (Figure 29). This finding is of strong support that high levels of Piezo1 in the tumor have causal and profound impact on disease progression.

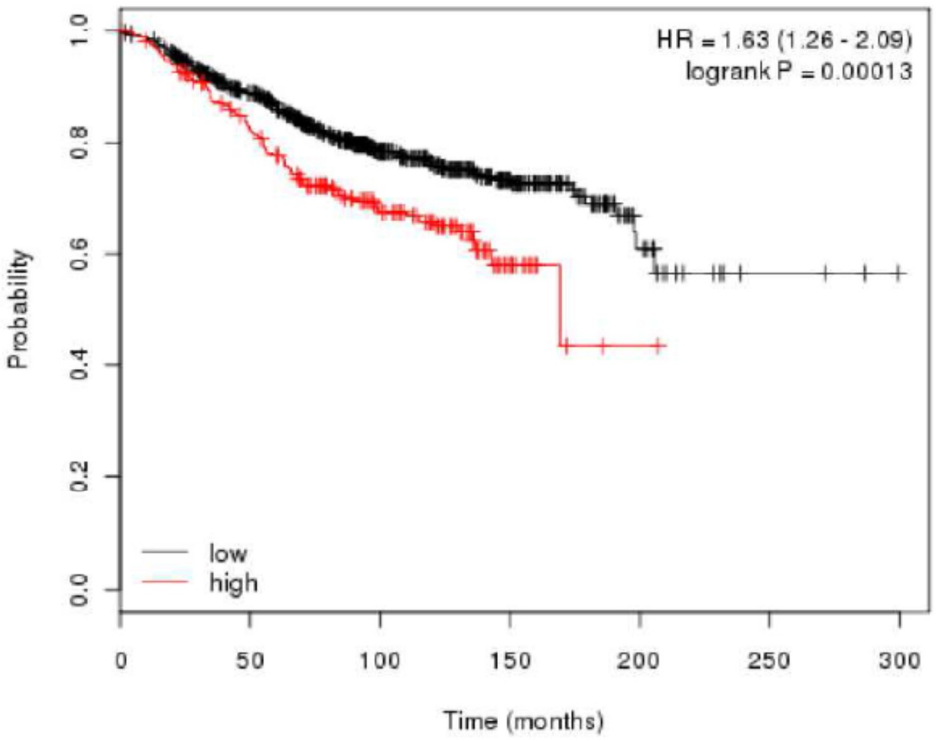

Figure 29.: Overall survival of breast cancer patients with low and high expression of Piezo1 mRNA in the primary tumor. [49]

Kaplan–Meier plot showing overall survival of breast cancer patients with low and high expression levels of Piezo1 mRNA. Grey line: patients with high expression of Piezo1; black line: patients with low expression. The cutoff value for distinguishing high and low expression was 1760 tpm (transcripts per million), calculated by the software. Hazard ratio (HR) was 1.63 (1.26 – 2.09; 95% confidence interval), P < 0.000013, N = 1115).

DISCUSSION

Here we report the existence of functional mechanosensitive ion channels in a malignant human MEC line. Wagner V., previously working with Prof. Schreibmayer as a PhD student and performing precursor work of my thesis project, and co-workers demonstrated a preliminary finding about MSC in MCF-7 cells when they tried to screen GIRK channel among human breast cancer celllines using single channel recording method [unpublished results]. In Wagner's preliminary pilot studies, 8 successful patches in MCF-7 cells were tested for presence of MSCs, among which MSC was observed in 6 patches. While, 5 successful patches were made from MCF-10A cells and no MSC appeared. Then we continued to screen and characterize this channel in MCF-7 cells transfected with different GIRK splice variants, looking for functional GIRK channels. The characterization of MSC, which indicated that it was not related with any of the GIRK splice variants, together with the large occurrence rate of MSC in MCF-7 cells, urged us to explore further role of MSC in human breast cancer cell.

Single channel analysis revealed, for the first time, that Ca^{2+} permeation of MSCs in the MCF-7 line is substantial. Furthermore, characteristic differences in G_Λ for Li^+ and Na^+, the smallest alkali metal ions tested in this project, were found when compared to G_Λ for other alkali metal ions (K^+, Rb^+, Cs^+; unexpectedly and also for the first time). Among monovalent and divalent cations studied, G_Λ was inversely related to the radius of the hydrated ion suggesting that these ions may pass the open pore in the hydrated configuration.

Not only single channel conductance and permeability for different cations was studied, the sensitivity of MSC to mechanical stress was also assessed for MSC in both native MCF-7 cells and HEK-293 cells overexpressed with hPiezo1 construct. Based on our studies, there are several facts that prompted us to identify Piezo1 as a component of MSCs in MCF-7 cells: (i) G_Λ's permeating potassium ions were indistinguishable between MSCs from MCF-7 and MSCs formed by overexpressed Piezo1 in both HEK-293 cells and MCF-10A cells, whose difference was not statistically significant; (ii) The particular ion permeation properties with respect to G_Λ's for different cations as described above were identical between MSCs from MCF-7 and MSCs formed by transiently overexpressed Piezo1 in HEK-293 cells, whose difference was not statistically significant, either; (iii) MSCs in cell attached patches of MCF-7 cells exerted similar mechanical sensitivity when

compared to MSCs formed by overexpression of Piezo1 in HEK-293as well as in MCF-10A cells [32, 34]. The dose response against negative pressure as was similar for MSC in native MCF-7 patches and MSC in HEK-293 overexpressed with hPiezo1 construct; (iv)Since canonical Trp subunits could also form a variety of mechano-sensitive ion channels (stretch-activated channels) [26, 27], we generated a cell line that Trp subunits were dominantly negative. MSC screening results indicated that the occurrence rate of MSCs in MCF-$7^{Trp\_k.o.}$ cells remained similar to that in native MCF-7 cells, and to that in another positive control cellline, MCF-7^{scr} cells, either. Therefore, we can conclude that our MSC was not mainly formed by canonical Trp family subunits.

When a benign MEC line MCF-10A, was screened via the patch clamp method, no functional MSCs were observed. Then we tried to introduce hPiezo1 construct into this silent benign MEC line to see whether identical channel can be observed. In our experiment, transfection of hPiezo1 construct into MCF-10A cells was much harder than other transfection in our study. In the beginning, several transfection reagents were used for hPiezo1 transfection into MCF-10A cells and nearly no fluorescence could be observed under fluorescent microscope used for patch clamp recording, and thus recordable cells cannot be localized during recording. The transfection was not completely failed, as faint fluorescence could be observed when the cells were excited by high energy laser set and captured by more sensitive microscope. Only lipofectomine was efficient enough for induce hPiezo1 construct into MCF-10A cells and the transfection cells could be localized for cell attach recording under the fluorescent microscope of patch clamp setup. However, transfection using lipofectomine caused much more cell death than using other transfection reagents, thus more confluent cell was required for lipofectomine transfection. Moreover, hPiezo1 construct is much bigger than other constructs we used before, which might be the reason why stronger reagent was needed only for hPiezo1 transfection into only MCF-10A cells, not for GIRK variants, or not for MCF-7 and HEK-293 cells. The difficulty of inducing hP1 construct into MCF-10A cells could also be demonstrated by the different transfection efficiency in HEK-293 and MCF-10A transfection, respectively. RT-PCR results indicated that after transfection, hP1 mRNA expression level increased by over 100-fold in HEK-293 transfected cells, while in MCF-10A transfected cells, only 10-fold level increase was detected after transfection. Under fluorescent microscope, a large number of HEK-293 and MCF-10A cells was successfully transfected with hGIRK1 construct in the control plate,

which could be observed with very good fluorescence, perfect cell morphology and good plasma membrane strength for long time patch clamp recording.

Expression levels for mRNA encoding Piezo1 were substantially lower in wild-type MCF-10A when compared to MCF-7, but not negligible. In this context it is worth mentioning that the cDNA encoding human Piezo1 has been initially extracted from wild-type HEK-293 cells line where no functional MSC was observed by us as results indicated, and could be used for point mutation studies [34]. MCF-10A is, however, frequently used as a negative control, both in biochemical and electrophysiological experiments, demonstrating that the endogenous mRNA levels are not sufficient to produce high amount of Piezo1 protein, as forming a functional Piezo1 ion channel may require four Piezo1 proteins [32]. Thus a low density (or even absence) of functional MSCs in the plasma membrane despite of moderate mRNA levels is not an unusual situation, thus researchers can isolate hPiezo1 construct in HEK-293 wild type cells, as mentioned before. There are several reasons that may account for the absence of functional MSCs within plasma membrane of native MCF-10A cells: (i) Since we only screened MCF-10A cells for 30 cell attach patches, and we haven't ever performed whole cell recording during our study, endogenous mRNA encoding Piezo1 does not produce MSCs at sufficient high numbers that can be detected by the cell-attached method within 30 trials; (ii) The resulting small amount of protein is not inserted into the plasma membrane, but into other intracellular membrane structure, like nuclear membrane or endoplasmic reticulum; (iii) Endogenous Piezo1 protein is directed towards protein complexes, where it cannot be activated by simple mechanical stimulation or its mechanosensitivity is blocked by certain protein within the complexes and only heterologous Piezo1, inserted somewhere else, can be stimulated by mechanical stress only; (iv) Endogenous Piezo1 protein doesn't bind with any other protein, but it is blocked by endogenous factors after translation. Such blocking effect is limited, as when the concentration of Piezo1 protein increases dramatically due to transfection, functional ion channel will appear on plasma membrane (see e.g.: [56]).

Several studies, that have been reviewed in reference [39], have addressed so far the effects of mechanical stress on cancerogenesis and tumor progression in benign and malign mammary epithelial celllines (MECs) and thereupon may shed light on potential roles of increased densities of MSCs in the plasma membrane of malignant MECs: Increased densities of MSCs in MCF-7 cells, which is malign breast carcinoma celllines, is being

regarded as response to the effect of compressive stress from extracellular matrix on proliferation, apoptosis, migration and cytoskeletal architecture of several MECs, while the disappearance of MSC in MCF-10A cells, which are non-tumorigenic and much less mechanosensitive than their malign counterparts, such as 4T1 and MDA-MB-231,indicating little response of MCF-10A cells to mechanical stress, may well be involved in the fact that the migration of this normal mammary epithelial cells were significantly suppressed by compressive stress[57]. Using a three dimensional microlithography based approach, it was found that proliferation and invasion of several lines of malignant MECs occurred preferentially in regions experienced high endogenous mechanical stress when those tumor cells were embedded in non-malignant tissue and surrounded by collagen [58]. This study confirmed the role of mechanical stress in promoting the malignant phenotype progression of potential tumor tissue, and further supported our speculation of MSCs in cancerogenesis and tumor progression. In another study, Shi Q. and his colleagues studied the impact of long-range mechanical interaction exerted via interconnected long collagen lines on the disorganization of ras-transformed mammary acini formed by MCF-10AT cells was well studied. Mechanical interaction between MCF-10AT acini was shown to facilitate the transition to the invasive phenotype. When such mechanical connection was disconnected, the speed of transition process reduced, and if MCF-10AT acini were fully mechanically isolated, the transition was blocked [59]. A review summarized the influence of physical cues on cellular signaling and further on generation and development of diseases, especially the general role of mechanical stress in pathogenesis and progression of breast cancer as well as the influence of mechanosensitive signaling transduction on proliferation, invasion and differentiation of peculiar MECs [60]. The findings about mechanical cues inside or outside cells described above fit reasonably to the hypothesis that a high density of MSCs in malignant MECs intensifies their reaction to the cues, thereby extremely promoting tumor malignancy. It must be stated, however, that in those studies or reviews mechanosensation and mechanotransduction by MECs is generally considered to be based on a molecular machinery that does not necessarily entail ion channels: The molecular chain of events comprises ligands of the extracellular matrix or from neighboring cell, that bind to integrins thereby inducing integrin clustering, formation of focal adhesion sites and subsequent activation of focal adhesion kinase (FAK), a central intracellular effector of mechanotransduction, which is necessary for the cell in response to matrix stiffness and further leading to intracellular signaling pathway activation, inducing invasive phenotype [61]. Many different protein subunits, to be specific 156 components, in this signaling net

where hundreds of interactions occurs in between (integrin-adhesome) (Figure 30), but also elements of the glycocalyx, which drives integrin clustering and promotes metastasis, have been identified to participate in and to regulate this process [62, 63].

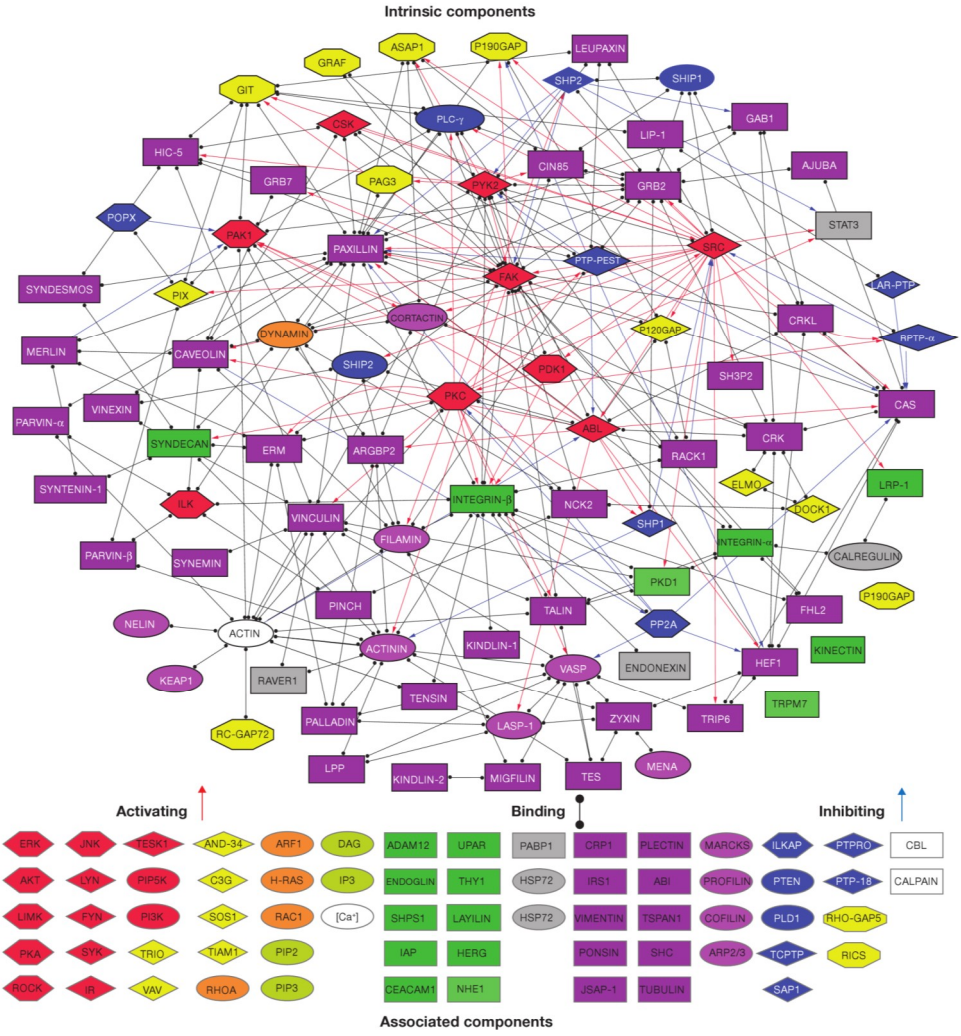

Figure 30: Interactions between all intrinsic components of the adhesome and a grouped list of the associated components.

Black lines with full circles at their ends demonstrat non-directional binding interactions, blue arrows represent directional inhibition (for example, dephosphorylation, G-protein inactivation or proteolysis) and red arrows represent directional activation (for example, phosphorylation or G-protein activation) interactions. The nodes are shape- and colour-coded according to the function of the proteins. Intrinsic components are surrounded by a black frame and associated components by a grey frame. [64]

Then the question is what role of MSCs plays in this network. Whether MSCs formed by Piezo1 are hitherto one of the unrecognized constituents of this molecular machinery where MSCs signaling acts together with biochemical signaling pathways or whether MSCs provide MECs with a sensorium for only mechanical cues that acts in parallel and independently as mechanosensitive signaling pathway. Piezo1 was demonstrated to play essential role in the former pathway since those researchers demonstrate that Ca^{2+} entry through MSCs of the plasma membrane is required to trigger mechanoreception via the integrin-adhesome, and the Piezos were proved to be related with Fam38 which is involved in regulating integrin affinity by facilitating Ca^{2+} release from endoplasmic reticulum. Together with the facts that TRPV4 channels are demonstrated to play a role in conformational integrin activation, researchers speculated that Piezo channels might modulate TRP class channels activity and downstream signaling pathways by provoking a transient calcium ion influx [65~68]. In addition, it is notable that the first biological function found for Piezo1 protein was integrin activation by increasing intracellular Ca^{2+} levels: Expression of a GFP-tagged Piezo1, which had been proved to localize predominantly to the endoplasmic reticulum in CHO (αβ-py) cells, triggered integrin dependent cell adhesion by influencing calcium ions release from ER while knockout of Piezo1 resulted in the opposite [69]. Thus it is presumable that Piezo1 play vital role in the whole integrin mechanosensation machinery. Upon overexpression of Piezo1 in malignant MCF-7 cells this machinery becomes hyperactive. On the other hand, Piezo1 ion channels may also provide a separate and parallel pathophysiological mechanosignaling transduction pathway that acts in addition to integrin signaling. More experimentation is required to allocate the exact location of Piezo1 in the molecular landscape of MEC mechanotransduction, which may help to answer the question why there is mRNA expressed in MCF-10A cell but no functional MSC observed. The operative mechanism of Piezo1 in MCF-7 cells is currently under investigation.

Although the Fam38a and Fam38b gene products (i.e.: Piezo1 and Piezo2) only recently have been identified as templates for mechanosensitive ion channel proteins [32], several physiological functions have already been identified so far: Piezo2 protein plays major role in somatosensation of touch in mice corneal afferent neurons, and in rat Merkel cells [70~72]. Piezo2 is also indispensible for mechanosensitivity and mechanotransduction of human stem cell-derived touch receptors [73]. Involvement of Piezo1 protein other than the nervous system have been found in many studies. Piezo1 also plays a role in regulating

live cell extrusion, which is important for maintaining homeostatic cell numbers in epithelia and may involve in a tumor-suppressive mechanism by preventing the uncontrolled proliferating epithelial cells [74]. As a sensor to shear stress in vascular endothelial cells, Piezo1 is important for embryonic development of the circulatory system and for triggering the response of urothelium to bladder extension [75~77]. The role of Piezo1 in erythrocyte volume homeostasis has also been demonstrated [78]. All these studies demonstrate that Piezos have been recognized as key sensor that links to transduce physical signal into physiological response of cells.

Piezo proteins have also been demonstrated to play pathological roles in many human diseases: Gain of function mutations in both Piezo1 and Piezo2 protein have been identified as the basis for different pathologies such as Xerocytosis and Distal Arthrogryposis, respectively, where mutations were identified within Piezos genome extracted from patients samples, causing mechanosensitive channels dysfunction [34, 79]. Besides, researchers found two missense mutations in Piezo1 channel within red blood cell membrane from patients with dehydrated hereditary stomatocytosis [80, 81]. Piezo1 mutations were found to induce many other diseases, such as hereditary xerocytosis and familial haemolysis, as well as dehydrated stomatocytic anemia [82, 83]. In addition to our findings other data suggest that Piezo1 protein is involved in cancer: There is a larger amount of expression of mRNA encoding Piezo1 has been detected in the lung and also in lung epithelial cells amongst the tissues studied. However, its exact physiological role still remains to be revealed [32, 84]. Researchers have tried to study the relation between Piezo1 expression and cancer development. McHugh B.J. and his colleague studied three small lung cancer cells where Piezo1 expression was found to be greatly reduced, while in normal lung epithelial cells the expression was observed high. They knocked down Piezo1 protein utilizing siRNA and found that depletion of Piezo1 in normal lung epithelial cells promoted an amoeboid, reduced integrin-dependent, mode of cell migration. Migration assay showed that after treatment, Fam38A siRNA cells migrated further than their control counterparts [84]. Interestingly, in the prevailing study we observed the opposite, i.e. that mRNA expression of Piezo1 was low in benign MECs (MCF-10A), while significantly higher levels in the malign MCF-7 cells, leading to functional MSCs within the plasma membrane of MCF-7 cells, which greatly influenced cell migration in the subsequent migration assay. Similar to our results, knockdown of Piezo1 in gastric epithelium cancer cells has been shown to co-localize with peptide that involves in epithelial restitution and cell motility, and reduce cell

migration. The authors also performed wound healing assay, suggesting that Piezo1 knockdown reduce invasion and metastasation of gastric cancer cell migration, while overexpression promotes [85]. Piezo1 was also amongst the most profoundly upregulated genes in thyroid cancers following Iodine-131 exposure after the Chernobyl accident [86]. In summary, existence of Piezo1 expression in various kinds of cancer indicating that deregulated Piezo1 expression may contribute to cancer of several types of tissue.

My colleague Sarah Kammerer assessed the relation between Piezo1 expression and breast cancer development of patients. Patients with relatively higher Piezo1 mRNA expression level in their primary breast cancer tissue showed significantly shorter overall survival time compared with those with lower expression level. High hazard ratio (1.63) indicated stronger influence of Piezo1 expression on the development of breast cancer, and further the survival time of patients. These two assessments substantiated the role of Piezo1 in progression of breast cancer. This novel role of Piezo1 in cancer biology seems to be a peculiar manifestation in breast cancer that is different to the role of Piezo1 in lung cancer, as we mentioned before, indicating tissue specificity of Piezo1 expression among different human tissues. Further research will reveal whether Piezo1 is causally involved in cancerogenesis and progression of breast cancer, and the its possible role in certain signaling pathway that influences pathogenesis of normal epithelial cell or cancer cell, which represents a potential therapeutic target or can be used as a prognostic factor.

ACKNOWLEDGEMENTS

M. Absenger (Core Facility Microscopy/ZMF, MUG, Graz, Austria) provided technical assistance for using the cell observer. We thank A. Patapoutian (HHMI, La Jolla, CA, USA) for providing the plasmid (pIRES2) containing the human Piezo1 and eGFP cDNA. Financial support by the Austrian Research Foundation is gratefully acknowledged (FWF P22974-B19 (WS); KLIF 182 (TB)).

I thank A. Gorischek for greatly help to my daily experiment, thank S. Rezania for the help on cellular work of my project, thank S. Kammerer for the help on WB and information from the university, thank T. Devaney for the help on ImageJ, and thank everyone in our department for the help during the past four years.

My wife Xu Hui gave me strong support when I wrote this thesis, even if she was pregnant during that time. I am fully thankful for her support when I cannot pay much attention taking care of her.

REFERENCES

[1] Horner VL, Wolfner MF. Mechanical stimulation by osmotic and hydrostatic pressure activates Drosophila oocytes in vitro in a calcium-dependent manner. Dev. Biol. 2008a;316:100-109.

[2] Mammoto T, Ingber DE. Mechanical control of tissue and organ development. Development 2010;137:1407-1420.

[3] Charras GT, Horton MA. Single cell mechanotransduction and its modulation analyzed by atomic force microscope indentation. Biophys J 2002;82:2970–2981

[4] Bukoreshtliev NV, Haase K, Pelling AE. Mechanical cues in cellular signalling and communication. Cell and Tissue Research 2013;352:77-94.

[5] Guolla L, Bertrand M, Haase K, Pelling AE. Force transduction and strain dynamics in actin stress fibres in response to nanonewton forces. J Cell Sci 2012;125:603–613

[6] Dupont S, Morsut L, Aragona M, Enzo E, Giulitti S, Cordenonsi M, Zanconato F, Le Digabel J, Forcato M, Bicciato S, Elvassore N, Piccolo S. Role of YAP/TAZ in mechanotransduction. Nature 2011;474:179–183

[7] Butcher DT, Alliston T, Weaver VM. A tense situation:forcing tumour progression. Nat Rev Cancer 2009;9:108-122.

[8] Krieg M, Arboleda-Estudillo Y, Puech PH, Käfer J, Graner F, Müller DJ, Heisenberg CP. Tensile forces govern germ-layerorganization in zebrafish. Nature Cell Biol. 2008;10:429–436.

[9] Page-McCaw A, Ewald AJ, Werb Z. Matrixmetalloproteinases and the regulation of tissueremodelling. Nature Rev. Mol. Cell Biol. 2007;8:221–233.

[10] Czirok A, Rongish BJ, Little CD. Extracellularmatrix dynamics during vertebrate axis formation. Dev. Biol. 2004;268:111–122.

[11] Engler AJ , Sen S, Sweeney HL, Discher DE. Matrix elasticity directs stem cell lineage specification.Cell 2006;126:677–689.

[12] Davies PF, Remuzzi A, Gordon EJ, Dewey CF Jr, Gimbrone MA Jr. Turbulent fluid shear stressinduces vascular endothelial cell turnover in vitro.Proc. Natl Acad. Sci. USA 1986;83:2114–2117.

[13] Schedin P, Keely PJ. Mammary gland ECM remodeling, stiffness, and mechanosignaling in normal development and tumor progression. Cold Spring Harbor perspectives in biology 2011;3:a003228.

[14] Neville MC. Introduction: Tight junctions and secretory activation in the mammary gland. J MammaryGland Biol Neoplasia 2009;14:269–270.

[15] Thery M, Racine V, Piel M, Pepin A, Dimitrov A, Chen Y, Sibarita JB, Bornens M. Anisotropy of cell adhesivemicroenvironment governs cell internal organizationand orientation of polarity. Proc Natl Acad Sci U S A 2006;103:19771–19776.

[16] Thubrikar MJ, Robicsek F. Pressure-induced arterial wall stress and atherosclerosis. Ann Thorac Surg 1995;59:1594–1603.

[17] Brown XQ, Bartolak-Suki E, Williams C, Walker ML, Weaver VM, Wong JY. (). Effect of substrate stiffness and PDGF on the behavior of vascular smooth muscle cells: implications for atherosclerosis. Journal of Cellular Physiology 2010;225(1):115–122. doi:10.1002/jcp.22202

[18] Shieh AC, Biomechanical forces shape the tumor microenvironment, Annals of biomedical engineering 2011;39:1379-1389.

[19] Nelson CM, Bissell MJ. Of extracellular matrix, scaffolds, and signaling: tissue architecture regulates development, homeostasis, and cancer, Annual review of cell and developmental biology 2006;22:287-309.

[20] Michor F, Liphardt J, Ferrari M, Widom J. What does physics have to do with cancer?. Nat Rev Cancer 2011;11:657-670.

[21] Efremov YM, Lomakina ME, Bagrov DV, Makhnovskiy PI, Alexandrova AY, Kirpichnikov MP, Shaitan KV. Mechanical properties of fibroblasts depend on level ofcancer transformation.Biochim Biophys Acta. 2014 May;1843(5):1013-9.

[22] Yu HM, Mouw JK, Weaver VM, Forcing form and function: biomechanical regulation of tumor evolution, Trends in Cell Biology 2011;21:47-56.

[23] Geiger B, Spatz JP, Bershadsky AD, Environmental sensing through focal adhesions, Nature reviews. Molecular cell biology 2009;10:21-33.

[24] Sukharev S, Sachs F. Molecular force transduction by ion channels: diversity and unifying principles. J Cell Sci 2012;125:3075-3083.

[25] Guharay F, Sachs F. Stretch-activated single ion channel current s in tissue-cultu red embryonic chick skeletal muscle. J Physiol 1984;352:685–701

[26] Wu LJ, Sweet TB, Clapham DE, International Union of Basic and Clinical Pharmacology. LXXVI. Current progress in the mammalian TRP ion channel family, Pharmacological reviews 2010;62:381-404.

[27] Patel A, Sharif-Naeini R, Folgering JR, Bichet D, Duprat F, Honore E. Canonical TRP channels and mechanotransduction: from physiology to disease states, Pflugers Archiv.: European journal of physiology 2010;460:571-581.

[28] Beech DJ. TRPC1: store-operated channel and more.Pflugers Arch 2005;451:53–60

[29] Dietrich A, Gudermann T. Trpc6. Handb Exp Pharmacol 2007;179:125–141

[30] Dietrich A, Kalwa H, Storch U, Mederos YSM, Salanova B, Pinkenburg O, Dubrovska G, Essin K, Gollasch M, Birnbaumer L, Gudermann T. Pressure-induced and

store-operated cation influx in vascular smooth muscle cells is independent of TRPC1. Pflugers Arch 2007;455:465–477

[31] Winn MP, Conlon PJ, Lynn KL, Farrington MK, Creazzo T,Hawkins AF, Daskalakis N, Kwan SY, Ebersviller S, Burchette JL, Pericak-Vance MA, Howell DN, Vance JM, Rosenberg PB. A mutation in the TRPC6 cation channel causes familial focal segmental glomerulosclerosis. Science 2005;308:1801–1804

[32] Coste B, Xiao B, Santos JS, Syeda R, Grandl J, Spencer KS, Kim SE, Schmidt M, Mathur J, Dubin AE, Montal M, Patapoutian A. Piezo proteins are pore-forming subunits of mechanically activated channels. Nature 2012;483:176-181.

[33] Kawashima Y, Kurima K, Pan B, Griffith AJ, Holt JR. Transmembrane channel-like (TMC) genes are required for auditory and vestibular mechanosensation, Pflugers Archiv.: European journal of physiology. 2015 Jan;467(1):85-94..

[34] Bae C, Gnanasambandam R, Nicolai C, Sachs F, Gottlieb PA, Xerocytosis is caused by mutations that alter the kinetics of the mechanosensitive channel PIEZO1, Proc Natl Acad Sci U S A, 110 (2013) E1162-1168.

[35] Coste B, Houge G, Murray MF, Stitziel N, Bandell M, Giovanni MA, Philippakis A, Hoischen A, Riemer G, Steen U, Steen VM, Mathur J, Cox J, Lebo M, Rehm H, Weiss ST, Wood JN, Maas RL, Sunyaev SR, Patapoutian A. Gain-of-function mutations in the mechanically activated ion channel PIEZO2 cause a subtype of Distal Arthrogryposis. Proc. Natl. Acad. Sci. U.S.A. 2013 March;110 (12):4667–72.

[36] Potier M, Joulin V, Roger S, Besson P, Jourdan M L, Leguennec J Y, Bougnoux P, Vandier C. Identification of SK3 channel as a new mediator of breast cancer cell migration. Mol Cancer Ther 2006; 5: 2946–2953

[37] Stringer B K, Cooper A G, Shepard S B. Overexpression of the G-protein inwardly rectifying potassium channel 1 (GIRK1) in primary breast carcinomas correlates with axillary lymph node metastasis. Cancer Res 2001; 61: 582–588

[38] McFerrin M B, Sontheimer H. A role for ion channels in glioma cell invasion. Neuron Glia Biol 2006; 2: 39–49

[39] Prevarskaya N, Skryma R, Shuba Y. Ion channels and the hallmarks of cancer. Trends in Molecular Medicine 2010;16:107-121.

[40] Lee J, Ishihara A, Oxford G, Johnson B, Jacobson K. Regulation of cell movement is mediated by stretch-activated calcium channels, Nature 1999;400:382-386.

[41] Wagner V, Stadelmeyer E, Riederer M, Regitnig P, Gorischek A, Devaney T, Schmidt K, Tritthart HA, Hirschberg K, Bauernhofer T, Schreibmayer W. Cloning and characterisation of GIRK1 variants resulting from alternative RNA editing of the KCNJ3 gene transcript in a human breast cancer cell line. Journal of cellular biochemistry 2010;110:598-608.

[42] Livak KJ, Schmittgen TD. Analysis of Relative Gene Expression Data Using Real-Time Quantitative PCR and the $2^{-\Delta\Delta CT}$ Method. Methods 2001; 25:402-408.

[43] Poteser M, Schleifer H, Lichtenegger M, Schernthaner M, Stockner T, Kappe CO, Glasnov TN, Romanin C, Groschner K, PKC-dependent coupling of calcium permeation through transient receptor potential canonical 3 (TRPC3) to calcineurin signaling in HL-1 myocytes, Proc Natl Acad Sci U S A 2011;108:10556-10561.

[44] Ogden D, Stanfield P. Patch clamp techniques for single channel and whole-cell recording. Microelectrode techniques: the Plymouth workshop handbook. The Company of Biologists Cambridge; 1987.

[45] Sakmann B, Neher E. Patch clamp techniques for studying ionic channels in excitable membranes. Annu Rev Physiol 1984;46:455-72.

[46] K. Li, "The image stabilizer plugin for ImageJ," http://www.cs.cmu.edu/~kangli/code/Image_Stabilizer.html, February, 2008.

[47] Cahalan MD, Parker I. Choreography of cell motility and interaction dynamics imaged by two-photon microscopy in lymphoid organs, Annu Rev Immunol 2008;26:585-626.

[48] Gyorffy B, Lanczky A, Eklund AC, Denkert C, Budczies J, Li Q, Szallasi Z. An online survival analysis tool to rapidly assess the effect of 22,277 genes on breast cancer prognosis using microarray data of 1,809 patients. Breast Cancer Res Treat 2010;123:725-731.

[49] Li C, Rezania S, Kammerer S, Sokolowski A, Devaney T, Gorischek A, Jahn S, Hackl H, Groschner K, Windpassinger C, Malle E, Bauernhofer T, Schreibmayer W. Piezo1 forms mechanosensitive ion channels in the human MCF-7 breast cancer cell line. Sci. Rep. 2014;5, 8364; DOI:10.1038/srep08364

[50] Gottlieb PA, Bae C, Sachs F. Gating the mechanical channel Piezo1: a comparison between whole-cell and patch recording. Channels 2012;6:282-289.

[51] Hao J, Delmas P. Recording of mechanosensitive currents using piezoelectrically driven mechanostimulator, Nature protocols 2011;6: 979-990.

[52] Neve RM, Chin K, Fridlyand J, Yeh J, Baehner FL, Fevr T, Clark L, Bayani N, Coppe JP, Tong F, Speed T, Spellman PT, DeVries S, Lapuk A, Wang NJ, Kuo WL, Stilwell JL, Pinkel D, Albertson DG, Waldman FM, McCormick F, Dickson RB, Johnson MD, Lippman M, Ethier S, Gazdar A, Gray JW. A collection of breast cancer cell lines for the study of functionally distinct cancer subtypes. Cancer Cell 2006;10:515-527.

[53] Soule HD, Maloney TM, Wolman SR, Peterson WD, Brenz R Jr, McGrath CM, Russo J, Pauley RJ, Jones RF, Brooks SC, Isolation and characterization of a spontaneously immortalized human breast epithelial cell line, MCF-10. Cancer Res. 1990;50:6075-6086.

[54] Hanahan D, Weinberg RA. Hallmarks of cancer: the next generation. Cell 2011;144:646-674.

[55] Bae C, Sachs F, Gottlieb PA. The Mechanosensitive Ion Channel Piezo1 Is Inhibited by the Peptide GsMTx4. Biochemistry 2011;50:6295-6300.

[56] Peyronnet R, Martins JR, Duprat F, Demolombe S, Arhatte M, Jodar M, Tauc M, Duranton C, Paulais M, Teulon J, Honore E, Patel A. Piezo1-dependent stretch-activated channels are inhibited by Polycystin-2 in renal tubular epithelial cells. Embo Reports 2013;14:1143-1148.

[57] Tse JM, Cheng G, Tyrrell JA, Wilcox-Adelman SA, Boucher Y, Jain RK, Munn LL. Mechanical compression drives cancer cells toward invasive phenotype. Proceedings of the National Academy of Sciences of the United States of America 2012;109:911-916.

[58] Boghaert E, Gleghorn JP, Lee K, Gjorevski N, Radisky DC, Nelson CM. Host epithelial geometry regulates breast cancer cell invasiveness. Proceedings of the National Academy of Sciences of the United States of America 2012;109:19632-19637.

[59] Shi Q, Ghosh RP, Engelke H, Rycroft CH, Cassereau L, Sethian JA, Weaver VM, Liphardt JT. Rapid disorganization of mechanically interacting systems of mammary acini. Proc Natl Acad Sci USA 2014;111:658-663.

[60] DuFort CC, Paszek MJ, Weaver VM. Balancing forces: architectural control of mechanotransduction, Nature reviews. Molecular cell biology 2011;12:308-319.

[61] Provenzano PP, Inman DR, Eliceiri KW, Keely PJ. Matrix density-induced mechanoregulation of breast cell phenotype, signaling and gene expression through a FAK-ERK linkage. Oncogene 2009;28:4326-4343.

[62] Zaidel-Bar R, Itzkovitz S, Ma'ayan A, Iyengar R, Geiger B. Functional atlas of the integrin adhesome. Nat Cell Biol 2007;9:858-867.

[63] Paszek MJ, DuFort CC, Rossier O, Bainer R, Mouw JK, Godula K, Hudak JE, Lakins JN, Wijekoon AC, Cassereau L, Rubashkin MG, Magbanua MJ, Thorn KS, Davidson MW, Rugo HS, Park JW, Hammer DA, Giannone G, Bertozzi CR, Weaver VM. The cancer glycocalyx mechanically primes integrin-mediated growth and survival. Nature 2014;511:319-325.

[64] Zaidel-Bar R, Itzkovitz S, Ma'ayan A, Iyengar R, Geiger B, Functional atlas of the integrin adhesome. Nat Cell Biol. 2007 August;9(8):858–867. doi:10.1038/ncb.0807-858.

[65] Ross TD, Coon BG, Yun S, Baeyens N, Tanaka K, Ouyang M, Schwartz MA. Integrins in mechanotransduction. Current opinion in cell biology 2013;25:613-618.

[66] Martinac B. The ion channels to cytoskeleton connection as potential mechanism of mechanosensitivity. Biochimica et biophysica acta 2014;1838:682-691.

[67] McHugh BJ, Buttery R, Lad Y, Banks S, Haslett C, Sethi T. Integrin activation by Fam38A uses a novel mechanism of R-Ras targeting to the endoplasmic reticulum. J Cell Sci 2010;123:51-61.

[68] Thodeti CK, Matthews B, Ravi A, Mammoto A, Ghosh K, Bracha AL, Ingber DE. TRPV4 channels mediate cyclic strain-induced endothelial cell reorientation through integrin-to-integrin signaling. Circ Res 2009;104:1123-1130.

[69] McHugh BJ, Buttery R, Lad Y, Banks S, Haslett C, Sethi T. Integrin activation by Fam38A uses a novel mechanism of R-Ras targeting to the endoplasmic reticulum. J Cell Sci 2010;123:51-61.

[70] Woo SH, Ranade S, Weyer AD, Dubin AE, Baba Y, Qiu Z, Petrus M, Miyamoto T, Reddy K, Lumpkin EA, Stucky CL, Patapoutian A. Piezo2 is required for Merkel-cell mechanotransduction. Nature 2014;509:622-626.

[71] Ranade SS, Woo SH, Dubin AE, Moshourab RA, Wetzel C, Petrus M, Mathur J, Bégay V, Coste B, Mainquist J, Wilson AJ, Francisco AG, Reddy K, Qiu Z, Wood JN, Lewin GR, Patapoutian A. Piezo2 is the major transducer of mechanical forces for touch sensation in mice. Nature. 2014 Dec 4;516(7529):121-5. doi:10.1038/nature.13980.

[72] Ikeda R, Gu JG. Piezo2 channel conductance and localization domains in Merkel cells of rat whisker hair follicles. Neurosci Lett. 2014 Nov 7;583:210-5. doi:0.1016/j.neulet.2014.05.055. Epub 2014 Jun 6.

[73] Schrenk-Siemens K, Wende H, Prato V, Song K, Rostock C, Loewer A, Utikal J, Lewin GR, Lechner SG, Siemens J. PIEZO2 is required for mechanotransduction in human stem cell-derived touch receptors. Nat Neurosci. 2015 Jan;18(1):10-6. doi:10.1038/nn.3894. Epub 2014 Dec 3.

[74] Eisenhoffer GT, Loftus PD, Yoshigi M, Otsuna H, Chien CB, Morcos PA, Rosenblatt J, Crowding induces live cell extrusion to maintain homeostatic cell numbers in epithelia. Nature 2012;484:546-549.

[75] Ranade SS, Qiu Z, Woo SH, Hur SS, Murthy SE, Cahalan SM, Xu J, Mathur J, Bandell M, Coste B, Li YS, Chien S, Patapoutian A. Piezo1, a mechanically activated ion channel, is required for vascular development in mice. Proc Natl Acad Sci U S A 2014;111:10347-10352.

[76] Li J, Hou B, Tumova S, Muraki K, Bruns A, Ludlow MJ, Sedo A, Hyman AJ, McKeown L, Young RS, Yuldasheva NY, Majeed Y, Wilson LA, Rode B, Bailey MA, Kim HR, Fu Z, Carter DA, Bilton J, Imrie H, Ajuh P, Dear TN, Cubbon RM, Kearney MT, Prasad RK, Evans PC, Ainscough JF, Beech DJ. Piezo1 integration of vascular architecture with physiological force. Nature 2014 Nov 13;515(7526):279-82. doi:10.1038/nature13701. Epub 2014 Aug 10.

[77] Miyamoto T, Mochizuki T, Nakagomi H, Kira S, Watanabe M, Takayama Y, Suzuki Y, Koizumi S, Takeda M, Tominaga M. Functional Role for Piezo1 in Stretch-evoked Ca2+ Influx and ATP Release in Urothelial Cell Cultures. The Journal of biological chemistry 2014;289:16565-16575.

[78] Faucherre A, Kissa K, Nargeot J, Mangoni ME, Jopling C. Piezo1 plays a role in erythrocyte volume homeostasis. Haematologica. 2014 Jan;99(1):70-5. doi: 10.3324/haematol.2013.086090. Epub 2013 Jul 19.

[79] Coste B, Houge G, Murray MF, Stitziel N, Bandell M, Giovanni MA, Philippakis A, Hoischen A, Riemer G, Steen U, Steen VM, Mathur J, Cox J, Lebo M, Rehm H, Weiss ST, Wood JN, Maas RL, Sunyaev SR, Patapoutian A. Gain-of-function mutations in the mechanically activated ion channel PIEZO2 cause a subtype of Distal Arthrogryposis. Proc Natl Acad Sci U S A 2013;110:4667-4672.

[80] Andolfo I, Alper SL, De Franceschi L, Auriemma C, Russo R, De Falco L, Vallefuoco F, Esposito MR, Vandorpe DH, Shmukler BE, Narayan R, Montanaro D, D'Armiento M, Vetro A, Limongelli I, Zuffardi O, Glader BE, Schrier SL, Brugnara C, Stewart GW, Delaunay J, Iolascon A. Multiple clinical forms of dehydrated hereditary stomatocytosis arise from mutations in PIEZO1. Blood. 2013 May 9;121(19):3925-35, S1-12. doi:10.1182/blood.2013.02.482489. Epub 2013 Mar 11.

[81] Albuisson J, Murthy SE, Bandell M, Coste B, Louis-Dit-Picard H, Mathur J, Fénéant-Thibault M, Tertian G, de Jaureguiberry JP, Syfuss PY, Cahalan S, Garçon L, Toutain F, Simon Rohrlich P, Delaunay J, Picard V, Jeunemaitre X, Patapoutian A. Dehydrated hereditary stomatocytosis linked to gain-of-function mutations in mechanically activated PIEZO1 ion channels. Nat Commun 2013;4:1884. doi:10.1038/ncomms2899.

[82] Shmukler BE, Vandorpe DH, Rivera A, Auerbach M, Brugnara C, Alper SL. Dehydrated stomatocytic anemia due to the heterozygous mutation R2456H in the mechanosensitive cation channel PIEZO1: a case report. Blood Cells Mol Dis. 2014 Jan;52(1):53-4. doi:10.1016/j.bcmd.2013.07.015. Epub 2013 Aug 23.

[83] Sandberg MB, Nybo M, Birgens H, Frederiksen H. Hereditary xerocytosis and familial haemolysis due to mutation in the PIEZO1 gene: a simple diagnostic approach.Int J Lab Hematol. 2014 Aug;36(4):e62-5. doi:10.1111/ijlh.12172. Epub 2013 Dec 6.

[84] McHugh BJ, Murdoch A, Haslett C, Sethi T. Loss of the integrin-activating transmembrane protein Fam38A (Piezo1) promotes a switch to a reduced integrin-dependent mode of cell migration. PloS one 2012;7:e40346.

[85] Yang XN, Lu YP, Liu JJ, Huang JK, Liu YP, Xiao CX, Jazag A, Ren JL, Guleng B. Piezo1 is as a novel trefoil factor family 1 binding protein that promotes gastric cancer cell mobility in vitro. Dig Dis Sci 2014;59:1428-1435.

[86] Abend M, Pfeiffer RM, Ruf C, Hatch M, Bogdanova TI, Tronko MD, Riecke A, Hartmann J, Meineke V, Boukheris H, Sigurdson AJ, Mabuchi K, Brenner AV. Iodine-131 dose dependent gene expression in thyroid cancers and corresponding normal tissues following the Chernobyl accident, PloS one 2012;7:e39103.